Title

Electric-field effects in Rb.sphaeroides chromatophores and excitation equilibration in wild-type and mutant Rb.sphaeroides intracytoplasmic membranes

Author

Steiger, Jana L.

Publication Date

2001-12-01

Thesis/dissertation

LBNL-49617

ERNEST ORLANDO LAWRENCE
BERKELEY NATIONAL LABORATORY

Electric-Field Effects in *Rb. sphaeroides* Chromatophores and Excitation Equilibration in Wild-Type and Mutant *Rb. sphaeroides* Intracytoplasmic Membranes

Jana L. Steiger

Physical Biosciences Division

December 2001

Ph.D. Thesis

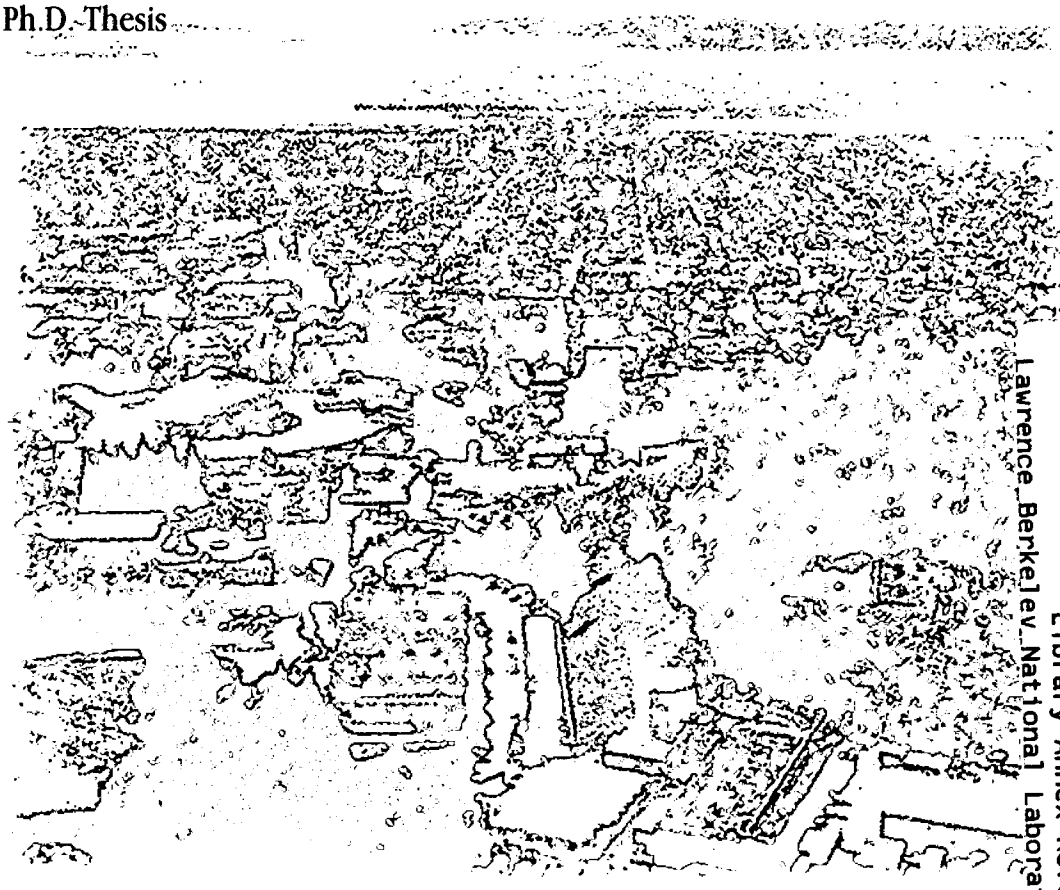

DISCLAIMER

LBNL-49617

Electric-Field Effects in *Rb. sphaeroides* Chromatophores and Excitation Equilibration in Wild-Type and Mutant *Rb. sphaeroides* Intracytoplasmic Membranes

Jana Lee Steiger
Ph.D. Thesis

Chemistry Department
University of California, Berkeley

and

Physical Biosciences Division
Ernest Orlando Lawrence Berkeley National Laboratory
University of California
Berkeley, CA 94720

December 2001

This work was supported by the Director, Office of Science, Office of Basic Energy Sciences, Division of Chemical Sciences, of the U.S. Department of Energy under Contract No. DE-AC03-76SF00098.

Electric-Field Effects in *Rb. sphaeroides* Chromatophores and Excitation Equilibration in Wild-Type and Mutant *Rb. sphaeroides* Intracytoplasmic Membranes

by

Jana Lee Steiger

Abstract

Electric-Field Effects in *Rb. sphaeroides* Chromatophores

and

Excitation Equilibration in Wild-Type and Mutant

Rb. sphaeroides Intracytoplasmic Membranes

by

Jana Lee Steiger

Doctor of Philosophy in Chemistry

University of California, Berkeley

Professor Kenneth Sauer, Chair

The purple photosynthetic bacterium *Rb. sphaeroides* is used to investigate processes of photosynthesis. Electric fields are applied along the membrane normal of *Rb. sphaeroides* chromatophore vesicles by the creation of a potassium chloride gradient across the membrane. The fluorescence emission is monitored as a function of the applied electric field potential.

The electric-field effect on the fluorescence emission is maximum (approximately 15% per 100 mV) in the Fm state, when the reaction center special pair is oxidized (P^+) and the reaction center cannot perform charge separation. The fluorescence changes we observe under these conditions are consistent with an electric-field effect directly on the fluorescence emission of the LH1 and LH2 antenna complexes. This theory is supported by an electric-field effect on the fluorescence emission of LM1.1, a mutant *Rb. sphaeroides* strain which expresses LH1 and LH2 but not reaction centers. In the wild-type Fo state, when the reaction center is capable of charge separation, the electric-field effect is diminished (approximately 8% per 100 mV). Assuming that the electric-field effect on the reaction center is separate from the electric-field effect on the antenna complexes, subtraction of

electric-field effect on the Fm state from the electric-field effect on the Fo state yields an estimate of the electric-field effect on the reaction center. Comparison of this effect with previous theoretical work supports the superexchange mechanism of charge separation in the reaction center.

Excitation equilibration is investigated in several mutant strains of *Rb. sphaeroides* which lack reaction centers, as well as the wild type. The Kennard-Stepanov analysis of absorption and fluorescence spectra is applied to membrane preparations of the mutants RC-1A, BALM/LH2, and LM1.1, which express LH1, LH2, and both LH1 and LH2, respectively. Good agreement with the Kennard-Stepanov (KS) relation is found over the majority of the spectral range, indicating rapid and complete excitation equilibration prior to fluorescence emission. One exception is a deviation on the red edge of the spectra, indicating a possible "dark" state in that spectral region which absorbs but does not fluoresce with the expected intensity.

The wild-type *Rb. sphaeroides* membrane preparation also shows a red-edge anomaly in the KS spectral analysis. Additionally, there is a second anomaly in the central spectral region which is not seen for mutants lacking a reaction center. Therefore we conclude that the presence of a reaction center disrupts the complete equilibration of excitation prior to fluorescence emission. Notably, this disruption of excitation equilibration is not observed in any previous KS analysis of PSI and PSII.

Table of Contents

Chapter One: Introduction

Chapter Two: Materials and Methods

Chapter Three: *Rb. sphaeroides* Characterization

Chapter Four: Electric-Field Effects in Chromatophores of *Rb. sphaeroides*

Chapter Five: The Kennard-Stepanov relation

Abbreviations

9AA	9-aminoacridine
ATP	adenosine triphosphate
B	monomeric bacteriochlorophyll in the L subunit of the reaction center
BChl	bacteriochlorophyll a
Bpheo	bacteriopheophytin a
Chl	chlorophyll
CM	cytoplasmic membrane
Cyt	cytochrome
dithionite	sodium dithionite; $Na_2S_2O_4$
DMSO	dimethyl sulfoxide
EDTA	ethylenediaminetetraacetic acid
FWHM	full width at half maximum
H	bacteriopheophytin in the L subunit of the reaction center
Hepes	4-(2-hydroxyethyl)-1-piperazineethanesulfonic acid
ICM	intracytoplasmic membrane
KS	Kennard-Stepanov
LH1	light harvesting complex 1 (absorption maximum at 875 nm)
LH2	light harvesting complex 2 (absorption maxima at 800 and 850 nm)
P	special pair in the reaction center
Q_A	primary quinone
Rb.	*Rhodobacter*
RC	reaction center
Rps.	*Rhodopseudomonas*
Rsp.	*Rhodospirillum*
RT	room temperature

Chapter One:

Introduction

"All life depends on plants."

Inscription at Kew Gardens, England

Photosynthesis:

Photosynthesis is the foundation of life on earth. In photosynthesis, sunlight is absorbed by photosynthetic bacteria, algae, or plants, and these organisms convert the absorbed light energy into chemical energy. In the reaction center of photosynthetic organisms, a photon of light triggers a charge separation event; a negative electron and a positive hole are generated within the reaction center. This charge separation event converts the energy of the photon into an electrochemical potential within the reaction center. The charge separation event which is initiated by light is extremely rapid and efficient, with very little charge recombination.[1] A full understanding of the photosynthetic process may someday allow us to mimic natural photosynthetic charge separation artificially, and develop efficient solar energy technology.

In the living cell, the electrochemical potential of the electron-hole pair that is created by absorption of a photon is used to generate high energy chemical compounds such as ATP, which are used as the currency of energy within the cell.[2] These high energy chemical compounds drive biological processes within the cell, such as the reduction of CO_2 into carbohydrates via the Calvin cycle.[3] Carbohydrates are ingested by other life forms, such as fungi, bacteria, and animals. Together with oxygen, these

carbohydrates are the energy source used to drive biological processes through respiration. Thus, photosynthesis is the foundation for life on earth.

Photosynthesis has been extensively studied for many decades. In spite of the great progress that has been made toward understanding photosynthesis, many fundamental questions remain unanswered. Photosynthetic bacteria are relatively simple photosynthetic systems, and as such they offer a practical approach to understanding general photosynthetic processes. Purple photosynthetic bacteria contain one type of reaction center, as opposed to two separate photosystems which are found in oxygen-evolving plants and cyanobacteria. Purple photosynthetic bacteria also have only one or two types of antenna complexes, while oxygen-evolving plants may have several types of antenna complexes.

Rhodobacter sphaeroides:

One of the most well-studied and well-characterized purple photosynthetic bacteria is *Rhodobacter (Rb.) sphaeroides*. *Rb. sphaeroides* is a Gram-negative, nonsulfur purple photosynthetic bacteria, with a rod-type cell shape approximately 0.7 μm in diameter.[4]

The photosynthetic apparatus of *Rb. sphaeroides* is located in a continuous internal membrane called the intracytoplasmic membrane (ICM).[4] In *Rb. sphaeroides*, the form of the ICM consists of multiple vesicular indentations in a continuous membrane sheet. The vesicle indentations are produced by a lateral asymmetry in the membrane bilayer. There is a higher percentage of phosphatidylglycerol (PG) phospholipids on the outer side of the bilayer membrane than the inner side, which produces an intrinsic curvature in the membrane.[5] When the cells are mechanically disrupted, for example by passage through a French press, the curved ICM indentations seal to form membrane vesicles with a preferential orientation. The ICM

membrane vesicles are called chromatophores, and can be isolated from the remainder of the cellular components (such as outer cell wall fragments) by differential centrifugation as described in Chapter Two. The formation of sealed chromatophore vesicles from the ICM of *Rb. sphaeroides* is important for our experiments, as will be discussed in Chapter Three and Chapter Four. The ICM contains the entire photosynthetic apparatus of *Rb. sphaeroides*, including both of the antenna complexes light harvesting complex 1 (LH1) and light harvesting complex 2 (LH2) as well as the photosynthetic reaction center.

The reaction center:

The reaction center from *Rb. sphaeroides* has been crystallized, and the structure has been determined at high resolution.[6] The reaction center consists of three protein subunits, L, M, and H. There is a pseudo-C_2 symmetry of the L and M protein subunits. See Figure 1.1 for a schematic of the reaction center L and M pigment-protein complexes. A dimer of BChl is located on the symmetry axis, and is called the special pair (P). The special pair absorbs light which creates the excited state special pair (P*). The excited state special pair originates charge separation by transferring an electron to a photosynthetic cofactor in the reaction center. The photosynthetic cofactor molecules bacteriochlorophyll a (BChl) and bacteriopheophytin (BPheo) are associated with the L subunit of the reaction center. The M subunit also contains a BChl and BPheo, in similar positions to those on the L branch. Despite the pseudo-C_2 symmetry, charge separation occurs almost exclusively along the L branch.[7] The reason for the asymmetry in the direction of charge separation is not yet known, although one hypothesis is that specific amino acids near the cofactors BChl and BPheo determine the direction of charge separation by influencing the potential energies of the charge separated states.[7]

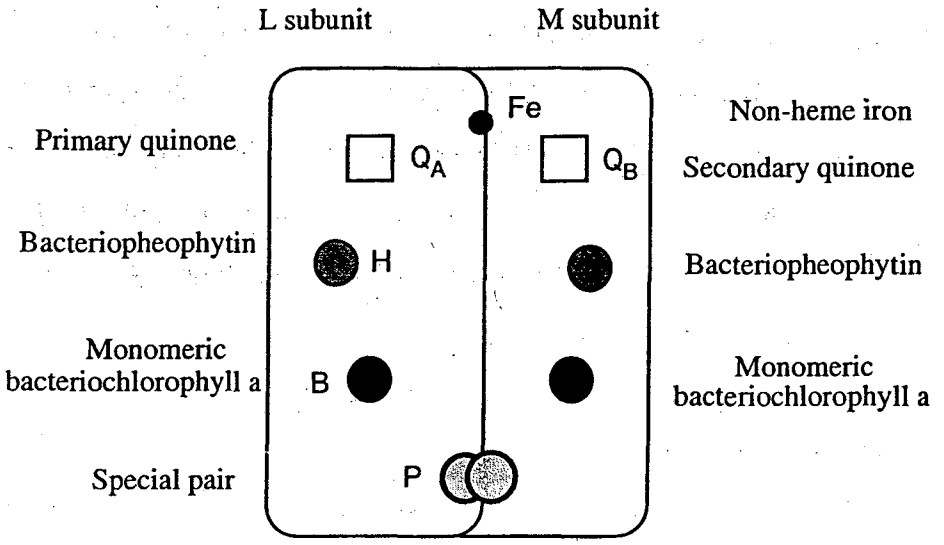

Figure 1.1: Schematic of the *Rb. sphaeroides* reaction center, showing the L and M subunits and the positions of the cofactors involved in charge separation.

Time resolved spectroscopic experiments reveal that there is an electron on the photosynthetically active L subunit BPheo (H) with a time constant of 2.8 ps after photon absorption by the special pair.[8] The nearest approach of the special pair (P) and the active BPheo (H) is approximately 7 Å.[6] The primary charge separation reaction is extremely rapid for such a large distance between electron transfer components; therefore, a BChl intermediary has been proposed. There are two main hypotheses how BChl may assist electron transfer from P to H. The BChl in the L subunit (B) may serve as a distinct reduced intermediate, B^-. This is called the two-step or sequential hypothesis, because the electron moves sequentially to B, then to H.[9] Alternately, B may serve as a virtual intermediate. This is called the superexchange mechanism. In the superexchange hypothesis, the presence of the B electronic state

facilitates direct electron transfer from P to H, although B^- is not formed as a discrete intermediate.[10] These two hypotheses will be further addressed in Chapter Four.

The antenna complexes LH1 and LH2:

The antenna complexes act as spectral funnels which direct absorbed light energy to the reaction center. LH2 antenna complexes from *Rhodopseudomonas (Rps.) acidophila*[11] and *Rhodospirillum (Rsp.) molischianum* [12] have been crystallized, and the structures of these LH2 complexes have been determined. The antenna complexes share a common motif of a circular protein ring containing closely packed BChl molecules and carotenoids within the protein matrix. These BChl and carotenoids absorb light over a range of wavelengths; the specific range of wavelengths depends on the unique pigment-protein interactions within the species-specific type of antenna complex. There are two types of antenna complexes in *Rb. sphaeroides.* LH2 has maximum absorption at 800 and 850 nm, while LH1 has maximum absorption at 875 nm. The carotenoids in both of the antenna complexes in *Rb. sphaeroides* absorb light in the range between 400 and 530 nm. The BChl and carotenoids in the antenna both convert absorbed light energy to electronic excitation, then transfer the excitation to the reaction center where the excitation may be used in charge separation events.[13] Thus, the antenna complexes extend the range of light wavelengths that can be used for photosynthetic charge separation beyond the absorption range of the reaction center alone.

Although the structure of the LH1 antenna has not yet been successfully determined at high resolution, a low-resolution projection map of two-dimensional crystals from *Rsp. rubrum* LH1 show a ring structure with a center hole wide enough to accommodate the reaction center.[14] One hypothesis for the three-dimensional arrangement of pigment-protein complexes in the membrane is a reaction center

surrounded by the ring of LH1, which is in turn surrounded by the LH2 rings. This physical arrangement will be discussed in terms of the energy equilibration between the three components LH1, LH2, and the reaction center in Chapter Four and Chapter Five.

References for Chapter One

[1]Gregory, R.P.F. (1989) *Photosynthesis*, Chapman and Hall, New York.

[2]Stock, D., Gibbons, C., Arechaga, I., Leslie, A.G. & Walker, J.E. (2000) *Current Opinion in Structural Biology* 10: 672-679.

[3]Calvin, M. (1976) *Photochemistry and Photobiology* 23: 425-444.

[4]Imhoff, J.F. (1995) in *Anoxygenic Photosynthetic Bacteria* (Blankenship, R.E., Madigan, M.T. & Bauer, C.E., eds.) pp. 1-15, Kluwer Academic Publishers, Dordrecht, The Netherlands.

[5]Kaplan, S. & Arntzen, C.J. (1982) in *Photosynthesis: Energy Conversion by Plants and Bacteria*, (Govindjee, ed.) Vol. 1, pp. 67-151, Academic Press, New York.

[6]Allen, J.P., Feher, G., Yeates, T.O., Komiya, H. & Rees, D.C. (1987) *Proc. Natl. Acad. Sci. USA* 84: 6162-6166.

[7]Woodbury, N.W. & Allen, J.P. (1995) in *Anoxygenic Photosynthetic Bacteria* (Blankenship, R.E., Madigan, M.T. & Bauer, C.E., eds.) pp. 527-557, Kluwer Academic Publishers, Dordrecht, The Netherlands.

[8]Martin, J.-L., Breton, J., Hoff, A.J., Migus, A. & Antonetti, A. (1986) *Proc. Natl. Acad. Sci. USA* 83: 957-961.

[9]Holzwarth, A.R. & Muller, M.G. (1996) *Biochemistry* 35: 11820-11831.

[10]Bixon, M., Jortner, J., Michel-Beyerle, M.E. & Ogrodnik, A. (1989) *Biochim. Biophys. Acta* 977: 273-286.

[11]Freer, A., Prince, S., Sauer, K., Papiz, M., Hawthornthwaite-Lawless, A., McDermott, G., Cogdell, R. & Isaacs, N.W. (1996) *Structure* 4: 449-462.

[12]Koepke, J., Hu, X.C., Muenke, C., Schulten, K. & Michel, H. (1996) *Structure*, 4: 581-597.

[13]Fyfe, P.K. & Cogdell, R.J. (1996) *Current Opinion in Structural Biology* 6: 467 472.

[14]Karrasch, S., Bullough, P.A. & Gosh, R. (1995) *The EMBO Journal* 14: 631-638.

Chapter Two:

Materials and Methods

Growth conditions of wild-type *Rb. sphaeroides*:

Rb. sphaeroides strain 2.4.1 (wild-type *Rb. sphaeroides*) was obtained from the American Type Culture Collection (ATCC, Rockville, MD; strain #17023) and grown anaerobically in RCV growth media with vitamin supplements. See Appendix A for details of the RCV growth media and vitamin supplements. The *Rb. sphaeroides* cultures are grown at 30-32 °C under low light intensity provided by five to seven 60-watt tungsten light bulbs. Low light intensity growth conditions of *Rb. sphaeroides* cells favor high expression of the photosynthetic reaction center (RC) and high expression of both antenna complexes, LH1 and LH2.[1,2] Low light intensity growth conditions also influence the morphology of the intracytoplasmic membrane (ICM) of *Rb. sphaeroides*, by increasing the formation of multiple membrane invaginations in the ICM.[3] This increases the chromatophore yield per cell.

Chromatophores are the sealed membrane vesicles that are formed from the ICM when the *Rb. sphaeroides* cell is mechanically disrupted. The chromatophore membrane vesicles of wild-type *Rb. sphaeroides* contain the photosynthetic reaction center, as well as both LH1 and LH2. In addition, these chromatophores contain the complete photosynthetic apparatus as found *in vivo*, and are capable of proton translocation.[4] Chromatophore vesicles from wild-type *Rb. sphaeroides* form with a preferential orientation, sealing the periplasm inside the vesicle. This is opposite to the orientation of the ICM in intact whole cells. In the whole cell, the periplasm is outside

the cytoplasmic membrane, between the cytoplasmic membrane and the outmost cell wall; the cytoplasmic space is inside the cytoplasmic membrane. In the chromatophore preparation, the periplasmic space is inside the vesicle and the cytoplasmic space is outside. Thus, chromatophores are sometimes called "inverted" or "inside-out" vesicles.[5]

New cultures of *Rb. sphaeroides* cells are typically inoculated with a steady-state or late-log phase culture of about 10% of the new culture total volume. The cultures are grown in 2-liter batches and harvested usually 5 to 6 days after inoculation, in the mid-to-late log phase. In the mid-to-late log phase, the cultures are optically dense and significant self-shading occurs. Self-shading reduces the overall light intensity experienced by the cultures.

Growth conditions of *Rb. sphaeroides* mutant strains:

Purple photosynthetic bacteria have a diversity of metabolic growth options which allows the growth of reaction-centerless mutants which cannot rely on photosynthesis. However, care must be taken in the growth conditions, because the growth conditions can affect the morphology of the cell and intracytoplasmic membrane (ICM). Well developed and vesiculated ICM are necessary for the sample preparation used in our experiments (see Chapter Three).

Semi-aerobic growth:

Mutants without reaction centers can be grown aerobically. The key factor in aerobic growth is the use of oxygen as a terminal electron acceptor. The aerobic metabolic pathway is efficient and reliable, producing healthy cultures within three to five days of growth. However, the presence of oxygen impairs bacteriochlorophyll a (BChl) biosynthesis[6] and inhibits ICM formation[7] in purple photosynthetic bacteria.

BChl biosynthesis and ICM development are both necessary for our experiments. *Rb. sphaeroides* has a species-specific cutoff for BChl biosynthesis above 0.66 kPa partial pressure of oxygen, or roughly 1% oxygen concentration at 1 atm.[5] Culturing the bacteria aerobically, but at lower oxygen partial pressures than the cutoff value for BChl biosynthesis, is semi-aerobic growth.

Each reaction-centerless strain that we use in our study is capable of growing under semi-aerobic conditions, and the mutant strains have been cultured under semi-aerobic conditions for some purposes. BChl biosynthesis is assayed by absorption spectroscopy. Semi-aerobic growth is achieved in Erlenmeyer or Fernbach flasks approximately one-third full of YCC+ media (see appendix A) at 32° C in an incubator shaker.

Anaerobic growth of mutant strains:

Purple photosynthetic bacteria also have metabolic capabilities that permit anaerobic, non-photosynthetic growth. One of these alternative metabolic pathways is the use of nitrates as terminal electron acceptors. However, anaerobic growth of *Rb. sphaeroides* using nitrates as terminal electron acceptors leads to morphological changes in the intracytoplasmic membrane. The ICM forms long tube-shaped structures rather than the vesiculated membrane found in photosynthetically grown cells.[8] These tubules can interfere with proper cell division and result in partially separated daughter cells under some conditions. The lack of vesiculated ICM renders this method of *Rb. sphaeroides* growth ineffective for our purposes.

Another anaerobic metabolic option available to *Rb. sphaeroides* is the use of dimethyl sulfoxide (DMSO) or trimethylamine-N-oxide (TMAO) as a terminal electron acceptor. DMSO reductase is capable of reducing S-oxides, N-oxides, or chlorate.[9] DMSO reductase can be expressed in *Rb. sphaeroides* under certain growth conditions.

DMSO reductase contains a pterin-type molybdenum cofactor; *Rb. sphaeroides* grown without molybdenum in the medium fails to assemble functional DMSO reductase enzymes.[10] Because of this requirement, all growth media for DMSO-based growth are supplemented with an additional 0.2 g/l of a molybdenum salt (see Appendix A). DMSO reductase exhibits some characteristics common to molybdenum enzymes, such as inhibition by tungsten.[10] Therefore, tungsten-containing compounds are excluded from the media used for DMSO growth.

DMSO cultures produce invaginated intracytoplasmic membrane structure similar to photoheterotrophically grown cells. The only morphological difference from photoheterotrophically grown cells reported in the literature is a thickening of the outer cell envelope.[11] The development of invaginated ICM makes DMSO growth a useful option for reaction-centerless mutants used in our study.

There are several conditions for successful culturing of *Rb. sphaeroides* using DMSO as a terminal electron acceptor. DMSO reductase is inhibited by the presence of oxygen or nitrogen/oxygen compounds, so the culture must be maintained in an anaerobic environment to prevent repression of DMSO reductase. The cultures are continuously sparged with nitrogen gas, bubbled first through sterile water to prevent dehydration of the cultures. Secondly, since toxic dimethyl sulfide (DMS) is evolved as a product of DMSO reduction, the culture is continuously purged. In practice this means continuous stirring of the culture, providing a sterile venting port, and allowing about nine times the culture volume of head space in the culture bottle.[12] The evolution of toxic DMS gas also requires venting the cultures into a hood. The cultures are maintained at 32° C in a warm water bath. While some DMSO growth is observed without reduced-carbon sources in the media, the growth rate is greatly improved with reduced-carbon supplements.[13] For *Rb. capsulatus*, 6 grams per liter each of pyruvate and glucose have proved effective in stimulating growth on DMSO media.[14] Since *Rb.*

sphaeroides is incapable of metabolizing glucose, 6 grams per liter fructose is substituted for the glucose (see Appendix A). The pyruvate and fructose supplements are filtered through a disposable sterile Nalgene filter and added to the growth media after the media have been sterilized in an Amsco 3043 autoclave for 45 minutes at 25 lb./in.^{2} and 250 F.

Preparation of the chromatophore solution:

Harvesting of the *Rb. sphaeroides* whole cells is accomplished by centrifugation in a GS3 rotor at 7000 rpm (8300 x g) for 20 min. at 5 °C in a Sorvall RC-5B refrigerated centrifuge. All preparation is done under dim light conditions and at cold temperatures. The sample is kept on ice and in the dark whenever possible. The pellet which results from the GS3 centrifugation is resuspended in 40 ml of a buffer of 100 mM sodium phosphate and 10 mM EDTA, pH = 7.0. This buffer reduces nonspecific interactions between the ICM and the outer cell wall.[15] The cells are then mechanically ruptured by three passes through a French press (Aminco French pressure cell #4-3396) at 96.5 MPa/m^2. The resulting solution is centrifuged at 17,000 rpm in an SS34 rotor (35,000 x g) for 30 min. at 5 °C, to pellet any remaining whole cells and membrane aggregates.

The supernatant is carefully decanted and ultracentrifuged at 50,000 rpm in a Ti60 rotor (180,000 x g) at 4 °C for one hour in a Beckman L8-70 ultracentrifuge. The pellet is resuspended in ice-cold buffer A and homogenized. Buffer A consists of 5 mM $MgCl_2$, 5 mM HEPES, 800 mM sucrose and 100 mM KCl at pH 7.5. Any portion of the pellet which appears white is not resuspended. The homogenized solution is then ultracentrifuged again at 50,000 rpm in a Ti60 rotor (180,000 x g) at 4 °C for two hours, and resuspended and homogenized in ice-cold buffer A again. This solution is diluted to a total volume of one liter in buffer A. This is the chromatophore

solution. It is stored on ice overnight and measurements are typically made the next day.

The final concentration of BChl in the chromatophore solution is approximately 1.8 μg BChl / ml. This concentration of BChl is determined using an extraction of the chromatophore solution with 7:2 acetone : methanol by volume. The extinction coefficient of BChl under these conditions is $\varepsilon = 82.4\ mg^{-1}\ cm^{-1}$ ml at 770 nm.[16]

An alternative method of mechanical disruption of *Rb. sphaeroides* whole cells is a bead-beater apparatus (Biospec Products Inc., Bartlesville, OK). Wild-type *Rb. sphaeroides* cells are suspended in 40 ml of 100 mM sodium phosphate and 10 mM EDTA, pH 7.0, and combined with an equal volume of fine glass beads (0.1 mm diameter). This mixture is chilled in an ice/water jacket for 20 min. The solution is then rapidly agitated with rotating blades for 20 seconds followed by 10 min. of cooling in the ice/water jacket, repeated seven times in succession. The solution is then carefully decanted from the beads and centrifuged at 17,000 rpm in an SS34 rotor for 30 min., which pellets any remaining beads and whole cells or membrane aggregates. The supernatant is carefully decanted, and the remainder of the preparation follows the same protocols described in the second paragraph of the French press preparation above. The bead-beater procedure results in a lower chromatophore yield than the French press procedure. Bead-beater preparations are suspended to approximately the same concentration of BChl, resulting in a smaller total volume of chromatophore solution; the bead-beater method results in a final chromatophore solution about 1/4 the volume of the French press method from the same amount of starting material. Absorption and fluorescence of the bead-beater chromatophore solution are identical to the chromatophore solution produced by the French press method.

Intracytoplasmic membranes are prepared from the mutant strains following the same protocols as the French press preparation for wild-type *Rb. sphaeroides* with the following modifications. Multiple cultures are harvested for each preparation of mutant strains, because the mutant strains develop to a lower cell density than the wild type. Semi-aerobic cultures are harvested approximately five to seven days after inoculation. DMSO cultures are harvested approximately seven to nine days after inoculation. The preparations of the reaction-centerless mutants are made under normal room light conditions.

Diffusion potentials across membranes:

The salt-jump technique, described in the next section, creates diffusion potentials across chromatophore membranes of *Rb. sphaeroides.* A diffusion potential is an electrical potential across a membrane caused by an unequal distribution of ions on the two sides of the membrane.

Prior to salt-jump measurements, 100 µl of 20 mM valinomycin in 100% ethanol is added to the chromatophore solution per liter, for a final concentration of 2 µM valinomycin in the chromatophore solution. Valinomycin is a potassium-specific ionophore which transports potassium across biological membranes. Therefore, in the presence of valinomycin, potassium ions are transported freely across the sealed membrane vesicles of *Rb. sphaeroides* chromatophores. The counterion in solution (chloride in our experiments) has a slower diffusion rate than potassium in the presence of valinomycin. For example, if the concentration of potassium outside the chromatophore is higher than the concentration inside, valinomycin will transport potassium along its own potential gradient to the inside of the vesicle. This results in a transient diffusion potential, because the chloride counterion in the solution outside the vesicle cannot diffuse as rapidly as potassium to the inside of the vesicle. The

diffusion potential decays with a half time of several seconds, correlated with the rate of counterion equilibration.[17] The diffusion potential can be described by the Goldman-Hodgkin-Katz equation[18] [2.1]:

$$\Delta\Psi = \frac{R\,T}{z\,F} \ln \frac{\sum_c P_c[C]_2 + \sum_a P_a[A]_1}{\sum_c P_c[C]_1 + \sum_a P_a[A]_2} \qquad [2.1]$$

In equation [2.1], $\Delta\Psi$ is the diffusion potential, R is the gas constant, T is the temperature, z is the number of electric charges of the ionic species, and F is the Faraday constant. The first term in the numerator of the natural log, $\Sigma\ P_C[C]_2$, is a summation over all the different cation concentrations [C] on one side of the membrane (side 2; $_2$) multiplied by the respective permeability of those cations (P_C). The second term is a summation over all the different anion concentrations [A] multiplied by their respective permeabilities (P_a) on the other side of the membrane (side 1; $_1$). The denominator is the summation of the cation concentrations multiplied by their respective permeabilities on side 1, plus the summation of the anion concentrations multiplied by their respective permeabilities on side 2.

If one of the ions in the solution has a high concentration and mobility compared with the concentrations of the other ions in solution, equation [2.1] reduces to the Nernst equation:

$$\Delta\Psi = \frac{R\,T}{z\,F} \ln \frac{[I]_2}{[I]_1} \qquad [2.2]$$

Here [I] is the concentration of the most abundant ion in the solution on side 2 ($[I]_2$) or on side 1 ($[I]_1$) of the membrane. The Nernst equation describes the diffusion potential generated by the salt-jump technique when the potassium concentration is

high relative to that of other ions in solution. This relation is relevant to our experimental conditions as described below.

Salt-jump measurements:

The diffusion potentials in our experiments are applied through a rapid mixing technique, the salt-jump technique.[19] The chromatophore solution is allowed to come to room temperature and is dark-adapted for at least half an hour before measurements begin. During the measurement, the chromatophore solution is continuously mixed with a buffer containing 5 mM $MgCl_2$, 5 mM HEPES (pH 7.5), and adjustable concentrations of sucrose and potassium chloride (buffer B). In the presence of the potassium-specific ionophore valinomycin the potassium membrane permeability is higher than chloride permeability by several orders of magnitude.[20] In all cases the concentrations are altered in a complementary way, such that the osmotic concentration of the buffer remains constant. Molal sucrose concentrations are determined by the relation:

$$[\text{sucrose}] = 1\ m - 2 \times [\text{KCl}].$$

The chromatophore solution is equilibrated with a solution containing 100 mM KCl, which defines the internal potassium concentration. Equilibration with 100 mM KCl means that the potassium and chloride concentrations are large compared to those of other ions in solution. Under these conditions, the potential difference across the chromatophore membrane is described well by the Nernst relation for potassium concentrations inside and outside the vesicle (see carotenoid electrochromism in Chapter Three).

During the course of a measurement, buffer B is rapidly and continuously mixed with the chromatophore solution by means of two synchronously driven peristaltic pump heads (Cole and Parmer Masterflex Drive 7520-25). The solutions are

mixed through a house-made maze connector and flowed through a tube of 12 cm length, which facilitates complete mixing. See Figure 2.1 for a schematic of the experimental layout.

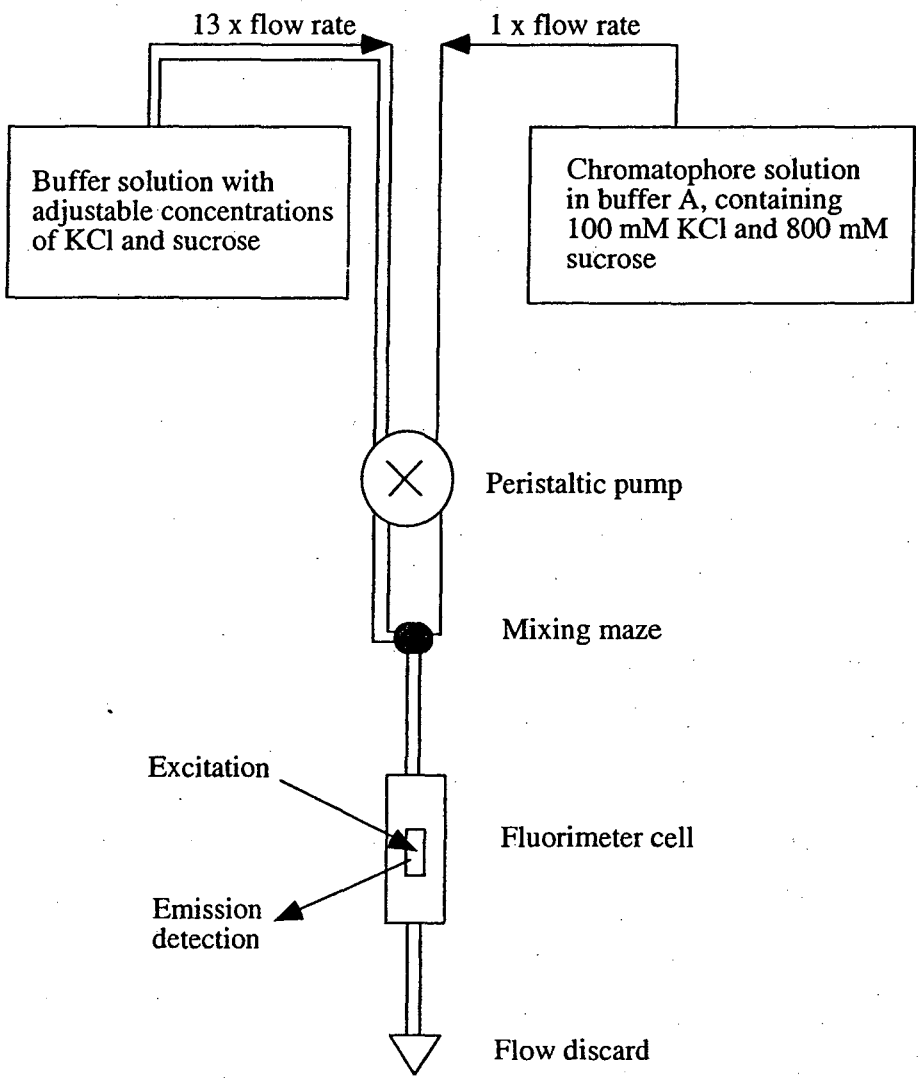

Figure 2.1: Experimental schematic for the salt-jump experments.

Unless otherwise noted, for all fluorescence measurements the ratio of the flow rate of buffer B to the flow rate of chromatophore solution is 13:1. This flow ratio results in a minimum possible external potassium concentration of 7.1 mM, because the internal potassium concentration of the chromatophore solution is 100 mM. The chromatophore absorption after mixing is approximately $A_{800} = 0.08$. An increase in external potassium concentration after mixing with a buffer B containing a higher potassium concentration than the chromatophore solution ([KCl in buffer B greater than 100 mM) is defined as positive applied potential (positive at the internal periplasmic side of the chromatophore vesicle). Negative applied potentials are achieved by dilution of the chromatophore solution into buffer B with lower potassium concentration ([KCl] less than 100 mM).

For carotenoid electrochromism measurements made on the Aminco spectrophotometer, the ratio of the flow rate of buffer B to the flow rate of chromatophore solution is 1:1. The 1:1 flow ratio results in a minimum possible external potassium concentration of 50 mM, because the internal potassium concentration of the chromatophore solution is 100 mM. For the absorption measurements, the chromatophore absorption after mixing is approximately $A_{800} = 0.5$. A relatively high concentration of the chromatophore solution after mixing is necessary to obtain good signal to noise in the measurement of the carotenoid electrochromism.

Optical measurements are made approximately 350 ms after mixing of the chromatophore solution and buffer B. Measurements are made in a flow cell 11 mm long and 1.5 by 1.5 mm cross section (Hellma QS flow-through cell).

In the case of measurements made with preillumination, the path from the mixing junction to the point of measurement is 45 cm, and measurement occurs about 1.3 s after mixing. The mixed solution flows through a secondary optical flow cell

prior to measurement and is illuminated with tungsten lamp light passed through a water filter and an 800 nm interference filter (FWHM = 11 nm). The duration of illumination is approximately 0.9 s. The preillumination is made in a secondary flow cell because actinic illumination inside the fluorimeter sample chamber results in light scattering artifacts; these light scattering artifacts could not be completely eliminated with bandpass filters and baffles inside the fluorimeter sample chamber.

Where specified, 10 mM sodium dithionite ($Na_2S_2O_4$, Sigma) is used to reduce the membrane-bound primary quinone Q_A in the reaction center.[21] Because sodium dithionite is slowly consumed in a reaction with oxygen in solution, experiments are performed within 30 minutes of addition of a fresh solution of sodium dithionite. The concentration of the reduced form of sodium dithionite can be monitored with UV absorption spectroscopy at 320 nm. There is a decrease of less than 50% in the 320 nm band within a 30 min. period under our experimental conditions. Purging the chromatophore solution with dry nitrogen during the course of experiments in the presence of dithionite showed no change in the experimental results, compared with results obtained without nitrogen purging.

Instrumentation:

Fluorescence measurements are made with a Spex Fluorolog 1680 double monochromator fluorimeter (SPEX Industries, Edison, NJ). Fluorescence detection is at right angles to the excitation beam. Excitation is provided by a 400 W Xenon arc lamp (FWHM = 8 nm). Emission slits are set to a maximum of 8 nm FWHM. The fluorescence emission passes through a Kodak Wratten red wavelength cutoff filter #26 (Eastman Kodak Co., Rochester NY) prior to detection. This filter exhibits negligible fluorescence. Detection is by single-photon counting with a near-infrared extended Hamamatsu R3310-02 photomultiplier tube (Hamamatsu Industries, Japan).

The photomultiplier tube is operated in a Products For Research TSA/RF temperature-controlled ceramic socket at -30° C (Products For Research, Illinois). The spectral response of the photomultiplier tube was calibrated, together with the optical emission path of the fluorimeter, using a standard lamp (Optronic Laboratories Inc., model 245 C). The correction function generated from the standard lamp calibration is applied to each fluorescence spectrum. A Spex DM 102 output discriminator is adjusted to maximize signal to noise, resulting in dark counts of about 70 counts per second. Excitation spectra are corrected for lamp intensity with a photodiode reference cell. Fluorescence measurements are made on samples in a Hellma QS flow-through cell of cross section 1.5 mm^2 unless noted otherwise. Fluorescence spectra are taken at an interval of one nm and each data point is averaged one second unless otherwise noted.

Absorption measurements are made on one of two instruments. The electrochromism measurements require high sensitivity to small changes in absorption. Therefore electrochromism measurements are made with an Aminco UV-vis spectrophotometer in the dual-wavelength mode. In dual-wavelength mode, the spectrophotometer excitation beam is split by a chopper and alternates rapidly between two wavelengths, the sample wavelength and the reference wavelength. The excitation beam passes through the same physical spot of the sample in both wavelength modes. This configuration allows sensitive detection of an absorption change at one wavelength relative to another. For carotenoid electrochromism of wild-type *Rb. sphaeroides*, the sample wavelength is set at 521 nm and the reference wavelength is 508 nm. These wavelengths correspond to a maximum and a minimum in the electrochromism difference spectrum. The excitation slits are set at 2.0 nm (FWHM = 2.0 nm). A photomultiplier tube (#9558QB, Thorn EMI, Rockaway NJ) is used for signal detection. The Hellma QS flow-through cell is used in the sample chamber for these measurements.

When actinic illumination is used, the actinic excitation is provided by a tungsten lamp. The light is passed through an interference filter with maximum transmission at 800 nm and FWHM = 20 nm. The filtered light is piped into the sample chamber of the Aminco spectrophotometer with a fiber optic cable.

The second instrument used for absorption measurements is an AVIV UV-vis-IR spectrophotometer model 14-DS (Aviv, Lakewood, NJ), with a fixed bandpass of 0.25 nm. This instrument is used for absorption spectra over a range of wavelengths. The sample cell used is a polystyrene cell of cross-section 1 cm^2 unless otherwise noted. A baseline correction is taken with the same cell containing only buffer solution; this baseline correction is subtracted from each absorption spectrum. Spectra are taken at an interval of one nm and each data point is averaged for 0.2 seconds unless noted otherwise.

References for Chapter Two

[1]Buggy, J.J., Sganga, M.W. & Bauer, C.E. (1994) *J. Bacteriol.* 176: 6936-6943.

[2]Shimada, H., Iba, K., & Takamiya, K.-I. (1992) *Plant Cell Physiol.* 33: 471-475.

[3]Golecki, J.R. Schumacher, A. & Drews, G. (1980) *Eur. J. Cell Biol.* 23: 1-5.

[4]Baltscheffsky, H. & von Stedingk, L.-V. (1966) in *Currents in Photosynthesis.* (Thomas, J.B. & Goedheer, J.C., eds.), pp. 253-261, Ad. Donker, Rotterdam.

[5]Drews, G. & Golecki, J.R. (1995) in *Anoxygenic Photosynthetic Bacteria* (Blankenship, R.E, Madigan, M.T. & Bauer, C.E., eds.), pp. 231-257, Kluwer Academic Publishers, Boston, MA.

[6]Kiley, P.J. & Kaplan, S. (1988) *Microbiology Reviews* 52: 50-69.

[7]Tai, S. & Kaplan, S. (1985) *J. Bacteriol.* 164: 181-186.

[8]Vermeglio, A., Joliot, P. & Joliot, A. (1995) in *Anoxygenic Photosynthetic Bacteria* (Blankenship, R.E, Madigan, M.T. & Bauer, C.E., eds.), pp. 279-295, Kluwer Academic Publishers, Boston, MA.

[9]McEwan, A.G. (1994) *Antonie van Leeuwenhoek International Journal of General and Molecular Microbiology* 66: 151-164.

[10]Yoshida, Y., Takai, M., Satoh, T. & Takami, S. (1991) *Journal of Bacteriology* 173: 3277-3281.

[11]Zannoni, D. & Marrs, B.L. (1981) *Biochim.Biophys.Acta* 637: 96-106.

[12]Williams, J.C. & Woodbury, N., private communication.

[13]McEwan, A.G., Jackson, J.B. & Ferguson S.J. (1984) *Arch. Microbiol.* 137: 344-349.

[14]Yen, H. & Marrs, B.L. (1977) *Arch. Biochem. Biophys.* 181: 411-418.

[15]Neiderman, R. & Gibson, K. (1978) in *The Photosynthetic Bacteria.* (Clayton, R.K. & Sistrom, W.R., eds.) pp. 79-118, Plenum Press, New York.

[16]Clayton, R.K. (1963) in *Symposium on Bacterial Photosynthesis* (Gest, H., San Peitro, A. & Vernon, L.P., eds.) pp. 498-508, Antioch Press, Ohio.

[17]Goodwin, M.G. & Jackson, J.B. (1993) *Biochim. Biophys. Acta* 1144: 191-198.

[18]Heinz, E. (1981) *Electrical Potentials in Biological Membrane Transport.* Springer-Verlag, New York.

[19]Dau, H. & Sauer, K. (1991) *Biochim. Biophys. Acta* 1098: 49-60.

[20]Stryer, L. (1988) *Biochemistry.* W.H. Freeman, New York.

[21]Godik, V.I. & Borisov, A.Y. (1980) *Biochim. Biophys. Acta* 590: 182-193.

Chapter Three:

Characterization of *Rb. sphaeroides*

Introduction:

The careful and thorough characterization of the *Rb. sphaeroides* chromatophores used in this study is particularly important for meaningful interpretation of the experimental results of the electric-field experiments. It is important to characterize the ionic integrity, or the degree of seal of these chromatophore membrane vesicles. Ionic integrity is defined as a lack of ionic permeability across the chromatophore vesicle on a timescale of several seconds. This is important for the generation and measurement of the extent of an electric field caused by potassium diffusion potentials (see Chapter Two). Additionally, the characterization of the orientation of the chromatophore preparation is important because the interpretation of the results of the electric-field experiments described in Chapter Four depends on the orientation of the chromatophore membrane relative to the direction of the applied electric field. It is therefore crucial to establish the orientation of the chromatophore membranes.

Furthermore, we wish in this chapter to introduce the spectral properties of *Rb. sphaeroides*. We will begin this chapter on characterization by defining the steady-state absorption and fluorescence characteristics of the *Rb. sphaeroides* chromatophore preparation, because it is a complex and heterogeneous system.

Spectral characterization:

The absorption spectrum of the wild-type *Rb. sphaeroides* chromatophore solution is shown in Figure 3.1. This is the final preparation as used in all experiments unless noted otherwise. The buffer is 100 mM KCl, 800 mM sucrose, 5 mM HEPES and 5 mM $MgCl_2$ with a pH of 7.5 (buffer A). The shortest wavelength band shown,

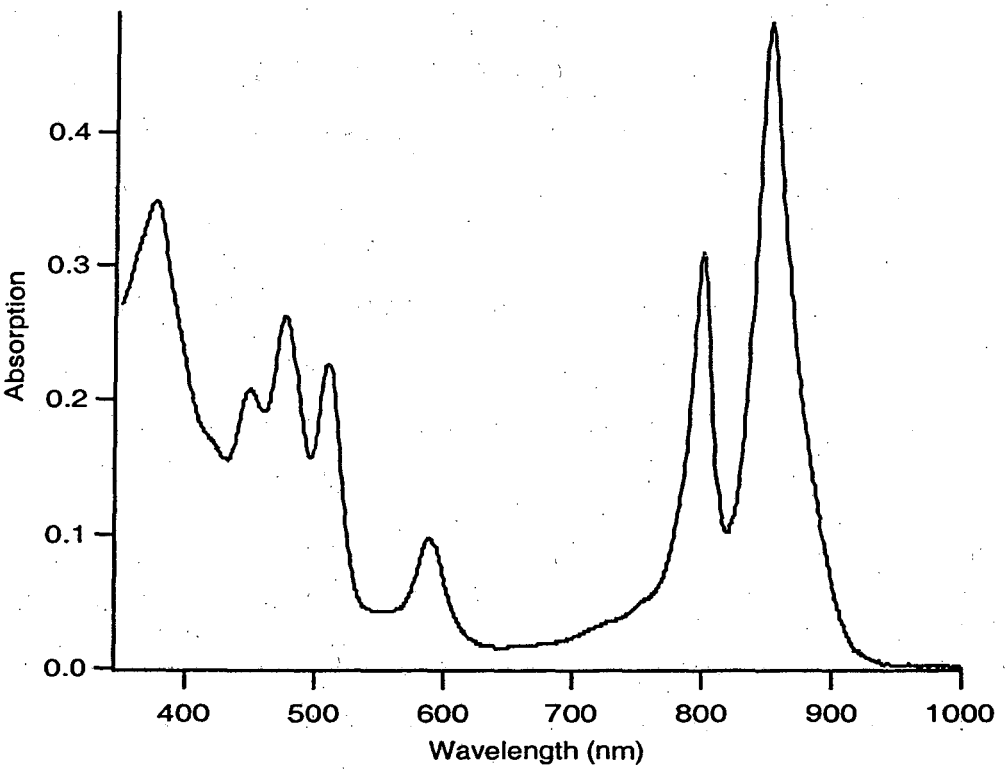

Figure 3.1: Absorption spectrum of wild type *Rb. sphaeroides* chromatophore preparation. Spectrum taken at room temperature in buffer A approximately five hours after chromatophore preparation.

at 375 nm, is the overlapping Bx and By transitions of the bacteriochlorophyll a (BChl) Soret band. There is a shoulder at 422 nm, corresponding to cytochrome c absorption. The next trio of absorption bands, at 450, 478, and 510 nm, are the carotenoid

absorption bands. In wild-type *Rb. sphaeroides*, the two most prevalent carotenoids are sphaeroidene and sphaeroidenone.[1] The absorption bands of these carotenoids will be discussed in more detail later in this chapter, in the section on carotenoid electrochromism.

The band at 590 nm is the Qx transition of BChl. At 800 nm and 850 nm are the two bands from the Qy transition of BChl in the LH2 antenna. A shoulder at 875 nm is the BChl Qy transition of the LH1 antenna. The absorption ratio $A_{875} : A_{850}$ depends on the ratio of LH1 : LH2 in the specific *Rb. sphaeroides* culture. This ratio varies depending on growth conditions and age of the culture. The reaction center absorption bands occur at 760, 800, and 865 nm. The absorption bands of the reaction center are mostly obscured by the more intense transitions of LH2. The chromatophore preparation is spectroscopically similar in the visible and near-IR region to the absorption of whole cell *Rb. sphaeroides*; the same chromophores are present in the intracytoplasmic membranes that are present in the whole cells of *Rb. sphaeroides.*

Fluorescence measurements are made with excitation into one of the BChl or carotenoid absorption bands. Excitation is at 800 nm unless stated otherwise, corresponding primarily to absorption in LH2. There is also some absorption into a reaction center absorption band and into LH1 at this wavelength.

Regardless of which absorption band is excited, the majority of the fluorescence emission of *Rb. sphaeroides* whole cells or chromatophores occurs in the near infrared region between 830 and 960 nm (Figure 3.2). Fluorescence occurs in this spectral region because energy is efficiently transferred from all absorbing chromophores to the long-wavelength spectral forms of BChl.[2] The majority of the fluorescence emission arises from LH1, which has a maximum emission at 890 nm. Some fluorescence also arises from LH2, which is maximum at 860 nm and appears as a shoulder in the emission spectrum.

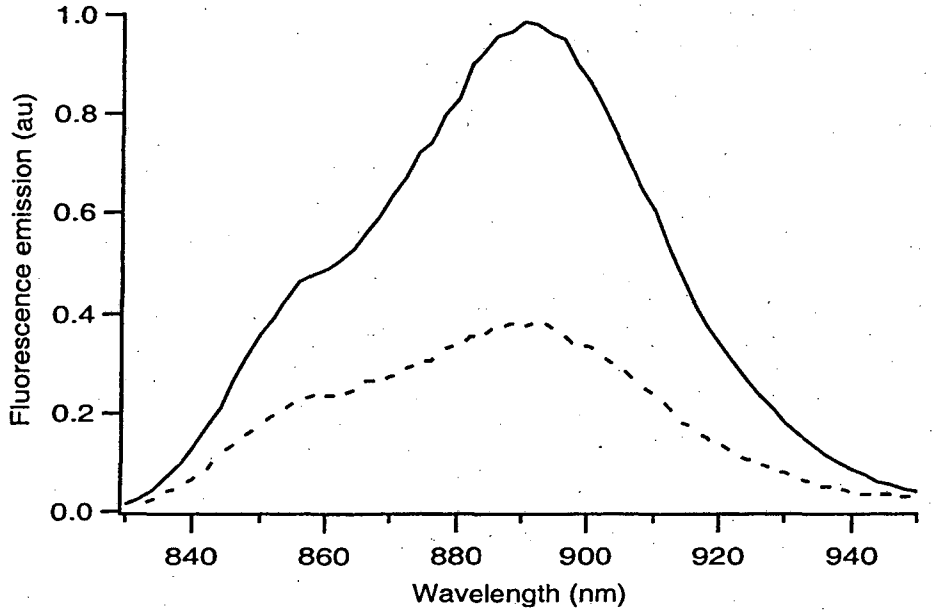

Figure 3.2: Fluorescence emission of *Rb. sphaeroides* chromatophores in the Fo state (dotted line) and the Fm state (solid line). Fluorescence emission from LH1 is maximum at 890 nm. Fluorescence emission from LH2 is visible as a shoulder maximum at 860 nm. Spectra taken at room temperature in buffer A.

Variable fluorescence:

Very little fluorescence arises from the reaction center. Instead, the reaction center uses excitation for charge separation if it is in the "open" or Fo state. In the Fo state, the special pair (P) is reduced and the bacteriopheophytin (H) is oxidized, so that primary charge separation can occur forming the state P^+BH^-. The efficiency of *Rb. sphaeroides* primary charge separation in the Fo state of the reaction center is very high, with a quantum yield of charge separation nearly 100%.[3] In the Fo state, the fluorescence from the detergent-isolated reaction center at room temperature is only 3×10^{-4}, or a 0.03% fluorescence quantum yield.[4,5]

In the "closed" or Fm reaction center state of *Rb. sphaeroides* chromatophores, the special pair is oxidized (P^+).[6] Under conditions of continuous illumination, the oxidized state of the special pair accumulates in *Rb. sphaeorides* chromatophores and the reaction center is closed. Soluble cytochrome c is responsible for the re-reduction of the oxidized special pair. The process of chromatophore preparation eliminates some of the soluble cytochrome c present in the whole cell. In the Fm state, primary charge separation cannot occur. However, the fluorescence from the detergent-isolated reaction center in the Fm state increases only about three times, to 10^{-3}, or a 0.1% fluorescence quantum yield.[4] The majority of the excitation in the Fm state reaction center is lost through non-radiative pathways. In the *Rb. sphaeroides* chromatophore vesicle, containing LH1 and LH2 in addition to the reaction center, the total fluorescence quantum yield in the Fm state is approximately 5%.[6]

The oxidation state of the reaction center (Fo or Fm) also affects the fluorescence yield of the antenna pigments[7], both LH1 and LH2 (Figure 3.2). For the *Rb. sphaeroides* chromatophore vesicle, which contains LH1 and LH2 in addition to the reaction center, the total fluorescence quantum yield in the Fo state is approximately 2%, and increases to approximately 5% in the Fm state.[8] The fluorescence emission intensity at 890 nm typically increases by a factor of about 2.7 in the Fm state compared to the Fo state. For example, if the fluorescence of *Rb. sphaeroides* chromatophores at 890 nm is 1.0 in the Fo state, it increases to 2.7 in the Fm state. The fluorescence at 890 nm arises mainly from LH1. The fluorescence from LH2 also increases in the Fm state relative to the Fo state, although to a lesser extent than the increase in the fluorescence of LH1. For example, if the fluorescence at 860 nm is 1.0 in the Fo state, it increases to approximately 2.0 in the Fm state (Figure 3.2) The variable fluorescence (Fvar) is defined as the difference between Fm and Fo; Fvar =

Fm - Fo. Because the LH1 fluorescence increases more than the LH2 fluorescence in the Fm state, the variable fluorescence has a maximum at 890 nm (Figure 3.3).

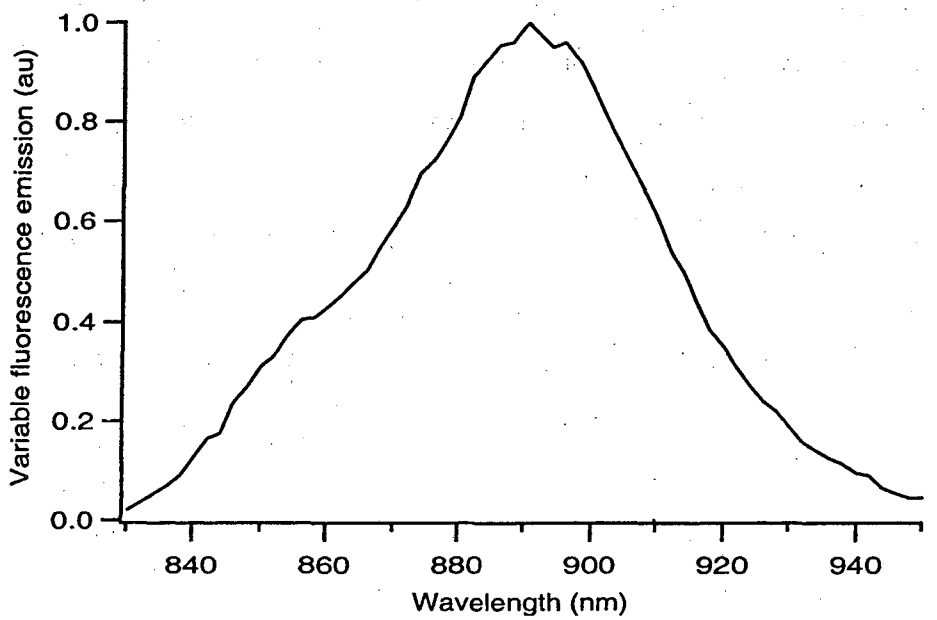

Figure 3.3: Variable fluorescence emission (Fm - Fo) of *Rb. sphaeroides*. Emission maxiumum of the variable fluorescence is at 890 nm. Spectra taken at room temperature in buffer A.

The extent of the variable fluorescence is taken as an indicator of the viability of the photosynthetic apparatus in our preparations of *Rb. sphaeroides* chromatophores. Reaction centers which are not functioning correctly do not produce variable fluorescence. Any preparations which have a low variable fluorescence (less than double the fluorescence in the Fm state than the Fo state at 890 nm) are not used in the salt-jump experiments.

One way to monitor changes in the rate of charge separation in the reaction center is to examine processes which directly compete with charge separation for excitation. Because the antenna fluorescence is sensitive to the state of the reaction center oxidation, the antenna fluorescence emission is a good candidate for reflecting charge separation processes in the reaction center.

Excitation equilibration:

The ratio of LH2 to LH1 fluorescence emission is indicated by the ratio of fluorescence at 860 nm compared to 890 nm; $F_{860} : F_{890}$. This ratio depends on four major factors. First, the $F_{860} : F_{890}$ ratio depends on the individual *Rb. sphaeroides* sample. That is because the ratio of the LH2 to LH1 is itself variable in *Rb. sphaeroides*, depending on specific growth conditions.[1] Second, the $F_{860} : F_{890}$ ratio depends on the state of the reaction center, Fo or Fm, as described in the section on variable fluorescence. Third, the $F_{860} : F_{890}$ ratio also depends on the efficiency of excitation transfer between LH1 and LH2.

When the previous three factors are constant, within the same sample and under the same experimental conditions, there is a fourth factor that influences the ratio of fluorescence at 860 nm compared to 890 nm. The fluorescence ratio $F_{860} : F_{890}$ depends on the illumination wavelength used to excite the fluorescence (Figure 3.4). For example, excitation at 800 nm, into one of the LH2 absorption bands, results in a higher fluorescence ratio $F_{860} : F_{890}$ than excitation into another absorption band, such as the Soret absorption band at 377 nm, the Qx band at 590 nm, or the carotenoid absorption band at 515 nm (Figure 3.4). The fluorescence spectra in Figure 3.4 are normalized at 890 nm. Excitation at 800 nm also results in a slight blue-shifting of the fluorescence emission compared to excitation at other wavelengths such as 515 nm. This variability in the fluorescence ratio as a function of excitation

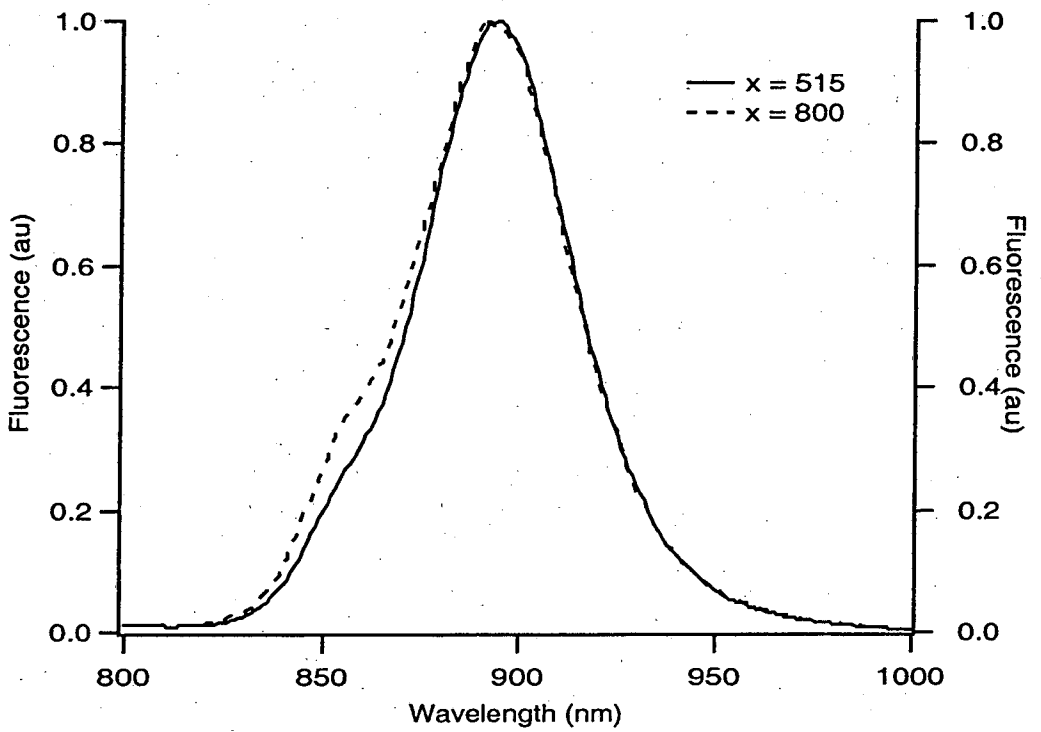

Figure 3.4: Normalized fluorescence emission from *Rb. sphaeroides* chromatophrores as a function of excitation wavelength. Solid line, excitation at 515 nm. Dotted line, excitation at 800 nm. Excitation at 800 nm (into an absorption band of LH2) results in higher relative emission at 860 nm (the maximum emission wavelength of LH2) than does excitation at 515 nm (into an absorption band of the carotenoids). Spectra are taken at room temperature in buffer A.

wavelength indicates that the fluorescing species in *Rb. sphaeroides* are not completely equilibrated before fluorescence emission occurs (see also Chapter Five).

The dependence of the fluorescence spectrum on the excitation wavelength demonstrates a lack of excitation equilibration between LH2 and LH1. This lack of excitation equilibration is surprising, considering that very rapid excitation transfer from LH2 to LH1 is observed using time-resolved spectroscopic techniques.[9] Excitation transfer from LH2 to LH1 in membranes of *Rb. sphaeroides* at room

temperature proceeds with two time constants, 4.6 ± 0.3 ps and 26.3 ± 1.0 ps.[10] The first time constant is interpreted as the excitation transfer from LH2 to LH1, and the slower time constant is interpreted as excitation migration within LH2 preceding transfer to LH1. These rates for excitation transfer from LH2 to LH1 are rapid on the timescale of other excitation transfer and loss processes in the chromatophore membrane. The fluorescence emission lifetime in *Rb. sphaeroides* chromatophores in the Fo state is approximately 60 ps, and in the Fm state the fluorescence lifetime increases to approximately 200 ps.[11] Trapping of excitation by the reaction center is estimated to occur in chromatophores at room temperature with a time constant of approximately 35-40 ps.[12] Excitation transfer from LH2 and LH1 is therefore rapid on the timescales of fluorescence emission and excitation trapping in *Rb. sphaeroides* chromatophores.

One possible explanation for the dependence of the fluorescence emission on excitation wavelength is that a portion of excitation in LH2 has a much slower equilibration time with LH1 than that which is observed in the time-resolved experiments. It may be that some LH2 is at a large distance from LH1, which results in a longer equilibration time, on the order of the fluorescence lifetime. Or possibly there is some portion of LH2 which is entirely uncoupled from LH1 and excitation equilibration does not occur between that portion of LH2 and LH1. In either case, excitation into an absorption band of LH2 would result in an increase in fluorescence emission from LH2 relative to LH1.

Carotenoid electrochromism:

The carotenoids in *Rb. sphaeroides*, sphaeroidene and sphaeroidenone, are long-chain poly-unsaturated hydrocarbons. The ratio of sphaeroidene to sphaeroidenone depends on the growth conditions of the culture. When grown

anaerobically and under low light conditions, as our cultures are, wild-type *Rb. sphaeroides* has approximately 90% sphaeroidene and 10% sphaeroidenone.[13] Both types of carotenoids can exhibit electrochromism, which is a shifting of the absorption bands in response to the presence of an electric field in the vicinity. The electrochromic bandshift of the carotenoid bands has a first-derivative lineshape.[14] Because sphaeroidenone has a very broad absorption band from 470 nm to 570 nm, the sphaeroidenone electrochromism is very difficult to observe.[15] Sphaeroidene, on the other hand, has three sharp absorption bands and the electrochromic shift is more easily detectable.

Electrochromism is a manifestation of the Stark effect. In the Stark effect, the presence of an electric field changes the energy levels of the ground and excited states of an atomic or molecular transition. Because the ground and excited states typically have different dipole moments, the electric field changes the energies of the ground and excited states to a different extent. The result is a net shifting of the transition energy between the ground and excited states; a shift in the absorption band.[4]

The Stark effect is typically quadratic with the intensity of the electric field. However, the observed electrochromic behavior of carotenoids in *Rb. sphaeroides* and other purple photosynthetic bacteria is linear with applied field strength. This discrepancy has been addressed by the hypothesis of a strong local electric field in the immediate vicinity of the carotenoids. Such a local electric field could be generated by charged amino acids[16] in the binding pocket of the carotenoids, or by interactions between the BChl molecules and the carotenoids.[17] In the presence of a local electric field, applying an additional electric field produces a pseudo-linear electrochromic effect in the absorption of the carotenoids.[4]

The extent of the observed carotenoid electrochromic bandshift depends on the specific species. For *Rb. sphaeroides*, an electrochromic shift is observed in the

absorption of the LH2 sphaeroidene carotenoids, but is not detectable in the LH1 carotenoid pool.[18] This fact lends credence to the hypothesis that the immediate local environment of the carotenoid is crucial to the observed electrochromic shift. The electrochromic shift that is observed in *Rb. sphaeroides* LH2 can be modeled as an absorption shift in a subset population of the carotenoids (33%) which are slightly red-shifted from the majority of the carotenoid absorption.[19]

The electrochromic shift of the carotenoid absorption in *Rb. sphaeroides* has been characterized by experiments with valinomycin and potassium.[14] The linear electrochromic shift in *Rb. sphaeroides* can be calibrated to describe the transmembrane potential difference, using the Nernst equation as described in Chapter Two. The electrochromic shift can be used as an internal voltmeter, to measure the potential difference near the carotenoids inside the chromatophore membrane. The electrochromic shift of the carotenoids has been observed under a variety of conditions which generate an electric field across the chromatophore membrane. These conditions include primary charge separation in the reaction center caused by illumination,[20] as well as valinomycin-induced potassium gradients across the membrane.

We have used carotenoid electrochromism of *Rb. sphaeroides* to characterize our experimental system. We have used actinic illumination, as well as potassium gradients (the salt-jump technique as described in Chapter Two) to generate charge separation in the reaction center. First we will address the results of actinic illumination.

Actinic illumination is provided by a tungsten lamp. The light is filtered through an 800 nm interference filter and introduced into the sample compartment via an optic fiber. The sample is not flowing during the actinic illumination experiments. The carotenoid electrochromism is measured using an Aminco spectrophotometer in dual-wavelength mode. The sample beam is at 521 nm and the reference beam is at

506 nm. These wavelengths correspond to a peak-to-trough difference in the *Rb. sphaeroides* carotenoid electrochromic shift.

Illumination of the sample results in an increase in the percent transmission at the measured wavelength pair, 521 nm versus 506 nm. The direction and magnitude of this absorption change agrees with previously published results for *Rb. sphaeroides*.[21] This confirms that the reaction centers in our chromatophore preparation are active and undergoing charge separation efficiently. Cessation of illumination results in a collapse of the absorption change and a return to baseline absorption.

Next we discuss the results of potassium-induced electrochromism. Briefly, valinomycin is added to the chromatophore solution which is pre-equilibrated with 100 mM potassium chloride buffer (buffer A). Just prior to the measurement the chromatophores are rapidly mixed with a second buffer containing a different potassium chloride concentration (buffer B). This results in a transient potassium gradient across the membrane. The sample is flowing continuously during potassium-induced electrochromism experiments. Measurements are made at the same wavelengths as described for the actinic electrochromism measurements, 521 and 506 nm (Figure 3.5).

The magnitude and direction of the potassium-induced electrochromic effect that we observe agrees well with previously published results[16] for *Rb. sphaeroides* chromatophores. The direction of the potassium-induced electrochromic shift for positive electric fields is the same as the direction of the light-induced electrochromic shift. A positive potential difference causes an increase in the percent transmission at 521 nm relative to 506 nm. Positive potential differences result from an increase in potassium ion (K^+) concentration inside the chromatophore vesicle.

The light-induced electrochromism results from protons (H^+) being transported across the chromatophore membrane. The direction of the light-induced change is the same as the direction of the change for increasing the K^+ ion concentration inside the vesicle, which means that light causes the vesicles to transport the H^+ ion to the inside of the vesicle. This verifies that the *Rb. sphaeroides* chromatophore vesicles as prepared in our hands have the same "inside-out" orientation as reported in the literature.

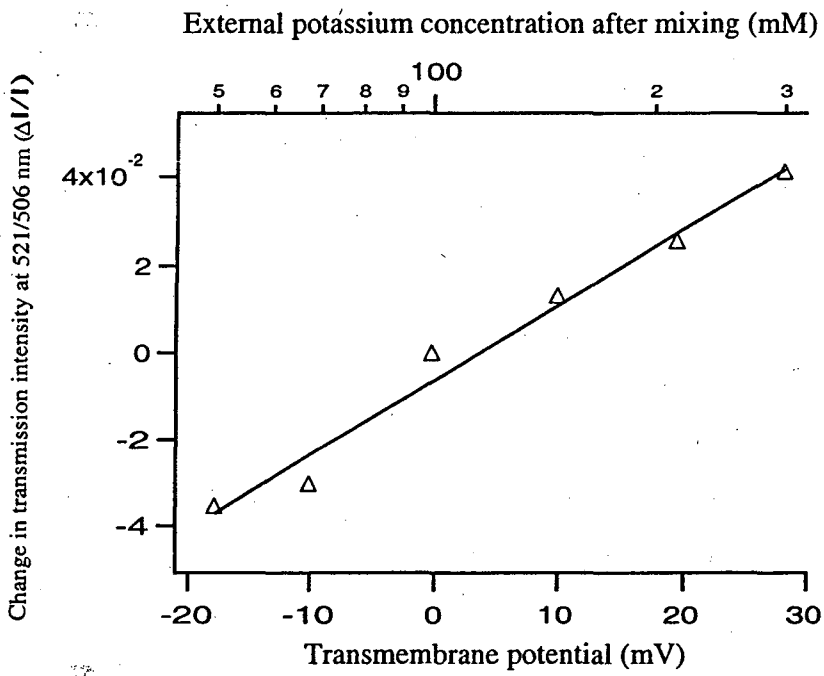

Figure 3.5: The change in the transmission intensity of *Rb. sphaeorides* chromatophores under conditions of mixing with various concentrations of potassium chloride (buffer B) in the presence of valinomycin.
Negative transmembrane potentials correspond to a decrease in the external potassium concentration relative to the internal 100 mM KCl concentration of the chromatophores. Positive transmembrane potentials correspond to an increase of the external potassium concentration relative to the internal 100 mM KCl concentration of the chromatophores. The absorption change is monitored at 521 nm with a reference wavelength of 506 nm, corresponding to a maximum shift in the electrochromism of the carotenoid bands.

The electrochromic shift that we observe under our experimental conditions is linear with the logarithm of the external potassium concentration. The electrochromic shift is linear for both positive and negative applied potentials. The transmembrane potential difference can be calculated from the Nernst relation as discussed in Chapter Two (Figure 3.5, bottom abscissa). This provides a valuable method for calibrating the transmembrane potential that is generated under our experimental conditions.

9-aminoacridine fluorescence quenching:

9-aminoacridine (9AA) is a fluorescent amine which can be used to detect transmembrane pH gradients.[22] The fluorescence emission of 9AA is sensitive to transmembrane pH gradients in a variety of membrane systems. 9AA fluorescence emission responds to pH gradients across chloroplast membranes[23] and phospholipid vesicles,[24] as well as the membranes of purple photosynthetic bacteria.[25] The unprotonated form of 9AA travels freely across these membranes. However, the protonated form aggregates at the surface of the membrane. This aggregation leads to quenching of the fluorescence emission.[26] In the presence of a transmembrane pH difference, the fluorescence of 9AA is strongly quenched.

We have used 9AA fluorescence quenching to confirm that our preparation of *Rb. sphaeroides* chromatophores is composed of sealed vesicles with a high degree of ionic integrity which are capable of proton translocation. We define sealed vesicles as vesicles which have a low permeability to ions. Vesicles which are not sealed cannot sustain a transmembrane pH gradient, therefore will not cause quenching of 9AA fluorescence. It is important to verify that our chromatophores are sealed vesicles for the salt-jump experiments described in Chapter Four.

Figure 3.6 shows the quenching of 9AA fluorescence in our *Rb. sphaeroides* chromatophore preparation. At the arrow, the flow of chromatophore solution is stopped and a pH gradient is formed across the chromatophore membranes from the excitation light illumination. Excitation is at 400 nm and emission is detected at 459 nm, corresponding to absorption and emission maxima of 9AA (not BChl). The fluorescence quenching of 9AA emission under conditions of continuous chromatophore illumination is eliminated under conditions which abolish the transmembrane pH gradient, such as addition of 2 mM FCCP (Figure 3.7).

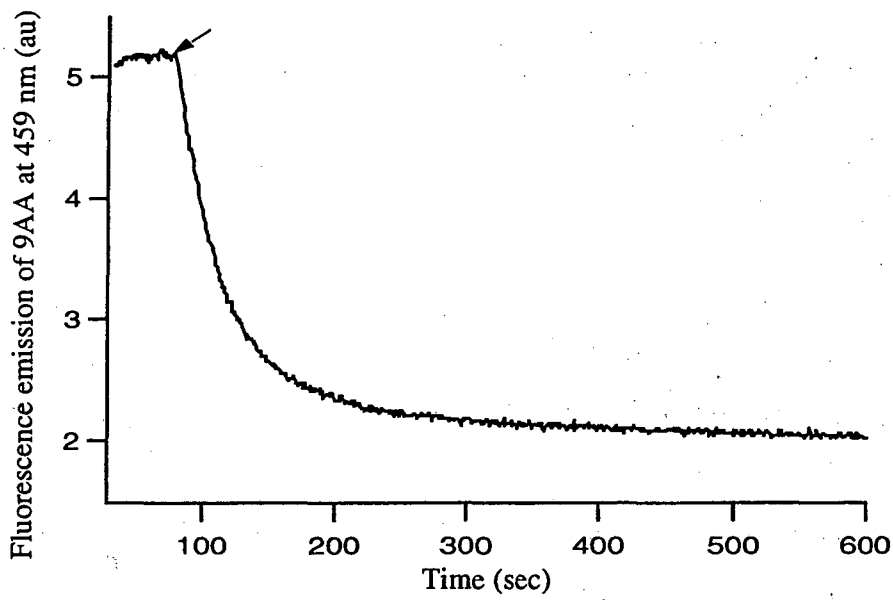

Figure 3.6: Fluorescence emission of 9AA with *Rb. sphaeroides* chromatophores. Excitation at 400 nm, emission detected at 459 nm. At the arrow, the flowing chromatophore solution is stopped and remains in the excitation beam. Quenching of the 9AA fluorescence emission begins as the transmembrane pH gradient forms across the chromatophore membrane under conditions of continuous illumination. See text for details.

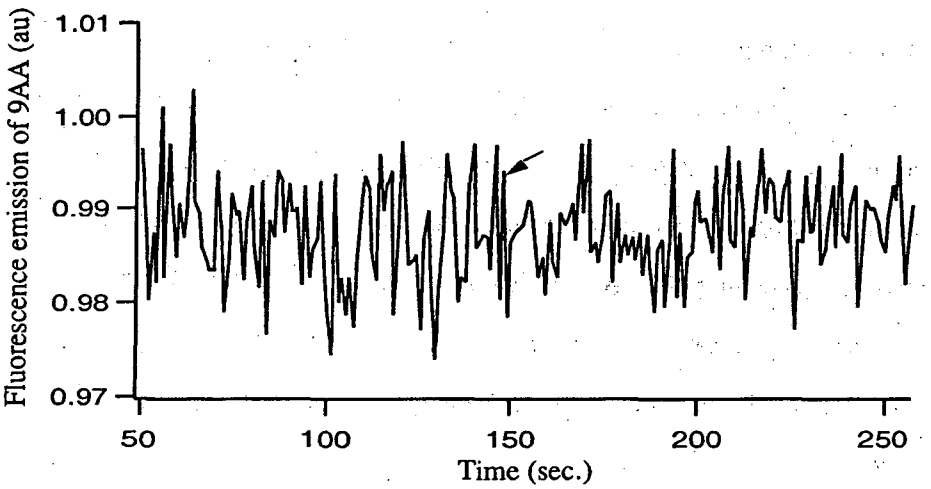

Figure 3.7: Fluorescence emission of 9AA with chromatophores in the presence of 2 mM FCCP, a proton uncoupler. Excitation at 400 nm, emission detected at 459 nm. There is little change in the emission intensity when the chromatophores are exposed to continuous illumination (at arrow).

Conclusions:

In summary, we have characterized our chromatophore preparation of *Rb. sphaeroides*. The steady-state spectral properties have been presented, including absorption, and fluorescence in the Fo and Fm state. The chromatophores have the "inside-out" configuration reported in the literature; this has been determined through the joint use of light- and potassium-induced carotenoid electrochromism. The extent of the electrochromic shift agrees well with the electrochromic shift reported in the literature. The chromatophores are capable of sustaining a transmembrane pH gradient, shown through the quenching of 9AA fluorescence. These experiments confirm that the chromatophores are tightly sealed vesicles with an "inside-out" orientation. This characterization has laid the foundation for an interpretation of the results from the electric-field experiments presented in the next chapter.

References for Chapter Three

[1]Yeliseev, A.A., Eraso, J.M. & Kaplan, S. (1996) *J. Bacteriol.* 178: 5877-5883.

[2]Herek, J.L., Polivka, T., Pullerits, T., Fowler, G.J.S., Hunter, C.N. & Sundstrom, V. (1998) *Biochemistry* 37: 7057-7061.

[3]Woodbury, N.W. & Allen, J.P. (1995) in *Anoxygenic Photosynthetic Bacteria* (Blankenship, R.E., Madigan, M.T. & Bauer, C.E., eds.) pp. 527-557, Kluwer Academic Publishers, Dordrecht, The Netherlands.

[4]Clayton, R.K. (1980) *Photosynthesis: physical mechanisms and chemical patterns*, Cambridge University Press, New York.

[5]Zankel, K. L.; Reed, D.W. & Clayton, R.K. (1968) *Proc. Natl. Acad. Sci USA* 61: 1243-1247.

[6]Godik, V.I. & Borisov, A.Y. (1977) *FEBS Lett.* 82: 355-358.

[7]Sebban, P. & Moya, I. (1983) *Biochim. Biophys. Acta* 722: 436-442.

[8]Wang, R.T. & Clayton, R.K (1971) *Photochemistry and Photobiology* 13: 215-224.

[9]Fleming, G.R. & van Grondelle, R. (1997) *Current Opinion in Structural Biology* 7: 738-748.

[10]Nagarajan V. & Parson W.W. (1997) *Biochemistry* 36(8): 2300-2306.

[11]Borisov, A.Y., Freiberg, A.M., Godik, V.I., Rebane, K.K. & Timpmann, K.E. (1985) *Biochim. Biophys. Acta* 807: 221-229.

[12]Visscher, K.J., Bergström, H., Sundström, V., Hunter, C.N. & van Grondelle, R. (1989) *Photosynth. Res.* 22: 211-217.

[13]Cogdell, R.J., Hipkins, M.F., MacDonald, W. & Truscott, T.G. (1981) *Biochim. Biophys. Acta* 634: 191-202.

[14]Jackson, J.B. & Crofts, A. R. (1969) *FEBS Letters* 4:185-189.

[15]Olivera, L.M. & Niederman, R.A. (1993) *Biochem.* 32: 858-866.

[16]Gottfried, D.S., Steffen, M.A. & Boxer, S.G. (1991) *Biochim. Biophys. Acta* 1059: 76-90.

[17]Krueger, B.P., Scholes, G.D., Jimenez, R. & Fleming, G.R. (1998) *J. Phys. Chem. B* 102: 2284-2292.

[18]Matsuura, K., Ishikawa, T., Nishimura, M. (1980) *Biochim. Biophys. Acta* 590: 339-344.

[19]Goodwin, M.G. & Jackson, J.B. (1993) *Biochim. Biophys. Acta* 1144: 191-198.

[20]De Grooth, B.G. & Amesz, J. (1977) *Biochim. Biophys. Acta* 462: 247-258.

[21]Matsuura, K. & Nishimura, M. (1976) *Biochim. Biophys. Acta* 458: 483-491.

[22]Azzone, G.F., Pietrobon, D. & Zoratti, M. (1984) *Curr. Top. Bioenerg.* 13: 2-77.

[23]Haraux, F. & De Kouchkovsky, Y. (1980) *Biochim. Biophys. Acta* 592: 153-168.

[24]Deamer, D.W., Prince, R.C. & Crofts, A.R. (1972) *Biochim. Biophys. Acta* 274: 323-335.

[25]Casadio, R. & Melandri, B.A. (1985) *Archives of Biochemistry and Biophysics* 238: 219-228.

[26]Grzesiek, S., Otto, H. & Dencher, N.A. (1989) *Biophysical Journal* 55: 1101-1109.

Chapter Four:

Electric-Field Effects in *Rb. sphaeroides* Chromatophores

Introduction:

In this chapter, we describe the use of electric fields to probe excitation dynamics and equilibration within the purple photosynthetic bacteria *Rb. sphaeroides.* We show that the application of external electric fields reveals details about excitation in the antenna complexes and charge separation in the reaction center of *Rb. sphaeroides*, studied through steady-state absorption and fluorescence spectroscopy. Before we present the results of our experiments, the introductory section of this chapter will 1) present the *Rb. sphaeroides* system to be studied, 2) discuss the theoretical work of Bixon and Jortner as applied to the *Rb. sphaeroides* system, and 3) give an overview of previous electric-field experiments on photosynthetic systems.

Rb. sphaeroides is a useful photosynthetic system to study, because it is simpler in many ways than oxygen-evolving plants. Oxygen-evolving plants contain two kinds of photosystems and multiple types of antenna complexes. The wild-type *Rb. sphaeroides* has only a single photosystem, which includes a reaction center and two types of antenna complexes (LH1 and LH2). The simpler photosynthetic system of *Rb. sphaeroides* is a useful model for studying the processes of photosynthesis. Additionally, X-ray crystallography studies have revealed the structure of the *Rb. sphaeroides* reaction center[1] and the structure of the LH2 antenna complex from a closely related photosynthetic bacterium *Rps. acidophila.*[2] The X-ray crystallography data provide information to help clarify excitation processes in *Rb. sphaeroides.*

Furthermore, mutant strains of *Rb. sphaeroides* are available which lack portions of the photosynthetic apparatus. These photosynthetic mutants can provide further information about excitation processes in *Rb. sphaeroides.*

Charge separation in the *Rb. sphaeroides* reaction center:

The two antenna complexes of *Rb. sphaeroides*, LH1 and LH2, absorb photons and transfer excitation to the reaction center in a process called trapping. When excitation reaches the reaction center (RC), a dimer of bacteriochlorophyll a (BChl) called the special pair (P) is excited, creating the state P*BH in the reaction center (excited special pair, P*, and neutral BChl, B, and BPheo, H). Next a dipolar, charge-separated state is generated from this excited state. The first well-defined isolated species in this process is P^+BH^-,[3] which has a hole at the special pair and an electron at the bacteriopheophytin a molecule (H) (Figure 4.1). This event is the primary charge-separation reaction. Subsequent redox reactions stabilize the charge separation across the reaction center which spans the photosynthetic membrane.

The dipolar charge-separated state P^+BH^- in the reaction center is oriented within the *Rb. sphaeroides* cell intracytoplasmic membrane[4] (see Chapter Two). The oxidized molecule, P^+, is adjacent to the periplasmic space. The reduced molecule, H^-, is closer to the cytoplasmic space (Figure 4.1).

As with any charge-separated state, the energy of the dipolar charge-separated state (P^+BH^-) relative to the neutral state (PBH) depends on the electric charges or electric fields in the vicinity. For example, a positive charge near the special pair would energetically oppose the formation of the charge-separated state P^+BH^- (Figure 4.1). In a similar way, an electric field oriented in the same direction as a dipolar state in the reaction center will energetically oppose the formation of the charge-separated state. Conversely, an electric field oriented in the opposite direction to the dipole will stabilize the charge-separated state and lower its energy. Therefore, the energies of the

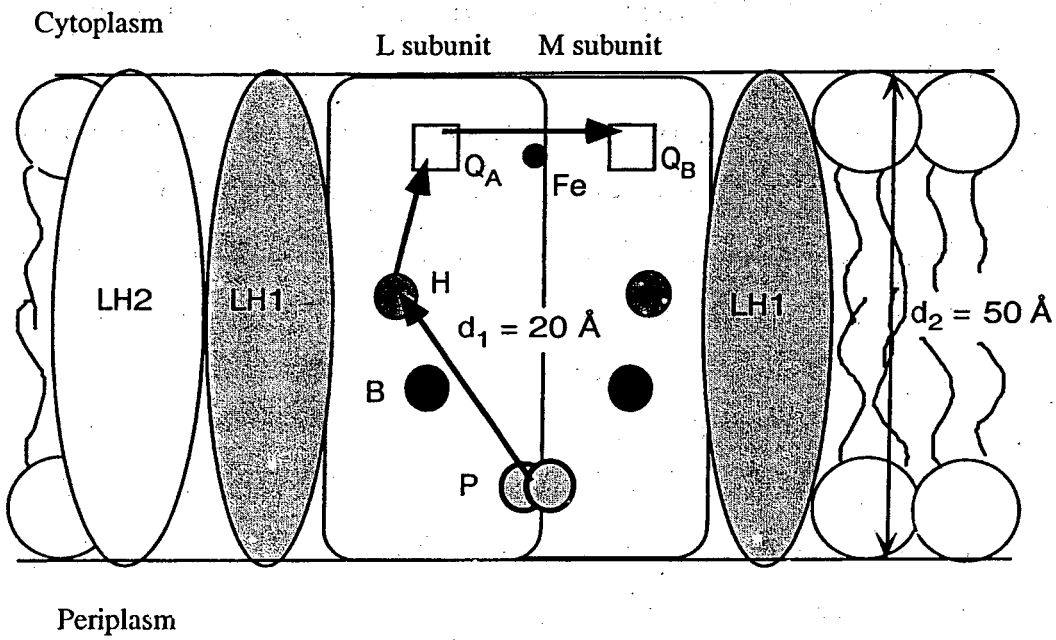

Figure 4.1: Schematic of the reaction center and the antenna complexes in the *Rb. sphaeroides* intracytoplasmic membrane. A possible path of charge separation is shown with arrows. The LH1 ring is shown surrounding the reaction center in cross-section, and the LH2 antenna ring is shown peripheral to LH1. Center-to-center distance between the special pair (P) and the bacteriopheophytin (H) is 20 Å. The membrane is 50 Å wide. The direction of the applied electric field vector is along the pseudo-C_2 symmetry axis of the reaction center, *i.e.*, vertical in this schematic.

charge-separated states in the photosynthetic reaction center will change when an external electric field is applied across the intracytoplasmic membrane. A change in the energy of the charge-separated state may be reflected in the rate of the formation of the charge-separated state. An increase in the energy of the charge-separated state relative to the ground state will decrease the probability of charge separation, and a decrease in the energy of the charge-separated state will increase the probability of charge separation. This model of the effects of an electric field on charge separation in a photosynthetic reaction center is based on the experiments of Dau and Sauer on electric-field effects in spinach thylakoid membranes.[9,18]

Theory of electric-field effects in the photosynthetic reaction center:

Bixon and Jortner have made calculations to predict more exactly what the effect of external electric fields will be on the rate of charge separation in the photosynthetic reaction center.[5] The effect that an external electric field has on the rate of charge separation depends on the specific mechanism of the primary charge separation. The mechanism of the primary charge separation is not known and cannot be determined from the known structure of the reaction center. Several competing theories of the mechanism of primary charge separation have been proposed. By comparison of the theoretical predictions with the experimental results of an external electric field across the photosynthetic reaction center, it may be possible to determine the mechanism of primary charge separation, or at least to eliminate some possible mechanisms of charge separation.

Three different mechanisms of primary charge separation will be addressed in this section, based on the theoretical work of Bixon and Jortner.[5] The theoretical work of Bixon and Jortner is developed from the nonadiabatic electron transfer rate:

$$k = (2\pi / h)V^2F \qquad [4.1a]$$

In equation [4.1a], k is the rate of electron transfer, h is Planck's constant, V is the electronic coupling between the initial and final states, and F is the Franck-Condon nuclear overlap factor. Two main assumptions are applied to the Franck-Condon factor. The first assumption is that the nuclear protein mode can be approximated by one average frequency, $h\omega = 100\ cm^{-1}$. The second assumption is the high-temperature limit, meaning that $hc\omega$ is less than k T. Applying these assumptions, the Franck-Condon factor can be expressed as the Marcus relation[6]:

$$F = (4\pi \lambda kT)^{-1/2} \exp\frac{-Ea}{kT} \qquad [4.1b]$$

In equation [4.1b], λ is the reorganization energy for electron transfer, k is the Boltzmann constant, T is the ambient temperature and Ea is the activation energy for electron transfer.

We will consider three possible mechanisms for primary charge separation in the reaction center; the one-step, the two-step and the superexchange mechanism. The theoretical calculations for these mechanisms take into account the effect of an electric field on the Franck-Condon factor.

The first mechanism of primary charge separation that we will address is the one-step model. In the one-step model the excited special pair P* transfers an electron directly to the bacteriopheophytin H, forming the state P^+BH^-; no intermediate state is involved in the process. The one-step model for bacterial charge separation is considered to be improbable, because the distance from the special pair to the bacteriopheophytin is large (20Å center-to-center distance),[1] and there is a very rapid rate of charge separation (2.8 ps).[3] The analysis of the one-step model is included here for comparison purposes with the electric-field effect on other models of charge separation. Equation [4.2] describes the theoretical dependence of an external electric field on a charge-separation process with a one-step mechanism:

$$\frac{k(E)}{k(0)} = \exp\frac{-\{\Delta\Delta G\}^2}{4\,\Delta G_o\, k\, T} \qquad [4.2]$$

In Equation [4.2] k(E) is the rate of charge separation in the presence of an external electric field, and k(0) is the rate of charge separation with no external electric field. ΔG_o is the change in free energy between P*BH (excited special pair) and P^+BH^- (charge-separated system) without any externally applied field. $\Delta G(E)$ is the change in free energy between P*BH and P^+BH^- in the presence of an external electric field, and $\Delta\Delta G$ [= $\Delta G(E) - \Delta G_o$] is the difference in the free energy change between

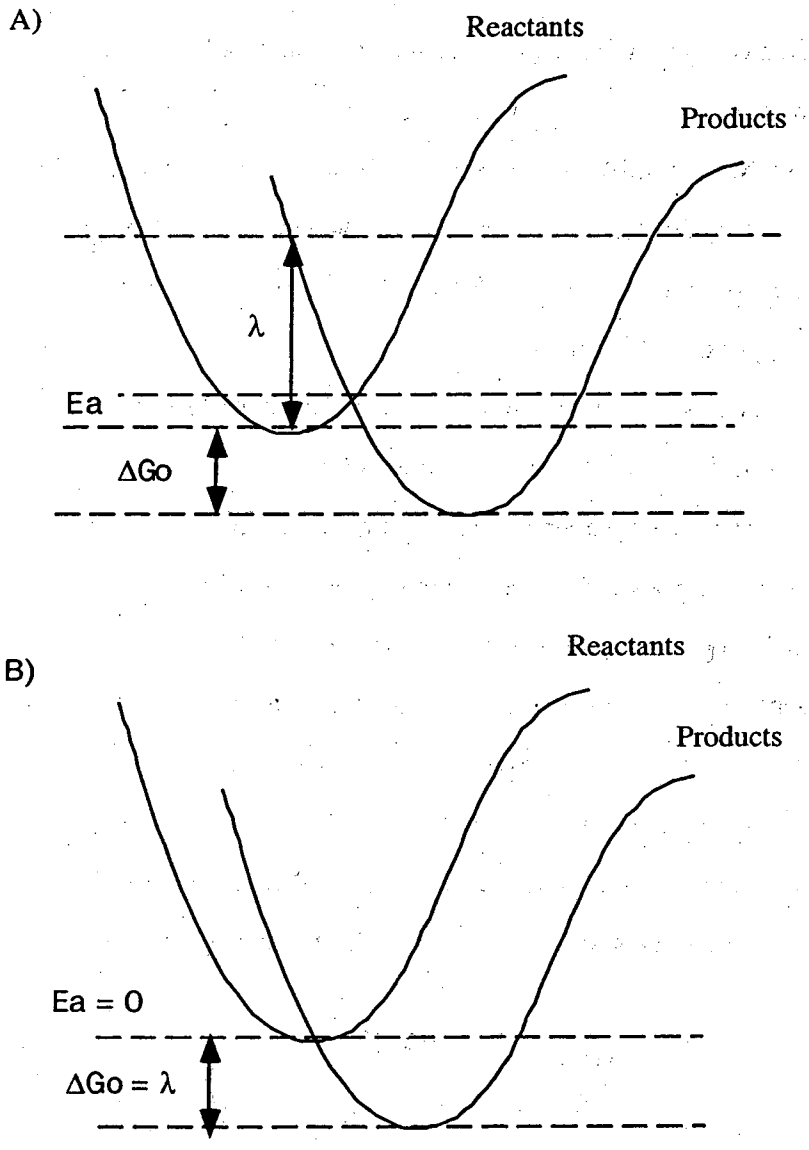

Figure 4.2: Potential energy curves showing the activation energy (Ea), change in free energy (ΔG), and reorganization energy (λ) for processes in the normal Marcus region (A) and the activationless region (B).

the external electric-field condition and the zero-field condition. $\Delta\Delta G$ is assumed to be directly proportional to the magnitude of the applied electric field. T is the temperature at which measurements are taken, and *k* is the Boltzmann constant. One assumption in equation [4.2] is that the process of charge separation is activationless. Bacterial charge separation is often assumed to be activationless because there is a very small temperature dependence of the rate of charge separation.[7] For a process which is not activationless, a decrease in temperature usually results in a slowing of the electron transfer rate because higher energy levels of the initial state are less populated at lower temperature. For an activationless process, the reorganization energy λ equals the change in free energy ΔG_o (Figure 4.2). The lack of temperature dependence is also consistent with charge separation in the inverted Marcus region, which is an intersection of initial and final states on the left side of the initial state curve (see Figure 4.23).[8]

Using this theory developed by Bixon and Jortner, we have estimated the effect that an externally applied electric field will have on the rate of charge separation in the reaction center of *Rb. sphaeroides.* The value of ΔG_o is not directly measurable and must be estimated for the process of *Rb. sphaeroides* charge separation. The value used in our calculations is derived from the rate of charge recombination from the state P^+BH^- to PBH in the detergent-isolated *Rb. sphaeroides* reaction center.[9] From this method, ΔG_o = 250 meV (2,000 cm^{-1}). The predicted results for the one-step mechanism applied to the reaction center of *Rb. sphaeroides* are shown in Figure 4.3 (open circles). The figure shows the ratio of the rate of primary charge separation expected under an applied electric field [k(E)] relative to the zero-field rate [k(0)].

For both positive and negative applied electric fields in *Rb. sphaeroides* the one-step mechanism predicts a decrease in the rate of charge separation k(E) relative to the zero-field condition. This can be understood intuitively because the rate-limiting step is assumed to be activationless (see Figure 4.2). The intersection of the product

potential energy surface is at the minimum of the reactant potential energy surface. Therefore, any shifting of the product potential energy curve by an applied electric field (in either direction) would displace the curve intersection from the minimum and result in an increase in the activation energy. This leads to a decrease in the observed rate of charge separation for both positive and negative applied electric-field directions. The decrease in k(E) is predicted to be symmetric around the zero-field condition, and is quadratic.

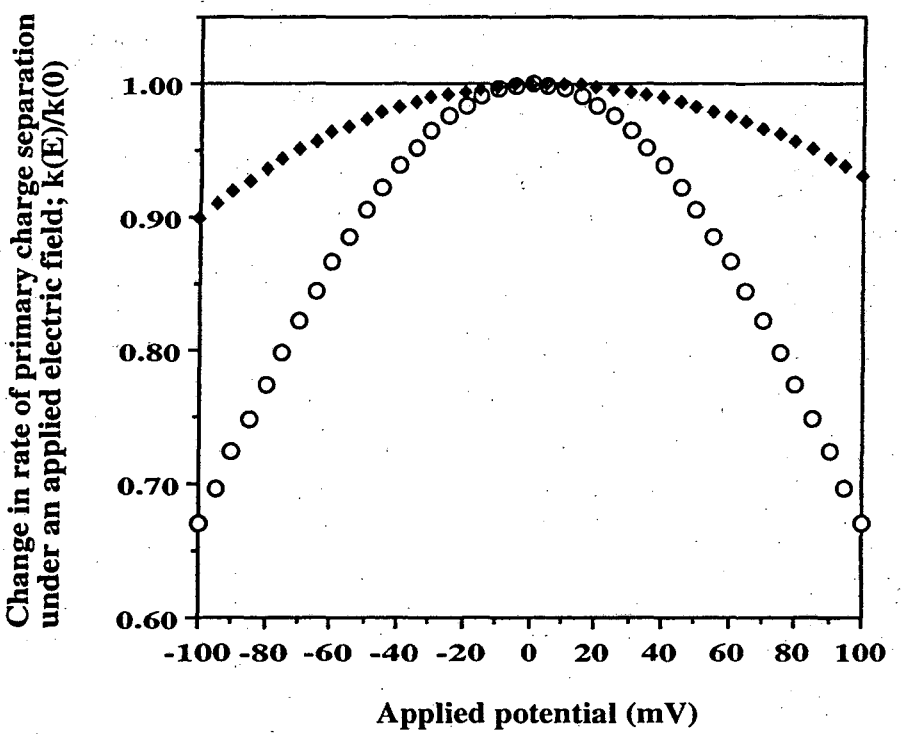

Figure 4.3: Model simulations of the effect of an electric field on the rate of primary charge separation in the *Rb. sphaeroides* reaction center. ΔG_o is taken to be 250 meV. Open circles, the one-step mechanism. Diamonds, the two-step mechanism.

A second possible model of primary charge separation is the two-step model. In the two step model, charge separation occurs first from the excited special pair state,

P*BH, to the monomeric bacteriochlorophyll, P^+B^-H. The two-step model is more realistic than the one-step model, because the monomeric bacteriochlorophyll (B) is a physical intermediate between the special pair (P) and the bacteriopheophytin (H). The initial charge separation to B must be the slow, rate-limiting step of the reaction. It is followed by very rapid charge transfer to the bacteriopheophytin (BPheo), creating the state P^+BH^-. These rate constraints are applied because the intermediate reduced monomeric BChl (B^-) has not been definitively isolated experimentally. Therefore, the reduced BChl (B^-) must be a very short-lived, transient intermediate state. Equation [4.3] has been derived by Bixon and Jortner to describe the effect of an externally applied electric field on the two-step model of charge separation.

$$\frac{k(E)}{k(0)} = \exp\frac{-\left[\frac{da}{da+db}\right]\Delta\Delta G^2}{4\ \Delta G_o\ k\ T} \qquad [4.3]$$

In equation [4.3], da is the distance between the special pair (P) and the monomeric BChl (B) projected along the membrane normal vector, and db is the distance between BChl (B) and BPheo (H) projected along the membrane normal vector. The other symbols are as previously defined.

This approach to the two-step model is oversimplified, because it does not consider the effect of an electric field on the rate of back transfer from P^+BH^- to the ground state PBH, or the electric-field effect on the secondary electron transfer from P^+B^-H to P^+BH^-. More sophisticated models which do account for both these factors yield similar results, provided that electron transfer to the monomeric bacteriochlorophyll (B) is the rate-limiting step.[10]

The distances da and db were calculated from the structure of the *Rb. sphaeroides* reaction center as determined by x-ray crystallography.[1] The result of the two-step simulation for *Rb. sphaeroides* is also shown in Figure 4.3 (diamonds). The

predicted electric-field dependence is qualitatively similar to that of the one-step mechanism; a symmetrical decrease of the charge separation rate for both positive and negative applied fields relative to the zero-field condition. The extent of the electric-field effect [k(E)/k(0)] predicted by the two-step mechanism is less than that predicted for the one-step mechanism at the same applied field intensity (Figure 4.3).

A third possible mechanism for charge separation is the superexchange model. In this model, the monomeric BChl (B) mediates electron transfer between the special pair and BPheo (H). However, B does not itself become reduced; the state P^+B^-H is not formed as a discrete intermediate. Instead, the electronic overlap of the initial (P*BH) and final (P^+BH^-) states is increased by the presence of a virtual state.[11] This virtual state, P^+B^-H, is higher in energy than the initial state P*BH by ∂E (Figure 4.4). The theoretical treatment of the superexchange mechanism takes into account the effect of an electric field on the Franck-Condon factor, as well as the effect of an electric field on the electronic coupling factor V. The effect on the electronic coupling factor V is expressed through the quantity ∂E.

In the superexchange mechanism, the effect of an electric field is considered on both the electronic coupling factor (V, see equation 4.1a) and the Franck-Condon factor. The effect of an external electric field on a superexchange mechanism is described to a first approximation by Bixon and Jortner in Equation [4.4]:

$$\frac{k(E)}{k(0)} = \frac{\delta E}{\left\{\delta E - \left[\frac{da}{da+db}\right]\Delta\Delta G\right\}^2 \exp\frac{-\Delta\Delta G^2}{4\ \Delta G_o\ k\,T}} \qquad [4.4]$$

The energy of the virtual state P^+B^-H relative to the initial state P*BH (∂E) is not known and must be estimated. The quantity ∂E has a large influence on the calculated rate of primary charge separation in the presence of an electric field. Two simulations of the superexchange model are presented for *Rb. sphaeroides* (Figure 4.5).

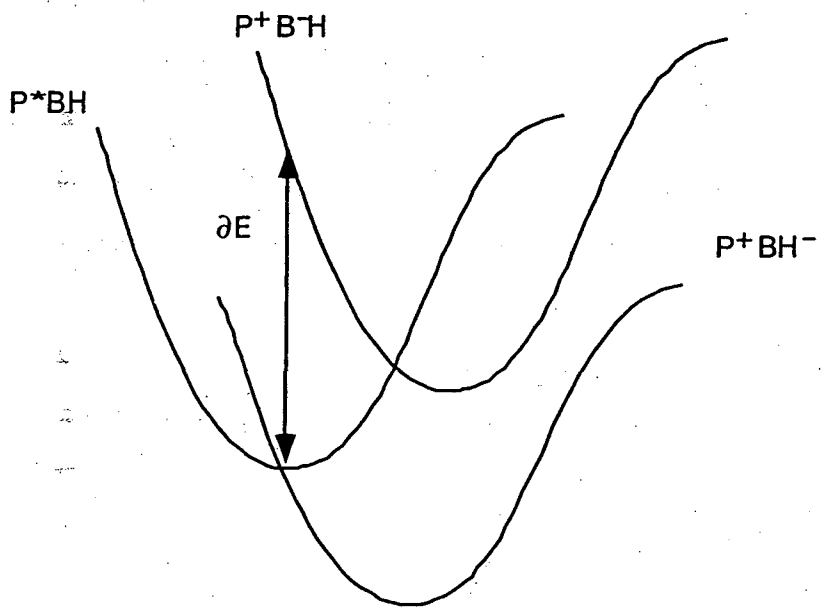

Figure 4.4: Potential energy surfaces of the superexchange model. ∂E is the vertical energy difference between the potential surfaces of P*BH and P^+B^-H at the intersection of the potential surfaces of P*BH and P^+BH^-.

In the first simulation (squares), ∂E = 250 meV (2000 cm^{-1}). The change in the primary charge separation is asymmetric for positive and negative applied fields. For positive applied potential, the electric field results in a decrease of primary charge separation rate, while for negative potential, the electric field results in an increase in the rate of primary charge separation. This is in contrast to the one- and two-step sequential models, which showed a symmetric decrease in the rate of primary charge separation for both positive and negative applied potentials (Figure 4.3).

The change in the rate of primary charge separation, k(E)/k(0), is larger than for both the one- and two-step calculations at a given applied field magnitude. In this superexchange simulation, there is a larger absolute change in k(E)/k(0) at negative applied potentials than at positive applied potentials.

The second simulation has a smaller ∂E; ∂E = 110 meV (887 cm^{-1}). The effect of a smaller ∂E is an increase in the magnitude of the electric-field effect on k(E)/k(0) (Figure 4.5, open circles) compared with a ∂E of 250 meV (squares). The rate of primary charge separation has a nearly linear dependence on the applied field intensity for both positive and negative potentials near the zero field mark; however, both functions are in fact quadratic.

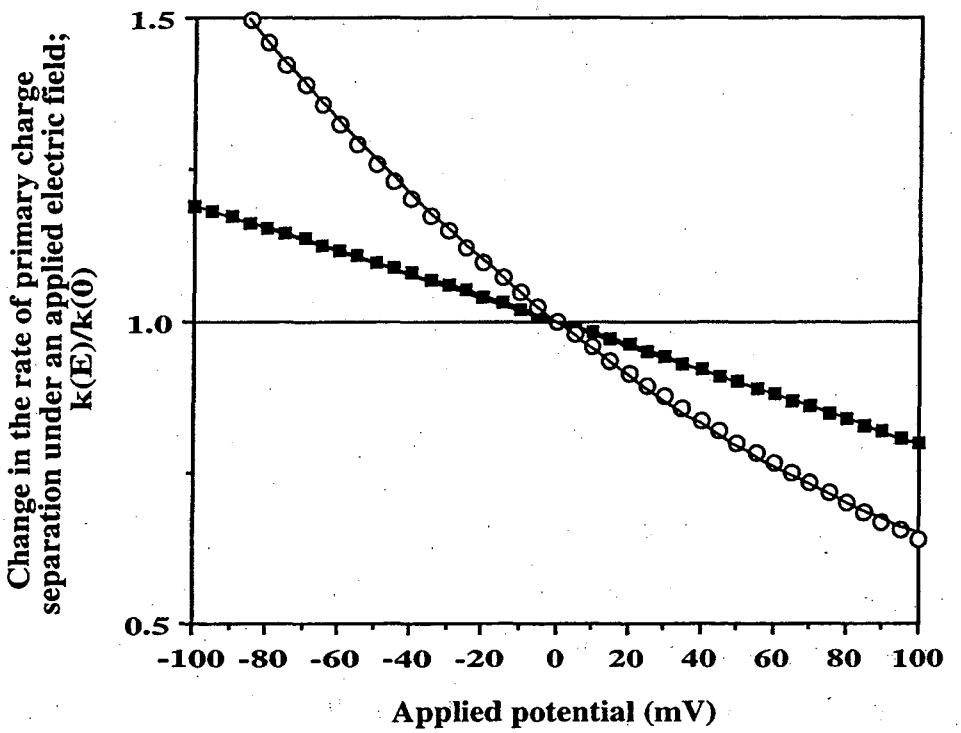

Figure 4.5: Model simulation of the effect of an electric field on charge separation in the *Rb. sphaeroides* reaction center. Both simulations are based on the superexchange mechanism with a ΔG_o of 250 meV. Open circles, ∂E = 110 meV. Squares, ∂E = 250 meV.

Review of previous experiments:

We will next present a brief overview of experiments in the literature which have used electric fields as a probe of photosynthetic systems. Electric fields are a useful tool for studying excitation in photosynthetic systems; however, analysis of the results has not always been straightforward. One source of complication in the analysis is the orientational disorder of the reaction centers and pigments relative to the external electric field in some of the studies.

Lockhart and Boxer have used electric fields to examine both the absorption and the fluorescence Stark effects on isolated *Rb. sphaeroides* reaction centers[12,13] which are orientationally isotropic in PVA matrices at 77 K. The difference spectrum of the absorption Stark effect of the reaction centers resembles the second derivative of the absorption band spectrum, in agreement with a broadening of the absorption band under an isotropic field.

However, the fluorescence of the reaction centers under an applied field was observed to increase with a predominantly "zeroth-derivative" component; *i.e.*, the increase in fluorescence emission had the same shape as the zero-field emission band. This was interpreted as an electric-field effect decreasing the rate of primary charge separation in the reaction center,[14] because fluorescence and charge separation compete for excitation in the reaction center. A decrease in charge separation therefore is reflected as an increase in fluorescence emission. Both the absorption and fluorescence effects were quadratic with the applied electric-field magnitude.

Ogrodnik *et al.* have used transient absorption measurements to study isolated *Rb. sphaeroides* reaction centers at 90 K suspended isotropically in PVA matrices under applied electric fields.[15] The results show different time constants for charge recombination events under applied field conditions. The quenching of the bacteriopheophytin bleaching (< 30 ps) is faster than the repopulation of the excited state P* (900 ps) during charge recombination, under the applied field conditions.

These results were interpreted as support for a model of an electric field-induced increase of an intermediate charge-separated state during charge recombination, possibly involving the monomeric accessory BChl (B).

Popovic *et al.* have used *Rb. sphaeroides* reaction centers embedded in Langmuir-Blodgett films, giving a partial net orientation.[16] The photo-induced electrical response of the film was measured as a function of external electric-field intensity. The results were interpreted as an effect on the energy of the initial dipolar state leading to a change in the rate of charge separation.[15,17]

The previous experiments reviewed here have all been performed on isolated *Rb. sphaeroides* reaction centers. There are few electric-field experiments which have been performed on the *Rb. sphaeroides* antenna complexes. One example of an electric-field experiment on antenna complexes is the study of Gottfried *et al.*, who have examined the absorption and fluorescence of photosynthetic antenna pigment-protein complexes isotropically oriented in 50% glycerol at 77 K under applied electric-field conditions.[18] *Rb. sphaeroides* LH2 antenna complexes and LH1 antenna complexes from *Rb. capsulatus* both exhibit an unusual strong fluorescence quenching behavior under applied electric-field conditions. The fluorescence quenching of LH2 and LH1 observed by Gottfried *et al.* will be addressed in greater detail later, in the discussion section of this chapter, together with the electric-field effect that they observe on the absorption of LH2 and LH1.

Aside from *Rb. sphaeroides*, another photosynthetic system which has been studied through application of electric fields is PSII. Dau and Sauer made electric-field measurements on the fluorescence of spinach thylakoid membranes.[5] The electric fields were applied using potassium diffusion potentials generated by a rapid mixing technique; this is the salt jump method described in Chapter Two. This approach allows measurements to be made on the pigment/protein complexes in the thylakoid membrane, which are naturally oriented in the membrane. Dau and Sauer measured the

fluorescence emission as a probe of charge separation reactions in the thylakoid, because fluorescence and charge separation compete for excitation. The change in fluorescence yield that they observed was linear with the magnitude of the applied electric field for all accessible electric-field intensities; there was a change in fluorescence emission intensity of about 9% per 100 mV. Fields oriented to oppose charge separation in the reaction center led to an increase in fluorescence of the system, and electric fields in the opposite direction caused a decrease in the fluorescence emission. Time-resolved fluorescence spectroscopy of the electric-field effect confirmed that the electric field does influence the rate of primary charge separation and recombination in the photosystem II reaction center.[19]

Results from a similar salt jump technique will now be reported here as applied to chromatophore membranes from *Rb. sphaeroides.*

Results

Electric-field effect on fluorescence emission:

The electric field is generated across the *Rb. sphaeroides* chromatophore vesicle using a salt jump gradient as described in Chapter Two. This salt jump technique creates an electric field which is normal to the surface of the vesicle. The orientation of the electric field and the magnitude of the electric field are controlled by the ratio of ions on both sides of the vesicle membrane. A positive electric field is defined as being positive on the inside of the chromatophore vesicle (the periplasmic side), and a negative electric field is defined as being negative on the inside of the vesicle. The periplasmic side of the membrane is adjacent to the special pair, P, which is oxidized to form P+ during charge separation. Therefore, a positive field, being positive on the periplasmic side of the membrane, is defined as being a field that is oriented in the

direction to energetically oppose charge separation in the reaction center. Conversely, a negative field is defined as being a field which is aligned to energetically stabilize charge separation in the reaction center. The orientation of the reaction center in *Rb. sphaeroides* chromatophore membrane is discussed in greater detail in the section on electrochromism experiments in Chapter Three.

We measure the fluorescence emission as a function of the electric-field intensity, because fluorescence and charge separation are competing pathways for excitation loss. An increase in the rate of charge separation will be reflected as a decrease in the fluorescence emission, if fluorescence and charge separation are in direct competition for excitation. Ideally, one could monitor the fluorescence emission of the reaction center directly. However, the reaction center of *Rb. sphaeroides* is only very weakly fluorescent; the quantum yield of fluorescence from the reaction center is only $Y_f = 4 \times 10^{-4}$ at room temperature.[20]

Most of the fluorescence emission of *Rb. sphaeroides* chromatophores comes from the antenna complexes, LH1 and LH2. Fortunately, the LH1 and LH2 fluorescence is sensitive to the state of the reaction center, as seen in the variable fluorescence (see Chapter Three). The variable fluorescence is the difference in fluorescence emission between the open reaction center state (Fo) and the closed reaction center state (Fm), and is maximum at 890 nm. If a change in the rate of charge separation is reflected in the antenna fluorescence emission, the difference spectrum will have the same spectral profile as the variable fluorescence, because that is the fluorescence which is sensitive to the state of the reaction center. However, it should be noted that 890 nm is also the maximum of the LH1 antenna emission and of the combined LH2 and LH1 fluorescence. If the electric field directly influences the emission of LH1 and/or LH2, the electric field-induced difference spectrum will also have a maximum at 890 nm.

The Fo state:

First let us consider the effect of electric fields on the fluorescence emission of *Rb. sphaeroides* chromatophores in the Fo state. In the Fo state, reaction centers are capable of undergoing the charge separation reaction. The Fo state is obtained with dark-adapted *Rb. sphaeroides* chromatophore samples under continuously flowing conditions where the sample was exposed only briefly to the measuring light (approximately 30 ms exposure). Under these conditions the measuring light did not produce any detectable actinic effect. This was confirmed by slowing the pump speed by 20% (from approximately 2 ml/sec to 1.6 ml/sec), which did not produce any change in the fluorescence emission intensity.

In the Fo state, positive electric fields applied across the oriented system of the *Rb. sphaeroides* chromatophore result in a decrease of the fluorescence emission. Negative electric fields cause an increase in the fluorescence emission.

There is a change in fluorescence intensity over the entire fluorescence emission band. Figure 4.6 shows the Fo state fluorescence emission spectra of *Rb. sphaeroides* chromatophores with a positive (dashed line) and negative (solid line) applied electric field. The transmembrane potential difference is 108 mV.

In *Rb. sphaeroides* chromatophores in the Fo state, fluorescence quenching occurs for a positive electric field (dashed line in Figure 4.6). A positive applied electric field is defined as one which is oriented to oppose charge separation in the reaction center. Therefore, a positive applied electric field would be expected to increase fluorescence emission if charge separation and fluorescence emission compete directly for excitation. Instead, a positive electric field causes a fluorescence decrease in *Rb. sphaeroides* chromatophores.

The fluorescence emission difference spectrum of the electric field-induced change in the Fo state (Fneg-Fpos) is shown in Figure 4.7.

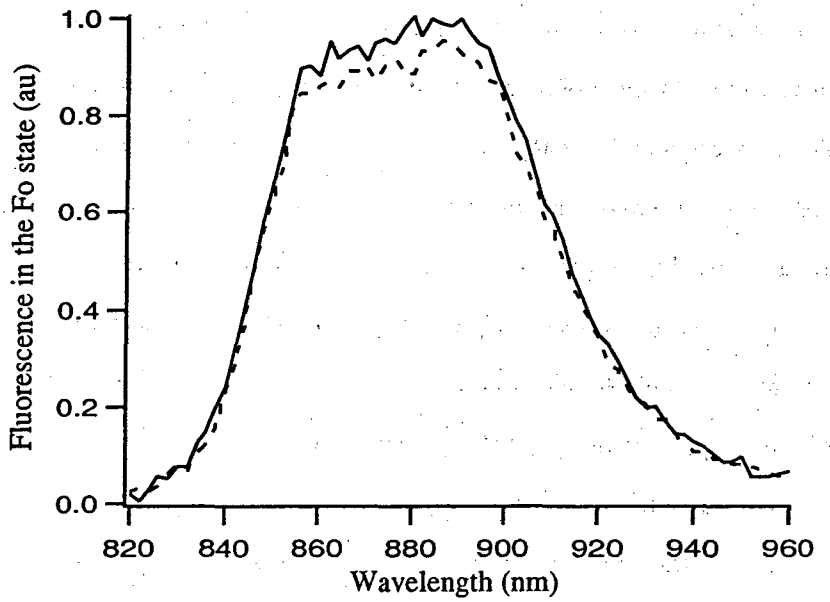

Figure 4.6 The Fo-state fluorescence emission of *Rb. sphaeroides* for positive applied electric fields (dashed line) and negative applied electric fields (solid line). The transmembrane potential difference is 108 mV.

The maximum of the electric field-induced fluorescence change in the Fo state occurs at 890 nm, which is the maximum of antenna fluorescence emission. 890 nm is also the maximum of the zero field variable fluorescence spectrum (Fm-Fo). The variable fluorescence is also shown for comparison (dashed line in Figure 4.7).

The magnitude of the change in fluorescence at 890 nm in the Fo state is shown in Figure 4.8a. This figure shows the change in fluorescence at 890 nm (ΔF) divided by the fluorescence intensity at 890 nm at zero field (F) as a function of the transmembrane potential difference; $\Delta F/F \times 100$ is the percent change in the fluorescence emission.

The transmembrane potential difference was calculated from the Nernst equation as described in Chapter Two. The ion concentrations used in these experiments (also described in Chapter Two) produce an accessible potential range of

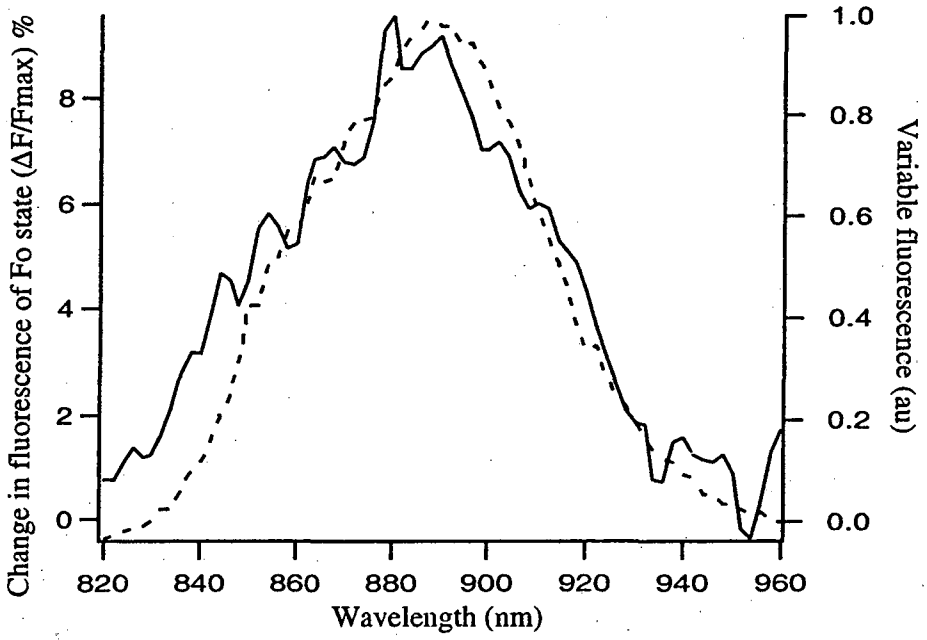

Figure 4.7: The electric field induced change in the Fo-state fluorescence spectrum of *Rb. sphaeroides* chromatophores (solid line). The variable fluorescence is also shown for comparison (dashed line).

-68 mV to +40 mV. The chromatophore membrane is approximately 50Å in thickness, therefore the maximum potential difference achieved in these experiments is approximately 2 x 10^4 V/cm.

The magnitude of the change in fluorescence at 890 nm in the Fo state can be fitted as a linear function (versus the transmembrane potential difference). Negative applied voltages result in an increase of fluorescence yield, and positive applied voltages result in a decrease of the fluorescence yield. The average value of the slope of five experiments was 8% per 100 mV. Linear regression analysis of the linear fit yields an r-squared value of 0.89. However, it should be noted that the best linear fit does not pass through the (0,0) mark.

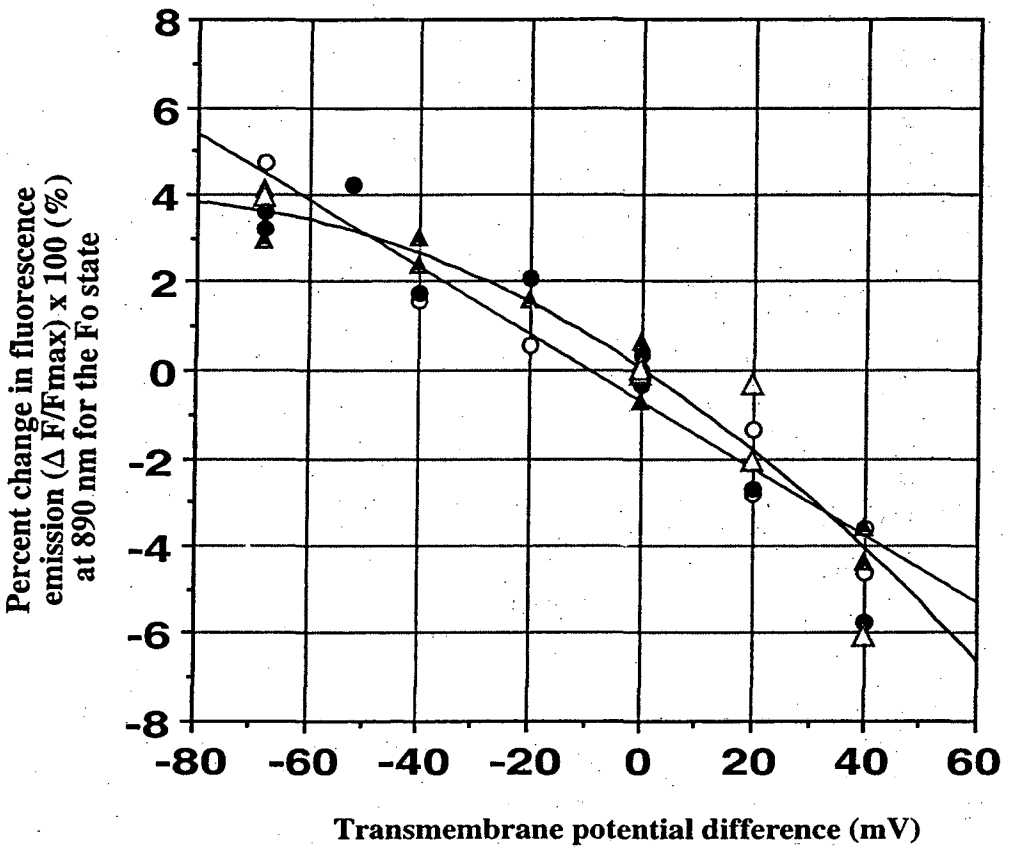

Figure 4.8a: Percent change in the fluorescence emission (ΔF/Fmax) for the Fo state of *Rb. sphaeroides* at 890 nm. Two fits are shown, a linear fit and a quadratic fit. The slope of the linear fit is approximately 8% per 100 mV.

The fluorescence change can also be fitted with a quadratic function. This results in an improved r-squared value of 0.95. Additionally, the polynomial fit does pass closely to the (0,0) mark at the origin. This increases the probability that the curvature in the data set is significant.

The linear and quadratic fits can be forced to pass through the origin (Figure 4.8b). This fitting constraint changes the r-squared value of the linear fit from 0.89 to 0.83. The quadratic fit, when constrained to pass through the origin, has an r-squared value of 0.94. The poor r-squared value of the linear fit through the origin enhances the likelihood of a true curvature in the data.

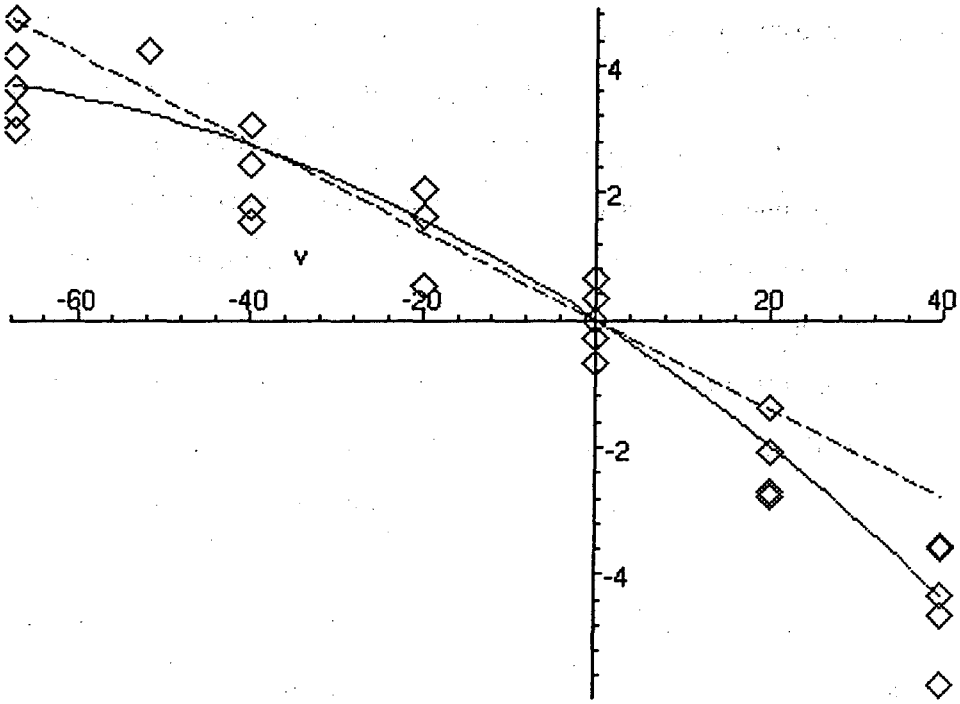

Figure 4.8b: Percent change in the fluorescence emission (ΔF/Fmax) for the Fo state of *Rb. sphaeroides* at 890 nm. Two fits are shown, a linear fit and a quadratic fit, both constrained to pass through the origin. The linear fit (dashed line) has an r-squared value of 0.83, and the quadratic fit (solid line) has an r-squared value of 0.94.

Partial trap closure:

Trap closure, or closing of the reaction centers, results in the state P^+BH in the reaction centers of *Rb. sphaeroides* chromatophores. In a fully closed-trap state (the Fm state) the reaction center cannot undergo further charge separation reactions. Closing the reaction center eliminates any effect that charge separation in the reaction center may contribute to the observed electric-field effect.

Partial trap closure was achieved by preillumination of the chromatophore solution. The degree of trap closure in a state "F" is expressed as the ratio of the fluorescence yield of closed and open traps, Q = (Fm-F) / (Fm-Fo). A Q of 1

corresponds to open traps (Fo), while a Q of 0 represents fully closed traps (Fm). Complete trap closure was not attainable by preillumination, due to charge recombination and relaxation processes before the fluorescence measurement; it was necessary to illuminate outside the fluorimeter sample compartment to prevent detection of scattered light. Approximately 400 ms elapsed between preillumination and fluorescence detection.

Figure 4.9 shows that at an intermediate Q of 0.45 or 0.55, there is a slight increase in the electric-field effect at the intermediate trap closure level. These results for *Rb. sphaeroides* chromatophores contrast with the behavior of spinach thylakoids.

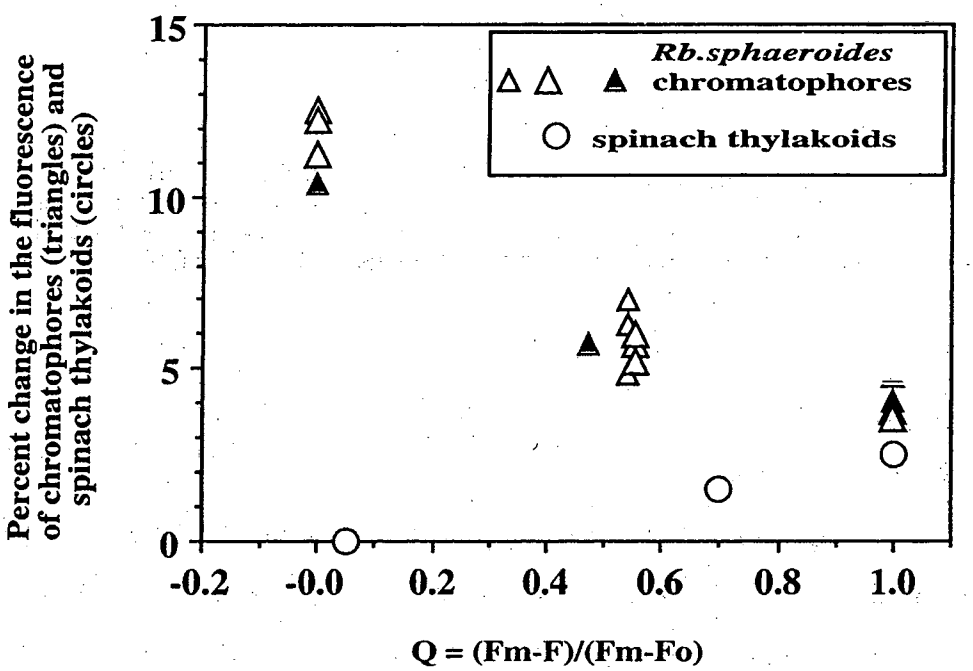

Figure 4.9: The electric field-induced change in fluorescence (ΔF/Fmax, %) as a function of trap closure for both *Rb. sphaeroides* chromatophores (triangles) and spinach thylakoids (circles). The data for spinach thylakoids, shown for comparison, are taken from Dau and Sauer, reference 9. For all data shown, the transmembrane potential is 40 mV. A Q of 1.0 corresponds to open traps (Fo state), and a Q of 0 corresponds to closed traps (Fm state).

For comparison, the results for spinach thylakoids are included in Figure 4.9 (open circles); data taken from Dau and Sauer.[9] For spinach thylakoids, a decrease in the electric field-induced fluorescence change was found for Q = 0.7. At a high degree of trap closure, Q = 0.05, the electric-field effect is entirely abolished in spinach thylakoids. The opposite behavior is observed for *Rb. sphaeroides* chromatophores; at lower Q values (higher degree of trap closure), the electric-field effect increases.

Figure 4.9 also displays the change in fluorescence for *Rb. sphaeroides* in the fully trap-closed state, Q = 0. This is the Fm state.

The Fm state:

The fully closed-trap state, the Fm state, is attained by stopping the pumps and exposing the sample to continuous illumination. Under these conditions an electric-field effect persists for several seconds. This is consistent with other observations of the duration of the electrochromic effects of the carotenoids generated by potassium diffusion potentials in *Rb. sphaeroides* chromatophores.[21,22] Measurements made within a few seconds after stopping the pumps demonstrated a large electric-field effect (Figure 4.9). In the Fm state, the electric-field effect has a larger magnitude than in the Fo state.

The spectrum of the electric-field effect in the Fm state is maximum at 890 nm, similar to that of the electric-field effect in the Fo state (Figure 4.10). The spectrum of the electric-field effect in the Fo state is also shown in Figure 4.10 for comparison (dashed line); the two spectra are normalized at the maximum. The magnitude of the effect for the same transmembrane potential difference is larger in the Fm state than in the Fo state across the spectral range of the emission; Figure 4.11 shows the spectrum of the electric-field effect for the Fo and the Fm state on the same scale.

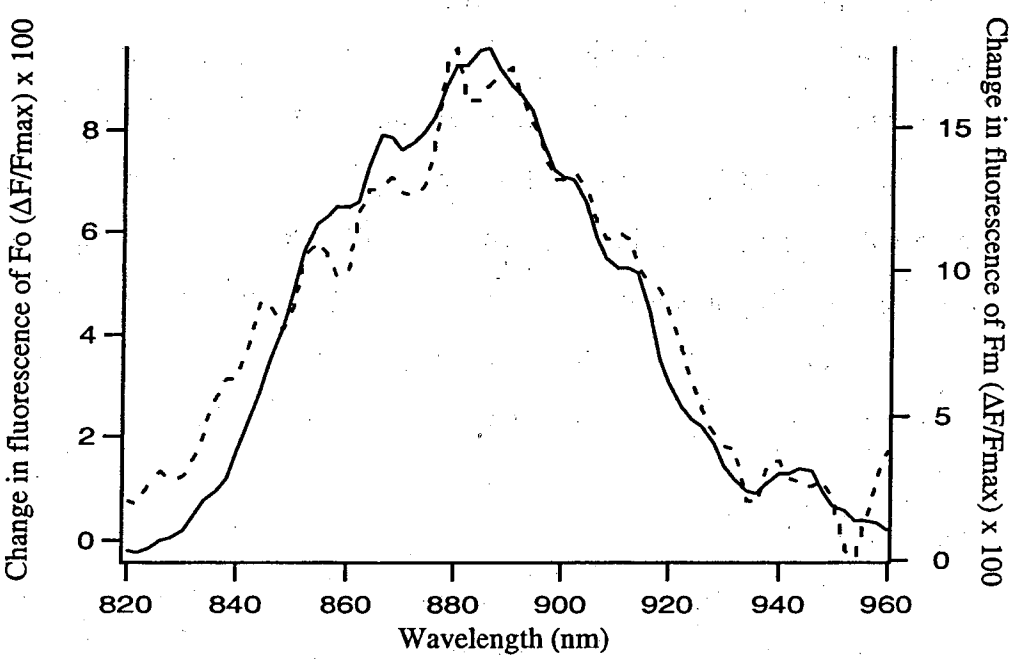

Figure 4.10: The electric field induced fluorescence change in the Fo state (dashed line) and the Fm state (solid line). The transmembrane potential difference is 108 mV. The spectra are normalized at 890 nm.

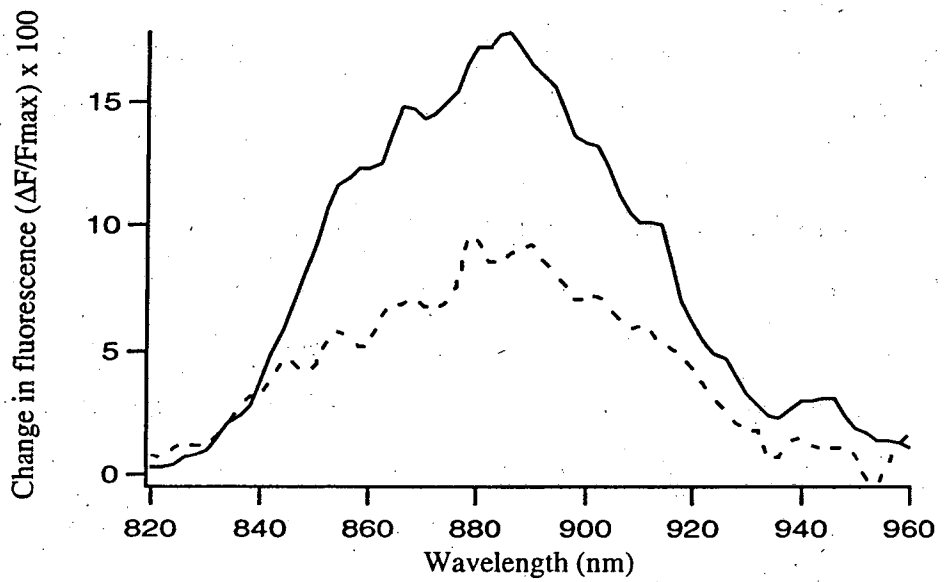

Figure 4.11: The electric field induced fluorescence change in the Fo state (dashed line) and the Fm state (solid line). The transmembrane potential difference is 108 mV.

The electric-field effect on the Fm state can also be fitted with a linear function versus the transmembrane potential difference from -68 to +40 mV, with a slope of approximately 15% per 100 mV (Figure 4.12a). This is approximately double the magnitude of the effect in the Fo state (Figure 4.8). Two fits are shown; the linear fit does not pass through the origin at (0,0) and results in an r-squared value of 0.92. The quadratic fit passes more closely to the origin and yields an improved r-squared value of 0.97. The Fm state fits can also be constrained to pass through the origin (Figure 4.12b). The constrained linear fit has an r-squared value of 0.91, and the constrained quadratic fit has an r-squared of 0.95. These results are similar to the results of the fits obtained for the Fo state. The percent change in fluorescence for the Fm and Fo state as a function of the transmembrane potential difference are displayed together on the same scale in Figure 4.13.

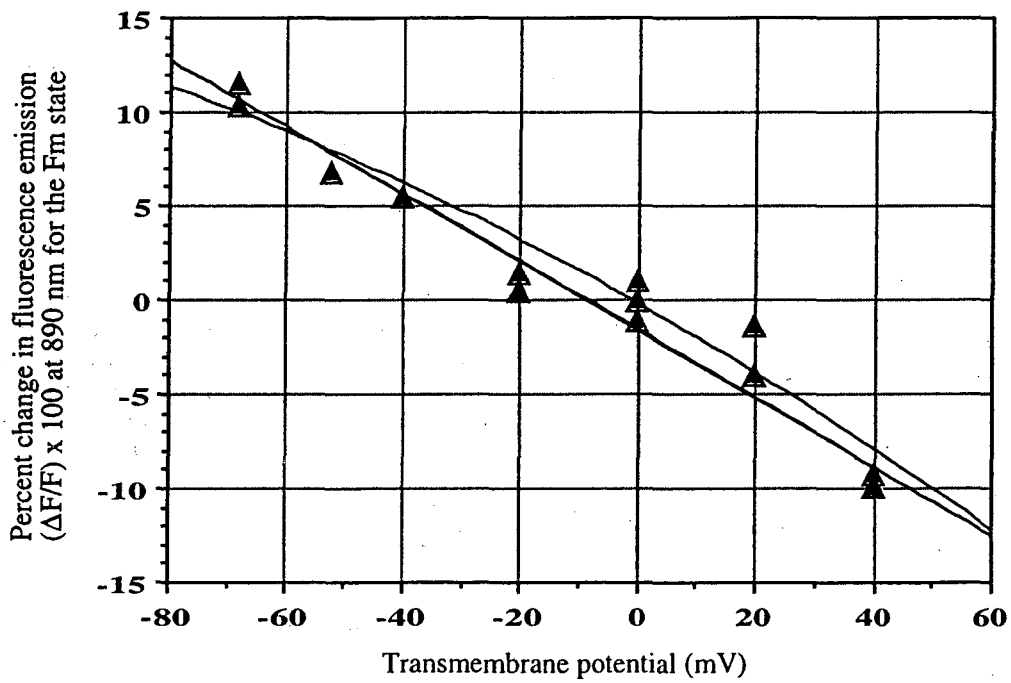

Figure 4.12a: Percent change in the fluorescence emission (ΔF/Fmax) for the Fm state of *Rb. sphaeroides* at 890 nm. Two fits are shown, a linear fit and a quadratic fit. The slope of the linear fit is approximately 15% per 100 mV.

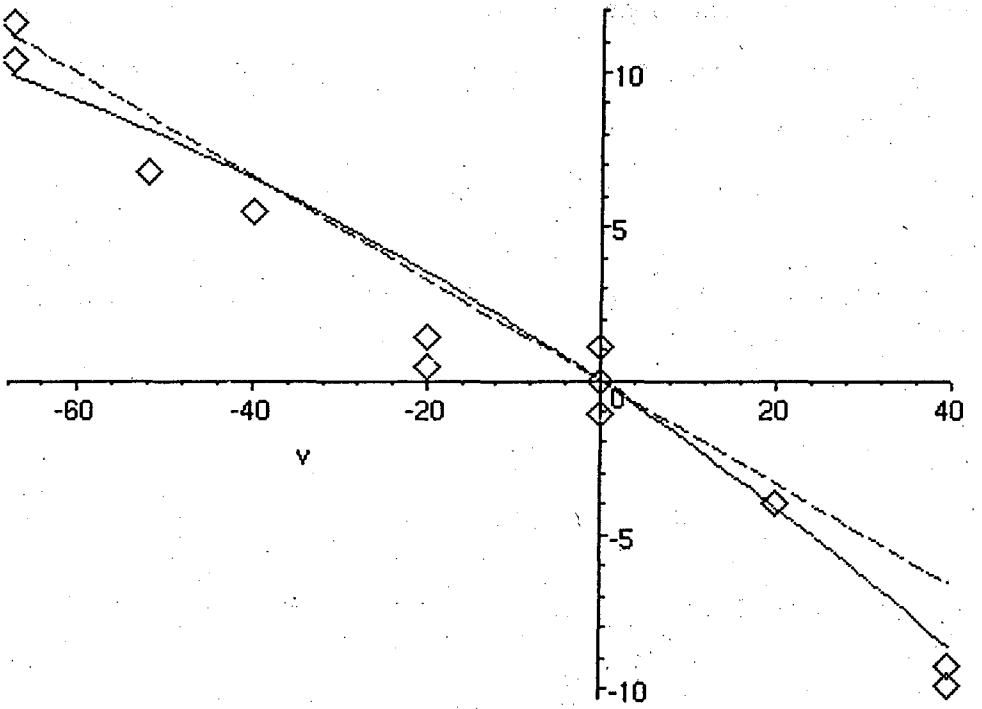

Figure 4.12b: Percent change in the fluorescence emission (ΔF/Fmax) for the Fm state of *Rb. sphaeroides* at 890 nm. Two fits are shown, a linear fit and a quadratic fit, both constrained to pass through the origin. The constrained linear fit has an r-squared value of 0.91, and the constrained quadratic fit has an r-squared value of 0.95.

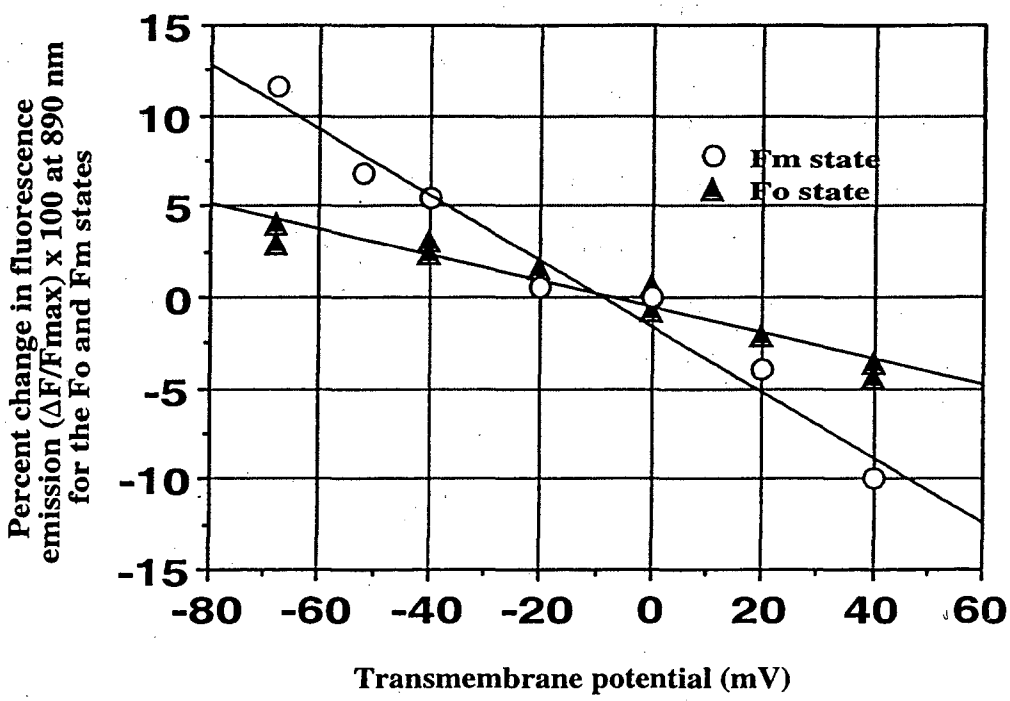

Figure 4.13: The electric field-induced fluorescence change at 890 nm in the Fo state (triangles) and the Fm state (circles). Linear fits are to both data sets are shown for comparison.

In the Fm state of *Rb. sphaeroides*, the electric-field effects on fluorescence emission are similar to those observed in the Fo state, but have a greater magnitude. In the Fm state of *Rb. sphaeroides*, the special pair is oxidized and charge separation cannot occur. Therefore, in the Fm state, a change in the rate of charge separation in the reaction center is not the origin of the observed electric-field effect.

Dithionite treatment:

Sodium dithionite is a strong reducing agent. The use of sodium dithionite as a specific reducing agent for the primary quinone in purple photosynthetic bacteria is frequently cited in the scientific literature. However, because sodium dithionite is a

powerful and indiscriminate reducing agent, we tested its effects on the antenna complexes in mutant strains of *Rb. sphaeroides* that do not contain reaction centers. As shown in Figure 4.14, addition of sodium dithionite to a final concentration of 10 mM did not significantly change the fluorescence emission of LM1.1, a strain containing both LH1 and LH2, but lacking reaction centers. Therefore we conclude that sodium dithionite does not have an effect on the fluorescence emission from the antenna complexes of *Rb. sphaeroides.*

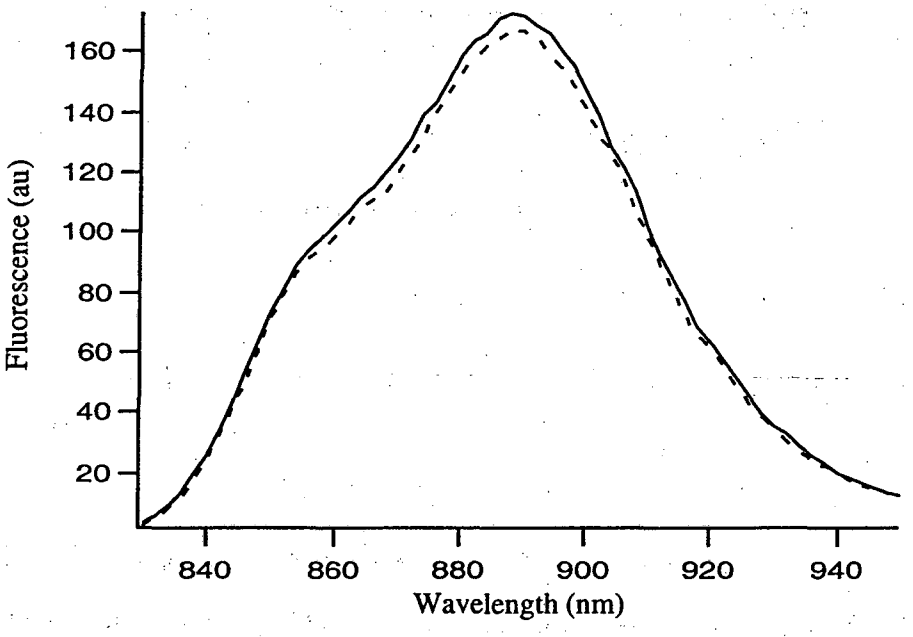

Figure 4.14: Fluorescence emission of LM1.1 before (solid line) and after (dashed line) addition of sodium dithionite to a final concentration of 10 mM. Excitation at 510 nm. Fluorescence taken at right angles in a polystyrene cuvette of cross section 1 cm.

Addition of sodium dithionite to a final concentration of 10 mM in the wild-type *Rb. sphaeroides* chromatophore sample reduces the primary quinone Q_A in the reaction center, producing the state PHQ_A^-.[23] The states Fo and Fm do not apply under these

conditions, because any charge separation producing the state $P^+H^-Q_A^-$ will result in a rapid recombination to the state PHQ_A^-.[24]

When the primary quinone is reduced by dithionite, the electric-field effect shows a striking reversal of direction (Figure 4.15). Positive electric fields now lead to an increase in fluorescence intensity, and negative electric fields cause a decrease in fluorescence intensity.

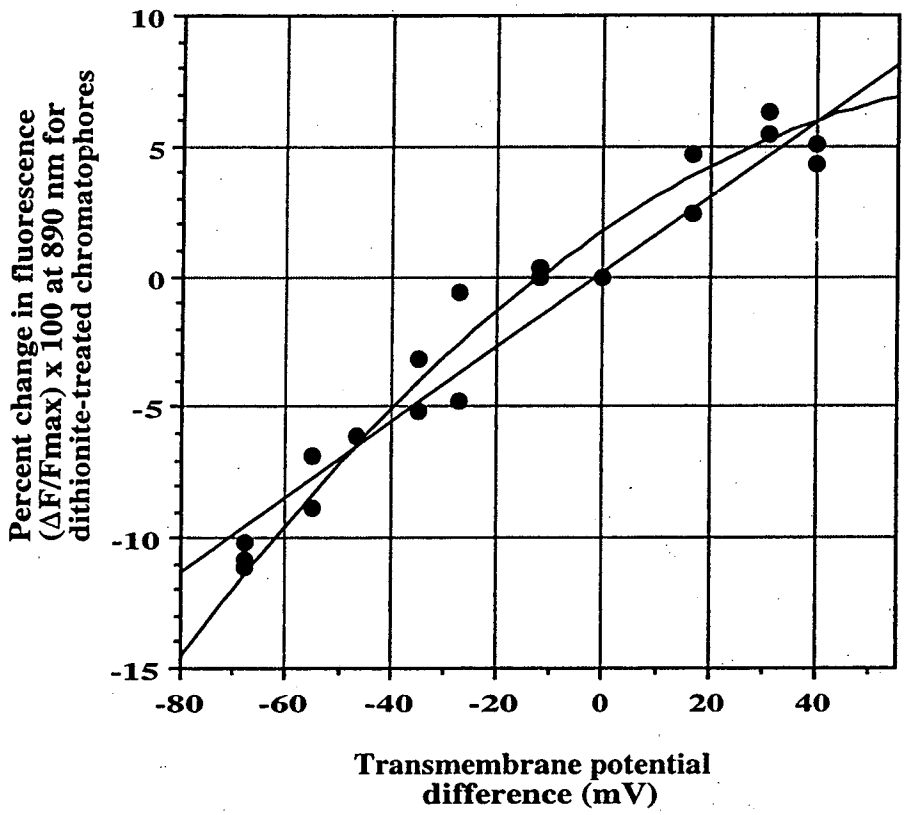

Figure 4.15: The electric field-induced fluorescence changes [(ΔF/Fmax) x100] in *Rb. sphaeroides* chromatophores in the presence of 10 mM sodium dithionite. A linear and a quadratic fit are both shown.

Two fits to the data are shown; the linear fit does pass through the origin at (0,0) and results in an r-squared of 0.95. The quadratic fit does not pass through (0,0)

and gives an only slightly improved r-squared value of 0.97. The magnitude of the effect is approximately 15% per 100 mV (compare with Figure 4.13).

The spectrum of electric field-induced effect under dithionite-treated conditions is maximum at 890 nm (Figure 4.16). The solid line is the ΔF/Fmax spectrum averaged one sec. every nanometer and the line with diamond markers is the ΔF/Fmax spectrum averaged for a longer time (four sec. averaging at every data point), taken every ten nanometers. Both of the ΔF/Fmax spectra in the presence of 10 mM dithionite are similar to the spectra of the electric-field effect for samples without dithionite in both the Fo and the Fm states; the spectrum for the untreated Fo state is displayed for comparison in Figure 4.17 (dashed lines).

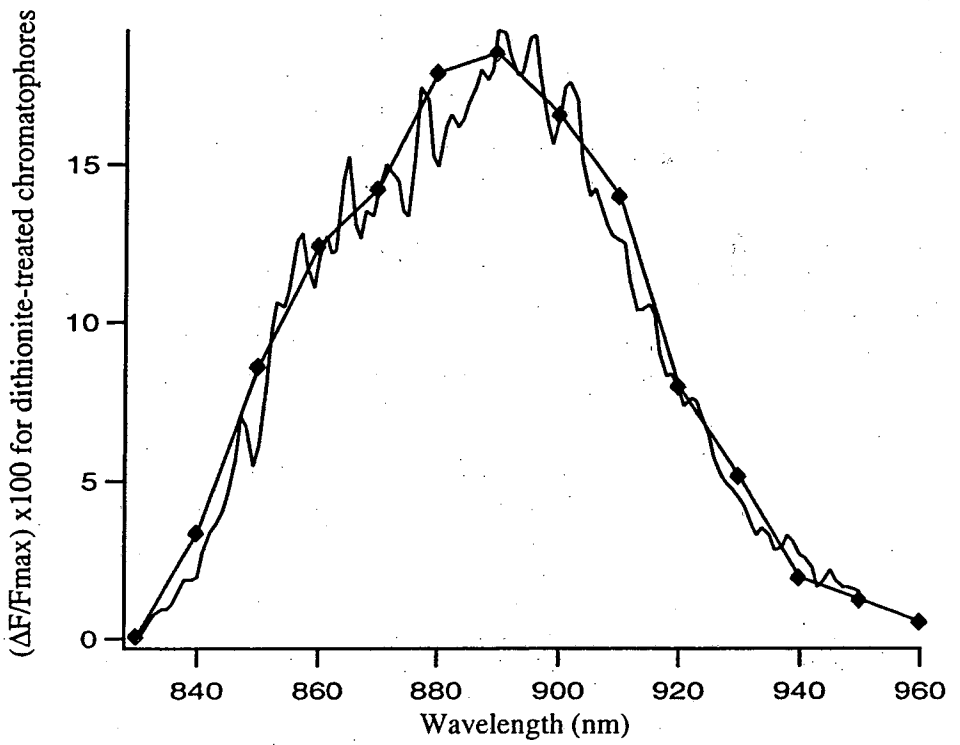

Figure 4.16: The electric field induced fluorescence change in *Rb. sphaeroides* chromatophores treated with 10 mM sodium dithionite. Solid line, one second averaging every one nanometer. Line with markers, four second averaging every ten nanometers. The transmembrane potential difference is 108 mV.

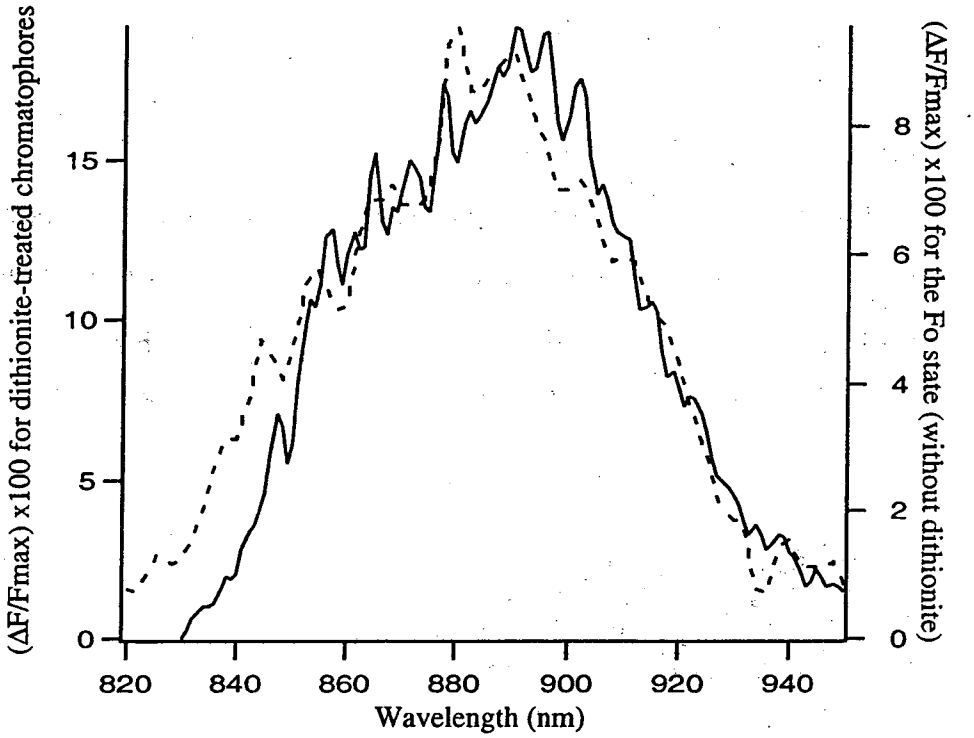

Figure 4.17: The electric field induced change in fluorescence [(ΔF/Fmax) x 100] for *Rb. sphaeroides* chromatophores in the presence of 10 mM dithionite (solid line) and in the absence of dithionite (dashed line). Both data sets are in the Fo state and the transmembrane potential difference is 108 mV.

LM1.1 - a mutant of *Rb. sphaeroides* without reaction centers:

To further investigate the effect of an electric field on the fluorescence emission of *Rb. sphaeroides*, mutant strains of *Rb. sphaeroides* lacking reaction centers were obtained as a generous gift from JoAnne Williams' lab at Arizona State University (see Appendix B for details of the mutant strains). LM1.1 is a strain which expresses both LH1 and LH2, but does not express reaction center polypeptides or assemble functional reaction centers. LM1.1 also fails to express PufX, a protein which may be

involved with intracytoplasmic membrane (ICM) topology and LH1/RC association (see Appendix B for further details).

Membrane morphology of LM1.1:

LM1.1 is grown using DMSO as a terminal electron acceptor (see Chapter Two), conditions which are more conducive to vesicular ICM formation than semi-aerobic growth.[25] However, electron microscopy of LM1.1 bacteria grown anaerobically with DMSO shows that in our hands under these conditions, LM1.1

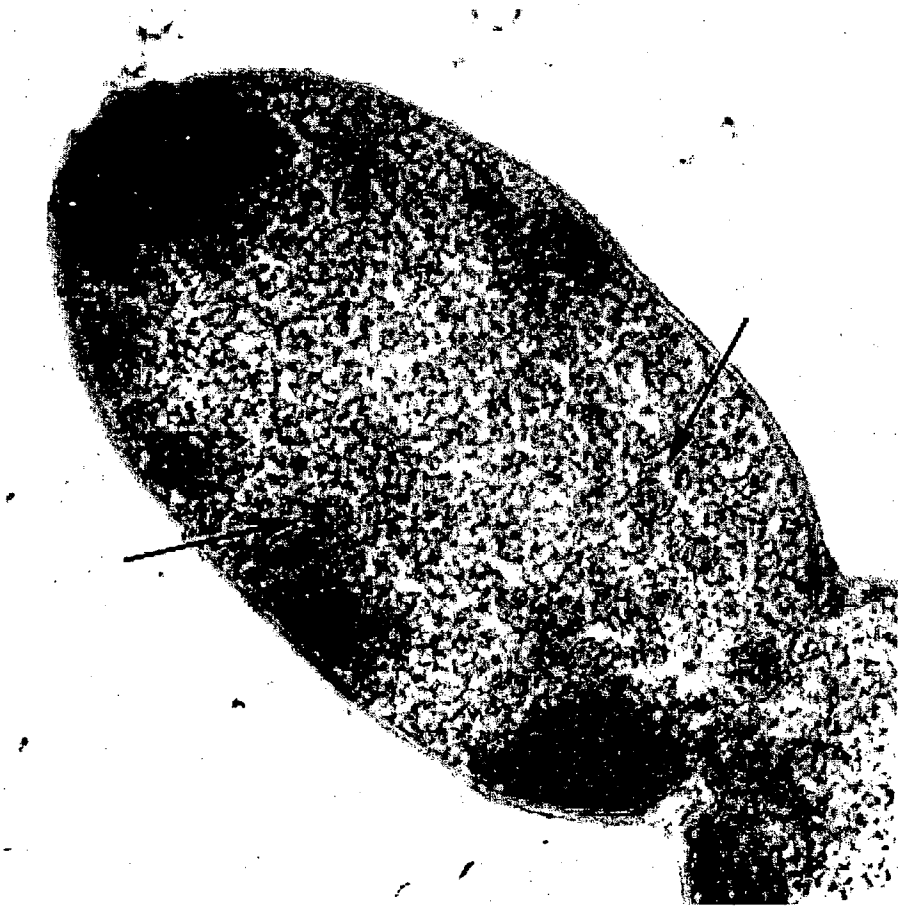

Figure 4.18: Ultrathin section of the mutant *Rb. sphaeroides* strain LM1.1 showing sporadic vesiculation of the ICM. Two of the vesicles are indicated by arrows. The image is taken at 33,000 times magnification.

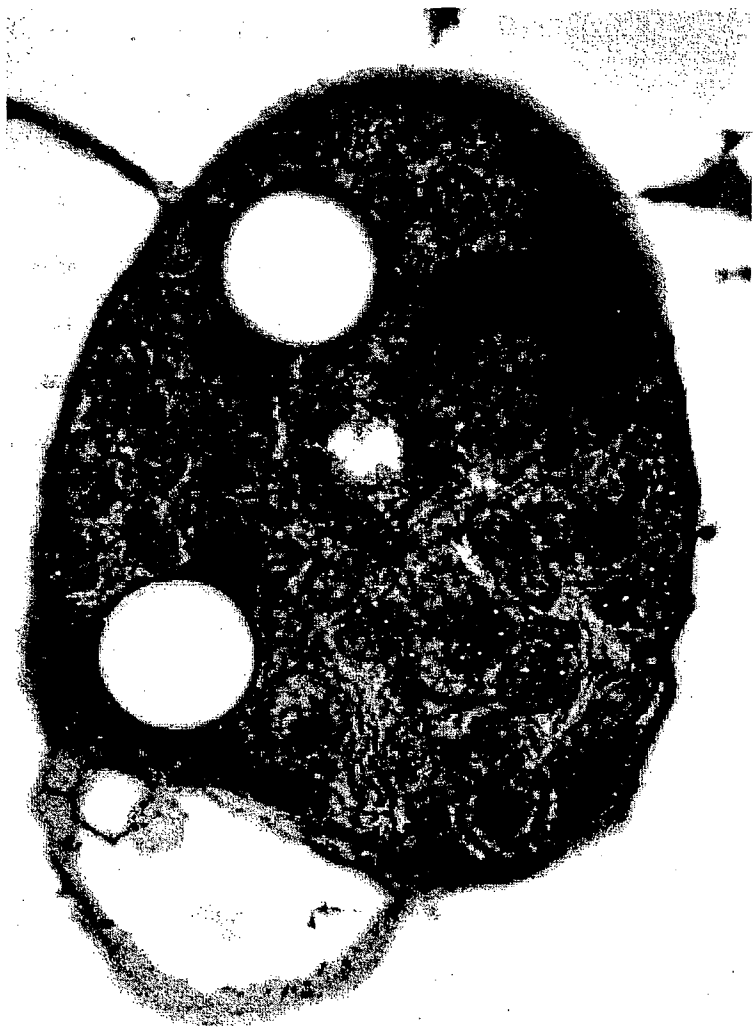

Figure 4.19: Ultrathin section of wild-type *Rb. sphaeroides* showing densely packed vesicles in the ICM. The image is taken at 25,000 times magnification.

exhibits only sporadic ICM vesicles (Figure 4.18). In contrast, the wild-type *Rb. sphaeroides* grown photosynthetically displays a densely packed ICM morphology (Figure 4.19).

The intracytoplasmic membranes of LM1.1 are isolated using the same preparation methods applied to the wild-type strain to generate chromatophores (Chapter Two). However, because of the difference in ICM structure in LM1.1 as

compared to the wild type, the result of the "chromatophore preparation" from LM1.1 may not be the same oriented and ionically sealed chromatophore vesicles as found for the wild type.

LM1.1 does not express functional reaction centers; therefore, it is difficult to assay the ionic integrity or degree of ionic seal of the LM1.1 membrane preparation. 9-aminoacridine, which is used to determine the ionic integrity of the wild-type chromatophore membrane (Chapter Three), relies on proton translocation across the membrane by the reaction center. Other pH-sensitive dyes often used for this purpose, such as oxanol dyes,[26] also depend on reaction center proton translocation. Obviously, these techniques do not apply to reaction-centerless mutant strains such as LM1.1.

However, LM1.1 does express BChl in LH1 and LH2. The BChl of LH2 is electrochromic. BChl electrochromism in the wild-type chromatophore membrane is linear at a measured wavelength pair of 865-850 nm (measurement beam at 865 nm and reference beam at 850 nm).[27] The absorption increases at this wavelength pair for positive internal potentials, and decreases for negative internal potentials. The magnitude of the electrochromic shift is approximately $\Delta A = 0.6\%$ for a 50 mV transmembrane potential difference in the wild type.[26]

Using potassium-induced transmembrane potentials, we have measured the electrochromic bandshift of the wild-type *Rb. sphaeroides* chromatophore preparation and the LM1.1 membrane preparation. For positive internal potentials, the wild-type chromatophore preparation shows an increase in absorption at the wavelength pair 865-850 nm, in agreement with the published literature.[26] However, the LM1.1 membrane preparation shows an absorption decrease at the wavelength pair 865-850 nm for positive internal potentials. The absolute magnitude of the absorption change in LM1.1 is less than that observed for the wild type, approximately 30% of the wild-type value.

The fact that the electrochromic absorption change of LM1.1 BChl is less than that observed for wild type indicates that either the extent of net orientation, or the degree of ionic integrity, is less for the LM1.1 membrane preparation than for the wild-type chromatophore preparation. The fact that the electrochromic absorption change of LM1.1 BChl is in the opposite direction from the wild type indicates that the net orientation of the LM1.1 membrane preparation is inverted from the wild-type chromatophore preparation.

Electric-field effect on the fluorescence of LM1.1:

A transmembrane potential is applied across the membranes of the LM1.1 preparation in the same way as described previously for the wild type. Positive applied

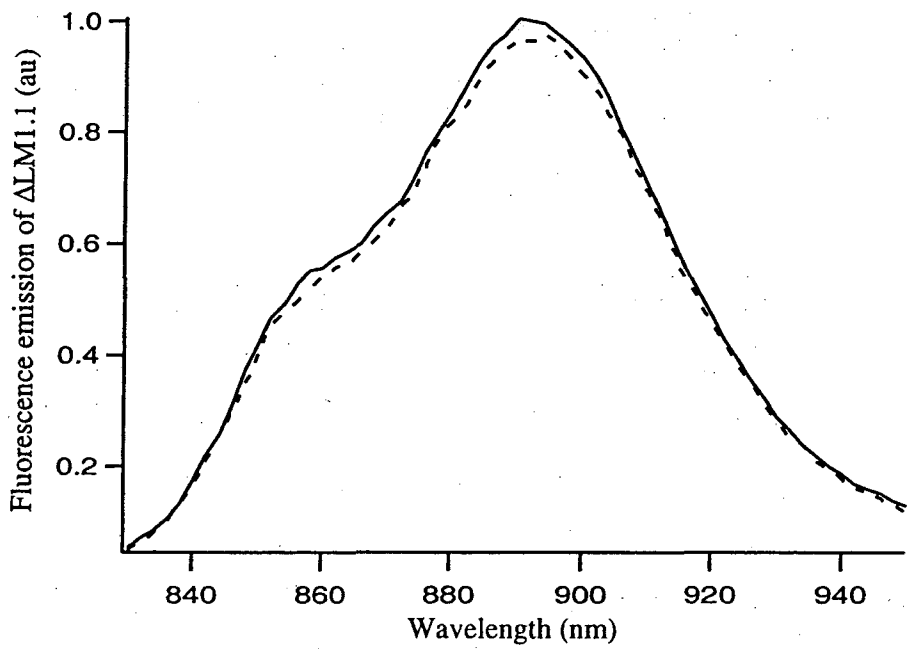

Figure 4.20: Fluorescence emission of the ΔLM1.1 membrane preparation for a positive transmembrane potential (+40 mV, solid line) and a negative transmembrane potential (-68 mV, dashed line). A positive internal potential causes an increase in the ΔLM1.1 fluorescence emission, unlike wild type.

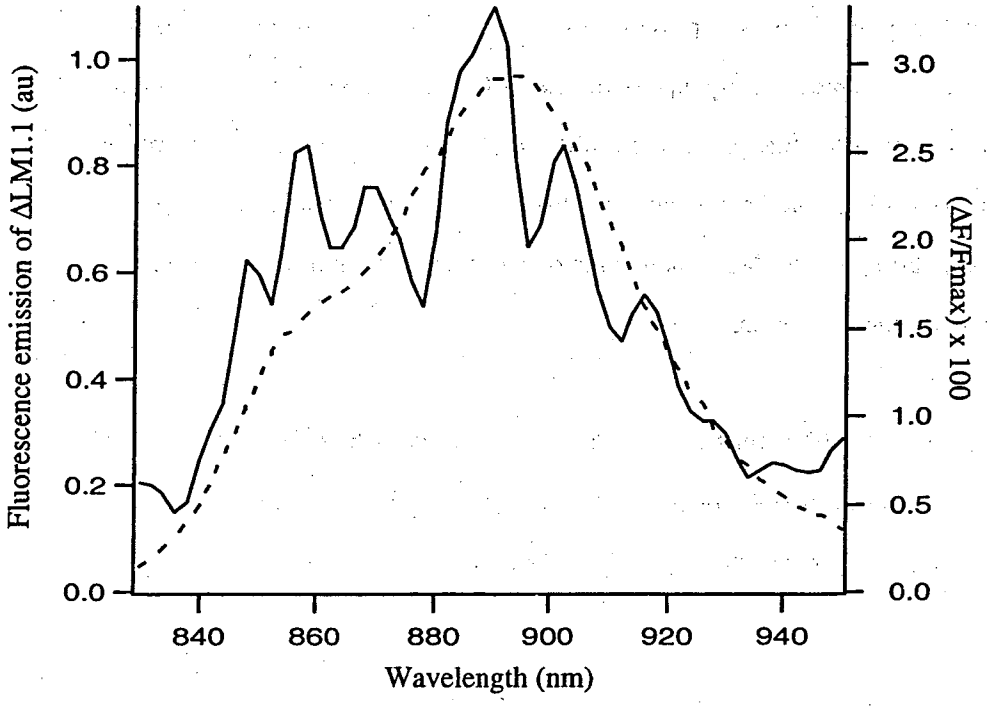

Figure 4.21: The electric field-induced change in the fluorescence emission of ΔLM1.1 [(ΔF/Fmax) x 100], solid line. The transmembrane potential difference is 108 mV. The fluorescence emission of ΔLM1.1 is also displayed for comparison (dashed line).

potentials, defined as being positive on the inside of the vesicle, lead to an increase in the fluorescence emission. Negative potentials lead to a decrease in the fluorescence emission. The fluorescence change is observed across the entire spectral range of the fluorescence emission of LM1.1 (Figure 4.20). The maximum of the electric field-induced fluorescence change is at 890 nm (Figure 4.21).

The direction of the electric field-induced fluorescence change in LM1.1 is opposite to the direction of the change observed for the wild-type chromatophore preparation. Recall also that the net orientation of the LM1.1 membrane preparation is opposite to the orientation of the wild-type chromatophore preparation. Taking the orientation of the membranes into account, the electric field-induced fluorescence

change is in the same direction for the wild type and the reaction centerless mutant strain LM1.1.

The magnitude of the electric field-induced fluorescence change in LM1.1 is less than the magnitude of the fluorescence change in the wild type. For a transmembrane potential of 100 mV, the fluorescence change in LM1.1 is approximately 2.5 % at 890 nm (averaged value of four experiments). For the wild-type chromatophore preparation, the electric field-induced fluorescence change is approximately 8% in the Fo state, or 15% in the Fm state. Recall that the absolute magnitude of the electrochromic absorption change of the LM1.1 membrane preparation is approximately 30% of the wild type, as determined from electrochromism experiments.

The membrane preparation of LM1.1 does not exhibit the same extent of electrochromism as the wild type, and therefore the membrane preparation of LM1.1 may have a decreased net orientation or an increased ionic permeability. Additionally, the electrochromic data show that the net orientation of LM1.1 is opposite to the orientation of wild type. Despite the differences in the membrane preparation between LM1.1 and wild type, the fact that LM1.1 shows an electric field-induced fluorescence change demonstrates that the presence of a functional reaction center is not required for an electric-field effect on the fluorescence emission of this strain of *Rb. sphaeroides.*

The results of the electric field-induced fluorescence changes at 890 nm are summarized in Figure 4.22 for wild-type *Rb. sphaeroides* in the Fo and Fm states, wild-type *Rb. sphaeroides* in the presence of 10 mM sodium dithionite, and LM1.1. The percent fluorescence change [(ΔF/Fmax) x 100] is shown for each condition at 890 nm with a transmembrane potential difference of 100 mV.

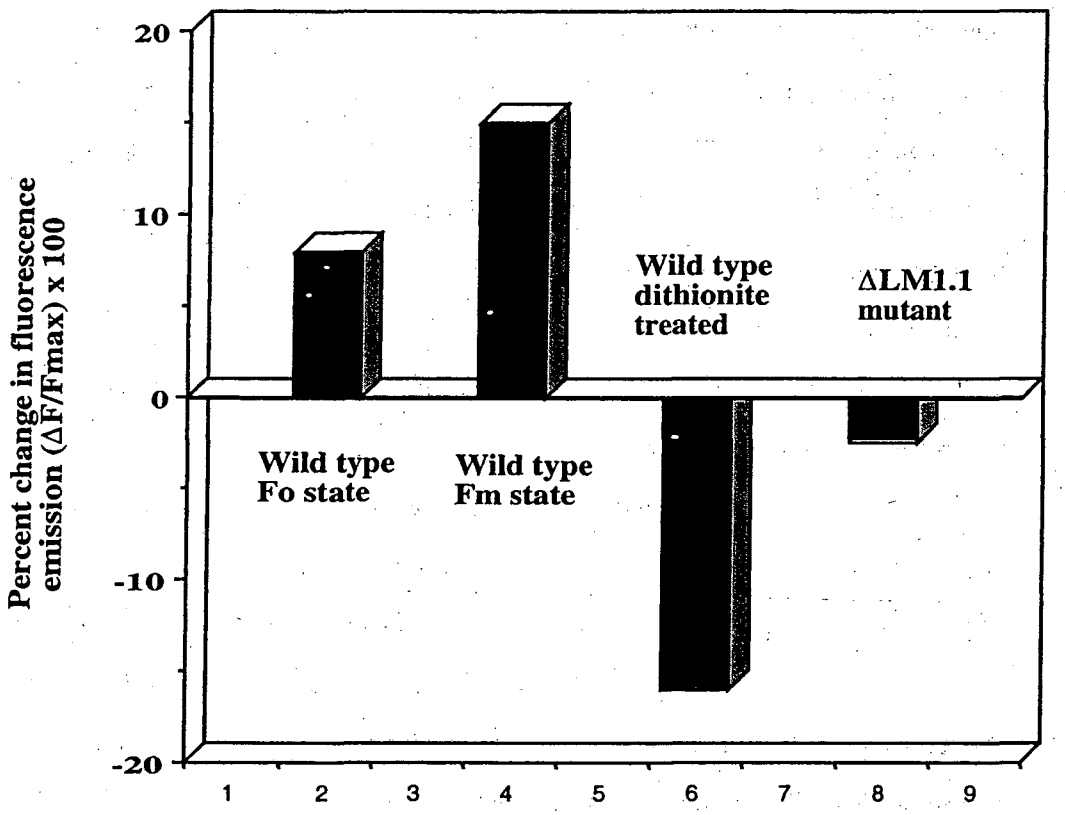

Figure 4.22: The percent change in fluorescence emission [(ΔF/Fmax) x 100] for wild-type *Rb. sphaeroides* in the Fo and Fm states, in the presence of 10 mM sodium dithionite, and for the reaction-centerless mutant strain LM1.1. The change in fluorescence was monitored at 890 nm for a transmembrane potential difference of 100 mV in all cases.

Discussion

At this point, let us briefly review our experimental findings.

- An electric field, which is oriented along the membrane normal of the *Rb. sphaeroides* chromatophore, causes a change in the fluorescence emission of the chromatophore preparation. This electric field-induced change in fluorescence can be best fitted as a quadratic function, versus the transmembrane potential.
- Fluorescence emission increases for negative potentials (negative defined as inside the chromatophore vesicle), and decreases for positive potentials (positive inside the vesicle).
- The effect of the electric field is greater in the Fm (P^+) state than in the Fo (P) state.
- The maximum of the electric-field effect is at 890 nm for both the Fo and the Fm state. 890 nm is the maximum of LH2 emission, as well as the maximum of the variable fluorescence emission.
- Addition of sodium dithionite, a strong reducing agent, reduces the primary quinone (Q_A^-) and causes a reversal of the direction of the electric-field effect. Under Q_A^- conditions, the electric field-induced change in fluorescence can be best modeled as a linear function versus the transmembrane potential, and is maximum at 890 nm.
- An electric-field effect is observed on the fluorescence emission from LM1.1, a strain lacking reaction centers. When the orientation of the membrane preparation is taken into account, the direction of the electric field-induced fluorescence change is the same as that seen for the wild type. The maximum of the electric-field effect on LM1.1 is at 890 nm.

Any model to explain the electric-field effects seen in *Rb. sphaeroides* chromatophores must be consistent with all of the above observations.

The inverted Marcus region:

In the Fo state of *Rb. sphaeroides* chromatophores, the direction of the electric-field effect is opposite to the direction predicted by electrostatic considerations of charge separation in the reaction center. If the Fo state results were the only experimental data available, the results might be explained by charge separation in the inverted Marcus region. Because charge separation in the inverted Marcus region has been proposed as a possible mechanism for primary charge separation in purple photosynthetic bacteria,[28] we will briefly discuss this mechanism.

Primary charge separation in the normal region of potential energy curve crossing is shown in Figure 4.23A. In this region, raising the free energy of the charge separated state P^+BH^- with an internally positive electric field would move the curve crossing intersection to higher energies. This would decrease the rate of charge separation. If charge separation occurred in the inverted Marcus region (Figure 4.23B), raising the free energy of the charge separated state with an internally positive electric field would bring the curve crossing closer to the activationless region and increase the rate of charge separation. Thus, charge separation in the inverted Marcus region could potentially explain the direction of the electric-field effect seen in the Fo state of *Rb. sphaeroides* chromatophores.

However, charge separation in the inverted Marcus region is not sufficient to explain the enhanced electric-field effect in the Fm state of *Rb. sphaeroides* (Figures 11 and 13). In the Fm state, the probability of primary charge separation is minimal and therefore an electric-field effect on charge separation in the reaction center should also be minimal. However, in the Fm state, the electric-field effect actually increases compared with the Fo state. Therefore, charge separation in the inverted Marcus region is not a valid explanation for all of the experimental data.

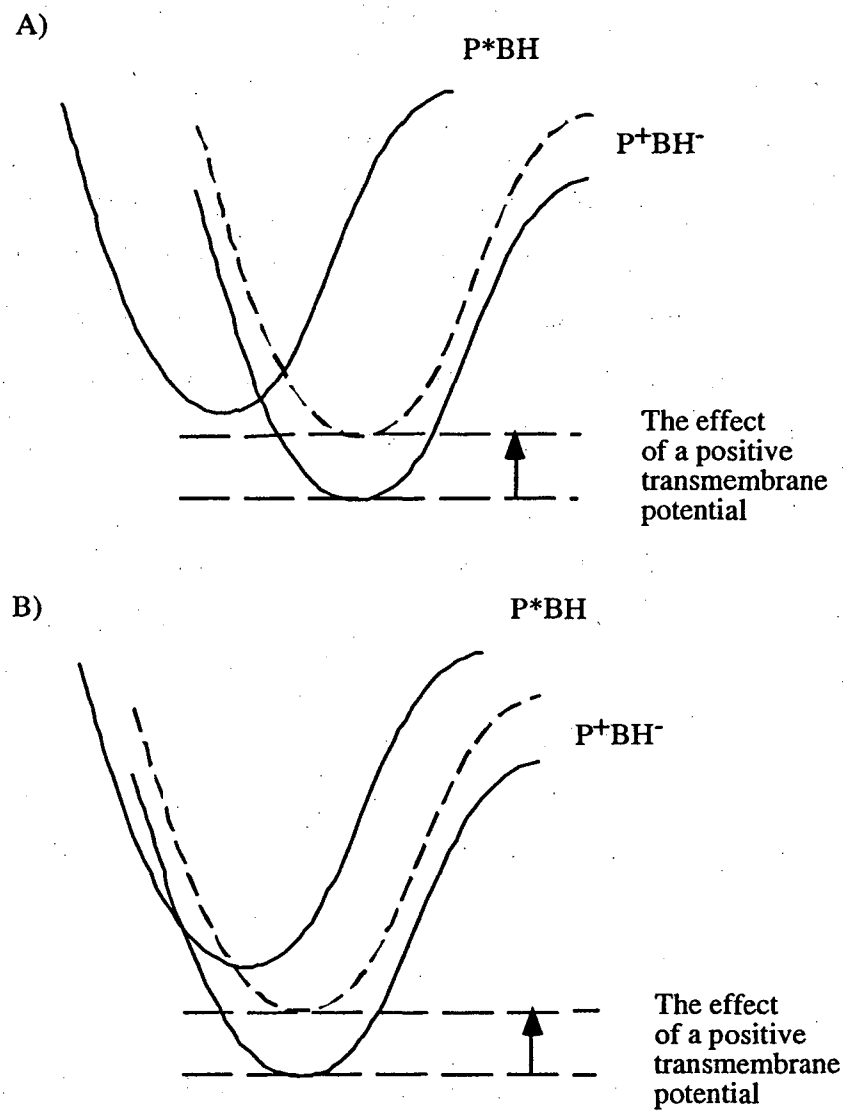

Figure 4.23: Potential energy curves for the normal (A) and inverted (B) Marcus regions. The effect of a positive internal transmembrane potential on the charge separated state P+BH- is shown for both conditions. A positive internal transmembrane potential increases the energy of the charge separated state. For a curve crossing in the normal (or activationless) Marcus region, raising the energy of the charge separated state moves that state farther away from the activationless curve crossing. However, for the inverted Marcus region, raising the energy of the charge separated state brings the curve crossing closer to the activationless region.

Model of the electric-field effect in *Rb. sphaeroides* chromatophores:

Our model of the electric-field effect in *Rb. sphaeroides* chromatophores is based on the fact that the fluorescence emission that we monitor in the experiment arises primarily from the antenna complexes, and not directly from the reaction center. Therefore, we must consider the possibility that **the externally applied electric field may have an effect directly on the fluorescence emission of the antenna complexes themselves**, independently from an electric-field effect on the reaction center.

Another consideration in our model is how excitation is shared between the reaction center and the antenna complexes in the wild type. Because the reaction center is very weakly fluorescent itself,[19] any electric-field effect on the reaction center will be evident only through the fluorescence emission from the antenna. Conditions which impair back transfer of excitation from the reaction center to the antenna may decrease the extent of any observed electric-field effect on the reaction center. Conversely, conditions which enhance the rate of back transfer from the excited state reaction center to the antenna complexes may cause an electric-field effect on the reaction center to be more pronounced in the fluorescence emission from the antenna.

Figure 4.24 is a schematic of a qualitative model which fits all our data for the effect of an applied electric field on the fluorescence emission of *Rb. sphaeroides* chromatophores. We propose that the electric field has an effect directly on the fluorescence emission from the antenna pigments. This hypothesis is consistent with the observed electric-field effect on LM1.1, a strain of *Rb. sphaeroides* that is lacking reaction centers.

In the wild type, the effect on the antenna fluorescence emission is in addition to a separate electric-field effect on the rate of charge separation in the reaction center. Figure 4.24 addresses the effect of an external electric field for three different

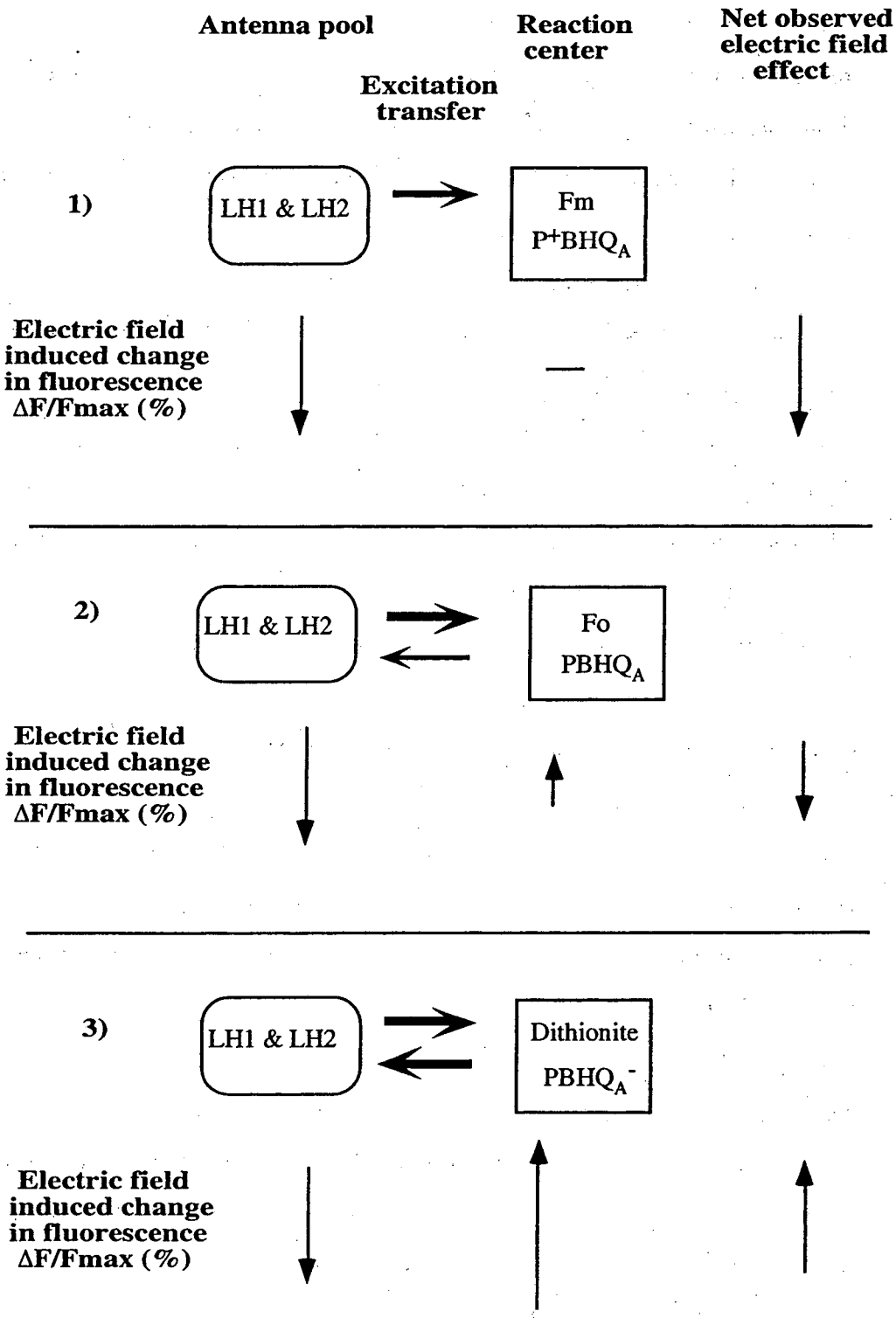

Figure 4.24: Schematic model of the electric-field effect in wild-type *Rb. sphaeroides.*

conditions of the wild type, which are presented separately in the three rows. The first condition, in the top row (1), is the Fm state of the reaction center. The second condition, in the middle row (2), is the Fo state of the reaction center. The third condition, in the bottom row (3), is the primary quinone reduced by addition of sodium dithionite.

In Figure 4.24, the percent electric-field induced change in fluorescence ($\Delta F/Fmax$) is indicated by vertical arrows below the antenna pool, in the left (antenna pool) column; the reaction center, in the middle (reaction center) column; and the net observed electric-field effect, in the right column. The change in fluorescence in Figure 4.24 is shown for a positive applied potential (positive inside the vesicle), which is defined as being oriented to energetically oppose charge separation in the reaction center. The direction of the electric field-induced fluorescence change (increase or decrease relative to the zero field condition) is indicated by the direction of the arrow (up or down). The magnitude of the electric field-induced fluorescence change is qualitatively indicated by the length of the arrow.

The electric-field effect on only the fluorescence emission of the antenna complexes is shown in the left (antenna pool) column of Figure 4.24. For all three conditions, Fo, Fm, and reduced primary quinone, the electric field has the same effect on the antenna fluorescence emission. The antenna fluorescence decreases by the same percent ($\Delta F/Fmax$) for each of these three conditions. The three different conditions (1,2 and 3) affect the reaction center and the transfer of excitation between the reaction center and the antenna, but do not affect directly the electric-field effect on the antenna fluorescence emission alone. The hypothesis of an electric-field effect directly on the fluorescence of the antenna complexes themselves is strongly supported by the experimental observation of an electric-field effect on the fluorescence of the membrane preparation of LM1.1, a mutant which expresses both antenna complexes but does not express functional reaction centers.

The electric-field effect on the charge separation in the reaction center is shown in the center column of Figure 4.24, as it would be reflected in the fluorescence emission. In the Fm state (case 1, P^+BHQ_A), where the probability of charge separation in the reaction center is minimal, the electric field has no effect on the rate of charge separation in the reaction center. In the Fo state (case 2, $PBHQ_A$), a positive field which is defined as a field oriented to energetically oppose charge separation, causes an increase in fluorescence emission; a decrease in the rate of charge separation is reflected by an increase in fluorescence emission.

Finally, in the Q_A^- state of the reaction center (case 3), the extent of the effect of the electric field on charge separation in the reaction center is increased. In the Q_A^- state, the reduced primary quinone itself opposes charge separation in the reaction center. Charge separation occurs from the excited state of the special pair, $P^*HQ_A^-$, to the state $P^+H^-Q_A^-$ with a decreased time constant of 5.6 ps[29] (versus 2.8 ps for charge separation to the state $P^+H^-Q_A$).[3] The presence of the reduced quinone slows the rate of charge separation in the reaction center. An electric field oriented in the same direction, a positive electric field as indicated in Figure 4.24, therefore has an even greater effect on the charge separation in the reaction center than in the Fo state (case 2).

Before we discuss the net observed electric-field effect under these three conditions (shown in the third column), the excitation back transfer from the reaction center to the antenna must also be considered. Excitation transfer is represented in Figure 4.24 by horizontal arrows between the antenna and reaction center. The direction of excitation transfer from between the antenna complexes and the reaction center is indicated by the direction of the arrows, and the extent of this excitation transfer is qualitatively indicated by the thickness of the arrows. In the Fm state (case 1), the electric field-induced effect on charge separation in the reaction center is assumed to be negligible because the Fm state reaction center has a very low

probability of charge separation. Furthermore, in the Fm state there is no back transfer of excitation from the excited state special pair (P*) to the antenna, because P* is not formed in the Fm state (P^+). Therefore, the net observed electric-field effect in the Fm state (the third column in Figure 4.24) is the effect of the electric field only on the antenna fluorescence emission.

In the Fo state (case 2), the antenna transfers excitation efficiently to the reaction center (thick arrow). In our model, the rate of back transfer in the Fo state of *Rb. sphaeroides* is estimated to be 25% ± 5% (thin arrow), similar to the case measured for the closely related purple photosynthetic bacteria *Rs. rubrum*.[30] The net observed electric-field effect in this case is estimated as:

$$[\Delta \text{ antenna}] + (0.25 \times [\Delta \text{ reaction center}]) \qquad 4.5$$

In equation 4.5, [Δ antenna] is the electric field-induced change in the fluorescence from the antenna, and [Δ reaction center] is the electric field-induced change in fluorescence caused by an electric-field effect on charge separation in the reaction center. It should be noted that multiplication of [Δ reaction center] by 0.25 is only an estimated scaling factor, and is not a rigorous number. The model that we are presenting is a qualitative model, to explain the direction and relative magnitude of the effect of the electric field on the fluorescence emission.

Because the electric field affects the fluorescence emission in opposite directions in the antenna and the reaction center, the net observed electric-field effect is actually a subtraction of the effect on the antenna from the effect on the reaction center (*i.e.*, one of the terms [Δ antenna] or [Δ reaction center] is negative, depending on the direction of the applied electric field). Because the direction of the electric-field effect is reversed between the antenna and the reaction center, the net observed electric-field effect on the fluorescence is smaller in the Fo state than in the Fm state. In the Fm

state, only the electric-field effect on the antenna fluorescence is observed. In the Fo state, the electric field affects both the antenna fluorescence and the rate of charge separation in the reaction center.

In the Q_A^- state (case 3), the back transfer of excitation from the reaction center to the antenna is enhanced. When the primary quinone is reduced, the rate of back transfer from the reaction center to the antenna increases from 25 ± 5% to 40% ± 5% in *Rs. rubrum*.[24] Assuming that a similar situation holds in *Rb. sphaeroides*, the net electric-field effect is now estimated by:

$$[\Delta \text{ antenna}] + (0.40 \times [\Delta \text{ reaction center}]) \qquad 4.6$$

Terms in equation 4.6 are as defined previously. The scaling factor has increased to 0.40, to reflect the increased extent of back transfer of excitation from the reaction center to the antenna. In the Q_A^- state (case 3), the effect of the electric field on charge separation in the reaction center is magnified in the final observed net electric-field effect relative to the Fo state (case 2), where the back transfer of excitation is approximately 25%. Additionally, the electric-field effect in the reaction center itself is enhanced relative to the Fo state by the presence of the reduced quinone, as discussed previously. The net observed electric-field effect under these conditions is dominated by the change in fluorescence arising from an electric-field effect on charge separation in the reaction center. Therefore, the observed electric-field effect for the Q_A^- state is in the opposite direction to that observed in the Fm state (case 1) and Fo state (case 2).

This model is also consistent with the observed behavior of *Rb. sphaeroides* fluorescence in the absence of any externally applied electric field. Fluorescence in the Fm state is greater than in the Fo state, because in the Fo state a larger portion of the excitation from the antenna is siphoned to the reaction center (thick arrow in the Fo

state versus thin arrow in the Fm state). In the primary quinone reduced state (case 3, Q_A^-), back transfer from the reaction center to the antenna pool is increased (thick arrow), consistent with the experimental observations of increased back transfer under these conditions.[29]

The preceding model accounts for the magnitude and direction of the changes in fluorescence observed in *Rb. sphaeroides* chromatophores under conditions of externally applied electric fields.

Other support for an electric-field effect on the antenna fluorescence emission:

Our model of the electric-field effect in *Rb. sphaeroides* proposes that there is an electric-field effect directly on the antenna fluorescence emission. There is evidence in the literature to support the theory of an electric-field effect directly on antenna fluorescence emission. Gottfried *et al.* have studied LH2 isolated from *Rb. sphaeroides* and LH1 isolated from *Rb. capsulatus* under conditions of externally applied electric fields.[17]

LH2 antenna complexes from *Rb. sphaeroides*, suspended isotropically in 50% glycerol at 77 K, show small changes in absorption (approximately 0.2% at 850 nm) under an externally applied electric field of 2.8 x 10^5 V/cm. The majority of these small absorption changes can be accounted for by the Stark effect, which describes the difference in polarizability and dipole moment between the ground and excited states of a molecule. The Stark effect is manifest as a first or second derivative of the zero-field spectrum. However, in the fluorescence of LH2, Gottfried *et al.* find that there is a strong quenching of the fluorescence emission under an applied electric field.[17] The fluorescence emission of LH2 decreases by 1.2% in a field of 2.6 x 10^5 V/cm. This strong quenching cannot be described by a Stark effect.

LH1 antenna complexes isolated from *Rb. capsulatus* (which is closely related to *Rb. sphaeroides*) orientationally disordered in 50% glycerol at 77 K also show a strong fluorescence quenching under an applied electric field.[17] LH1 fluorescence emission decreases by approximately 1% in a field of 2.2 x 10^5 V/cm. Similar to the case for LH2, the absorption changes of LH1 under an applied field of 1.9 x 10^5 V/cm are much smaller (approximately 0.1% at 889 nm) than the electric-field effect on the fluorescence emission, and can be explained by a Stark effect on the absorption. However, the fluorescence quenching of LH2 under an applied field cannot be explained by a Stark effect. The explanation that Gottfried *et al.* have proposed for the electric-field quenching of LH1 and LH2 fluorescence is an electric-field enhanced coupling to an excited state of the antenna which has a very high rate of non-radiative decay.

These experiments show that there is an electric-field effect directly on the fluorescence emission of isolated LH1 and LH2. However, there are several differences between the isolated antenna studies and our experiments which must be noted. In the work of Gottfried *et al.*, the antenna complexes are isolated with detergents and suspended in 50% glycerol, and the experiments are conducted at 77 K. The antenna complexes are oriented isotropically with respect to the applied electric field. The fluorescence quenching of LH1 and LH2 is observed to be quadratic with applied field intensity. The electric field-induced fluorescence quenching is observed between 1.7 x 10^5 V/cm and 10^6 V/cm; below 1.7 x 10^5 V/cm no results are reported.

In our experiments, the antenna complexes are in the native intracytoplasmic membrane of *Rb. sphaeroides*, and our experiments are conducted at room temperature. The antenna complexes are oriented with respect to the applied electric field. The highest transmembrane potential difference attainable in our experiments is approximately 2 x 10^4 V/cm, about an order of magnitude less than the lowest field intensities reported for Gottfried *et al.*

The near-linear change in fluorescence that we observe in our experiments with oriented samples would mostly cancel for an isotropically disordered sample. This is consistent with the fact that at the electric-field intensities that are accessible in our experiments (2×10^4 V/cm), no electric-field effect was reported for the isotropic samples. Our experimental results for the electric field-induced change in fluorescence on the antenna (the Fm state results) are best fitted with a quadratic function. This is also consistent with the quadratic results from Gottfried *et al.* For example, assume that the quadratic function $y = ax^2 + bx + c$ is the function which gives the best fit to our experimental Fm state results. If the same experimental data were determined from an isotropic experiment, the function would have the form $y(x) + y(-x) = (ax^2 + bx + c) + (ax^2 - bx + c) = 2ax^2 + 2c$. This function derived from the isotropic experiment is also a quadratic function. Therefore, the quadratic change in fluorescence emission observed in the isotropic experiments of Gottfried *et al.* is consistent with the quadratic results obtained in our oriented experiments.

Speculation on the nature of the antenna state affected by the electric field:

One hypothesis that is consistent with both the results of Gottfried *et al.* and our own observations, invokes a second excited state of the antenna which is coupled to the initial antenna excited state. This second antenna excited state has a high non-radiative decay rate and is energetically shifted in an externally applied electric field. The second antenna state may be a subset of bacteriochlorophyll or an excitonic state within the manifold of excitonic states.[31]

Consider, as shown in Figure 4.25, an initial excited state of the antenna [Ant 1*] (dark solid line) and a second excited state of the antenna [Ant 2*] (light solid line) which has a very high rate of non-radiative excitation loss. The second excited state [Ant 2*] is energetically shifted by the presence of an external electric field. The

relative positions of the curves shown in Figure 4.25 are shown merely as one possible example; the energetic positions of the states are not known.

For small values of the electric field (short dashed lines in Figure 4.25), such as those attained in our salt-jump experiments, the electric field-induced change around the zero-field condition is small and in the pseudo-linear region of the curve crossing. The extent of the coupling between the initial state and the secondary state is enhanced for the direction of the electric field, which brings the secondary state closer to the activationless region (reducing the activation energy necessary to cross between states). Increased coupling to the secondary state results in more excitation being lost through non-radiative paths, and thus a quenching of fluorescence from the antenna. Conversely, the opposite orientation of the electric field raises the secondary state in energy, and decreases the extent of excitation reaching [Ant 2*]. Thus, less excitation is lost through non-radiative channels and the fluorescence emission increases in intensity. Because the direction of the energetic shift of [Ant 2*] depends on the orientation of the electric field, these small, approximately equal changes in fluorescence emission cancel for an isotropic orientation as in the experiments of Gottfried *et al.*

However, when the magnitude of the external electric field is large (long dashed lines in Figure 4.25), the state [Ant 2*] is shifted to an even greater extent. An electric field orientation which raises the energy of [Ant 2*] increases the level of the curve crossing well beyond the thermal energy available to reach the level of the curve crossing, and additional increases in energy do not further affect the fluorescence emission; the non-radiative path through [Ant 2*] is now energetically inaccessible. However, electric fields oriented in the opposite direction continue to increase the coupling to the non-radiative state (until the curve crossing is in the activationless region). Thus, the fluorescence quenching effect increases quadratically for an isotropic sample under very high electric fields.

It may be possible to test the model presented in Figure 4.25 by changing the excitation wavelength used to stimulate the emission in the isotropic experiment of Gottfried *et al.* If the proposed model is correct, a higher excitation energy (for example, into the Soret band of BChl or into a blue edge of the Qy band) may increase the energy available in the initial antenna excited state [Ant 1*], compared with the amount of energy available with a long-wavelength excitation (for example, into the center or red edge of the Qy band of BChl). If the rate of excitation transfer between the two states [Ant 1*] and [Ant 2*] is on the same timescale as intramanifold relaxation within [Ant 1*], the onset of fluorescence quenching as a function of the transmembrane potential difference will be shifted to higher field intensities. More energy in the initial excited state of the antenna [Ant 1*] will allow access to higher energy states of [Ant 2*]. Therefore, for an isotropic orientation, the effects from positive and negative oriented fields will cancel for a larger range of electric field magnitudes. For high energy excitation, larger electric fields would be required to produce the same quenching of the fluorescence emission that is observed for lower energy excitation.

What is the origin of this secondary excited state [Ant 2*] in the antenna complexes? One possible explanation why the energy of [Ant 2*] is affected by an electric field is that [Ant 2*] is a subset of BChl within the antenna that has substantial charge-transfer character. For example, a closely coupled dimer of BChl may produce an excited state containing a partial charge separation between the BChl molecules; the excited state wavefunction may have some character of $BChl^{+}BChl^{-}$. Or possibly one of the excitonic states within the antenna manifold may have a partially charge separated character. Such a state would be energetically shifted by the presence of an electric field. While the identity of such a subset of BChl is not known, it is possible that the red-shifted subset of BChl, which has been proposed for the LH1 and LH2

antenna complexes,[32] is the same subset with charge-transfer character in the excited state (see also Chapter 5).

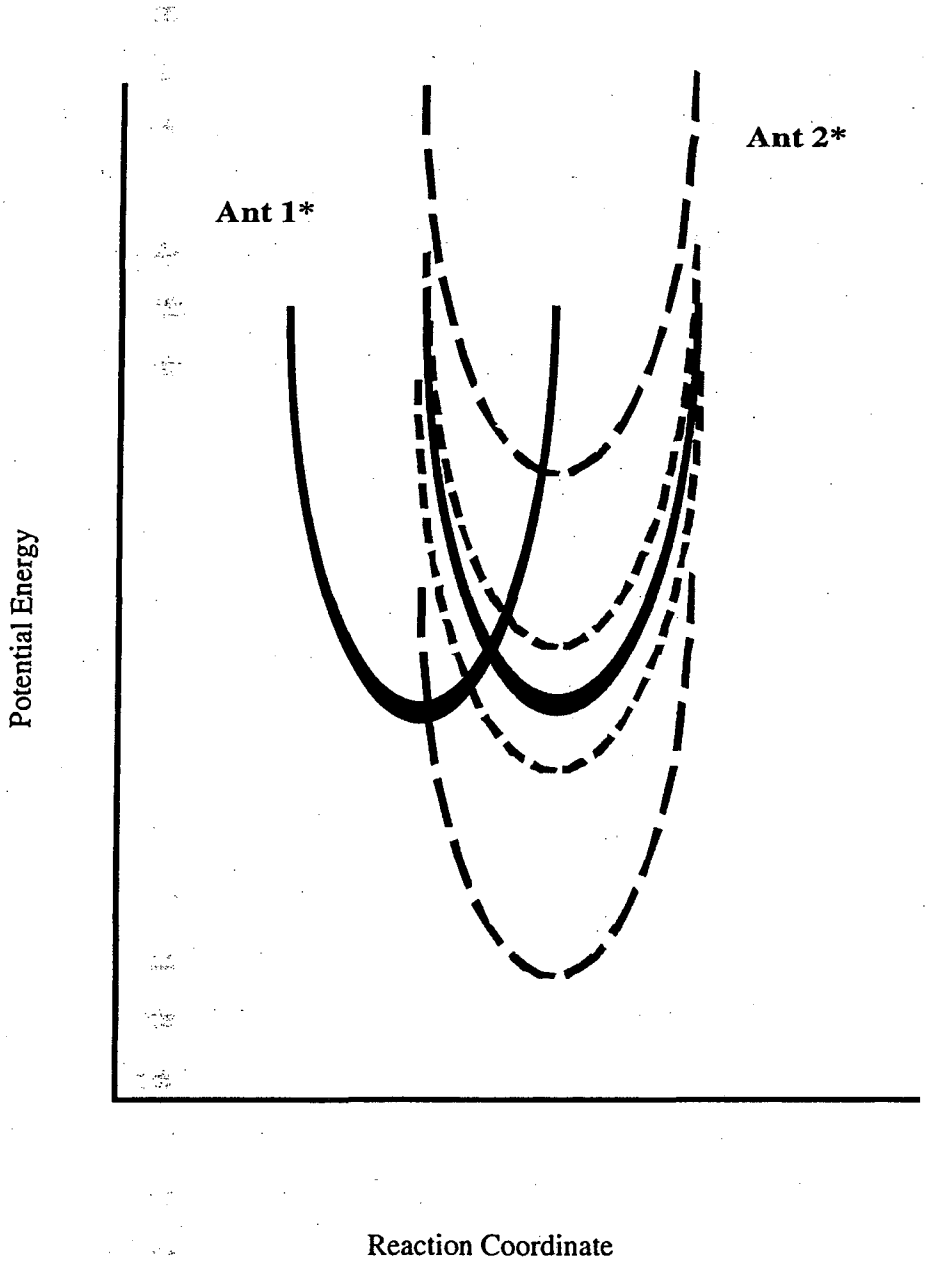

Figure 4.25: A theoretical second antenna state with a high non-radiative rate which is energetically shifted in the presence of an electric field. Dotted lines, low field intensity, dashed lines, high field intensity.

Comparison with theoretical work on charge separation:

If the model presented in Figure 4.24 is an accurate description of the origin of the fluorescence changes in *Rb. sphaeroides* under an applied field, then comparisons can be made with the theoretical predictions made by Bixon and Jortner,[5] as they relate to the mechanism of charge separation in the *Rb. sphaeroides* reaction center.

Our model proposes that the observed electric-field effect on the fluorescence is composed of two factors: the electric-field effect on charge separation in the reaction center, and the electric-field effect on the antenna complexes. Therefore, the effect of an electric field on the charge separation in the reaction center can be estimated by subtraction of the electric-field effect on the antenna complexes (ΔFm) from the net observed electric-field effect (ΔFo). This process produces an estimate for the change in fluorescence arising from the effect of an external electric field on charge separation in the *Rb. sphaeroides* reaction center (Figure 4.26). The fluorescence competing with charge separation increases for positive applied potentials and decreases for negative applied potentials. The change in fluorescence arising from the electric-field effect in the reaction center is approximately 11% per 100 mV.

In comparison with the theoretical predictions of an electric-field effect on charge separation, the one- and two-step models predict that the rate of charge separation will decrease for both positive and negative applied potentials, quadratically and symmetrically around the zero-field mark (Figure 4.3). Because charge separation and fluorescence emission compete for excitation, this indicates that the fluorescence emission will increase for both positive and negative potentials. This is clearly not the case observed experimentally; instead, the change in the fluorescence emission arising from an electric-field effect in the reaction center increases for positive potentials and decreases for negative potentials (Figure 4.26).

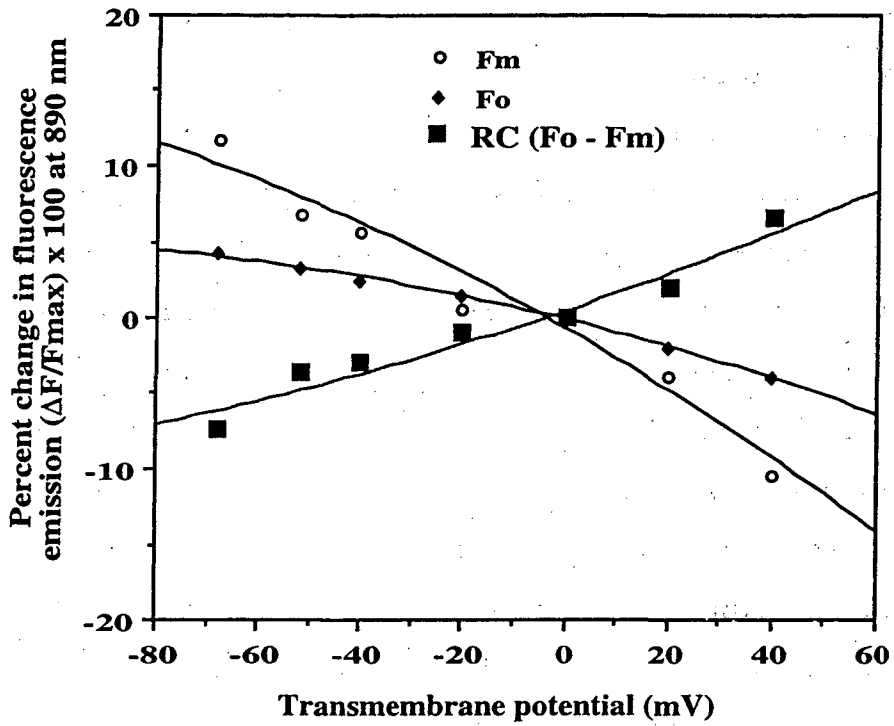

Figure 4.26: The electric field-induced change in Fm (circles), Fo (diamonds) and RC (squares), ΔF/Fmax x 100. RC points represent the effect on the fluorescence emission arising from an electric field-induced change in the rate of primary charge separation in the reaction center. RC is estimated from Fo - Fm.

In the superexchange case, the change in the charge separation rate is theoretically predicted to be asymmetric around the zero field mark. The superexchange theory predicts that the rate of charge separation in the reaction center will increase for negative applied potentials, and decrease for positive applied potentials. Our data is consistent with the superexchange rather than the two-step theory of charge separation in the reaction center. The compatibility of our experimental results with the superexchange model are not consistent with other experiments in the literature which identify a transient reduced bacteriochlorophyll

anion (B_A^-) absorption band at 1020 nm.[33,34] These experiments by Zinth *et al.* support the two-step theory of charge separation. We have no explanation for the discrepancy between these experimental results and our own at this time.

For comparison of our results with the theoretical predictions of Bixon and Jortner,[5] it is necessary to convert the fluorescence data from the form ΔF/Fmax x 100 (or [F(E) - F(0)] / F(0), which is a percent change in fluorescence emission) to F(E)/F(0) (a ratio of the fluorescence under conditions of an applied electric field to the zero-field fluorescence). Furthermore, since the charge separation rate and the fluorescence vary inversely from one another (an increase in the charge separation rate is reflected as a decrease in the fluorescence), the data for the fluorescence change are inverted to F(0)/F(E) for comparison with the ratio of rate constants k(E)/k(0) This direct comparison between the superexchange theory (open circles and squares) and the experimental data for the fluorescence change caused by an electric-field effect on the reaction centers of *Rb. sphaeroides* (filled circles) are displayed in Figure 4.27.

Two cases are shown for the superexchange theory in Figure 4.27, corresponding to different values of ∂E. Recall that ∂E is the energy difference between the virtual state P^+B^-H and the initial state P*BH (Figure 4.4). The value of ∂E is not known and is a free parameter in the fitting. The open circles represent a ∂E of 110 meV, and the squares represent a ∂E of 250 meV. The ΔG_o was estimated to be 250 meV for both cases, based on charge recombination data for detergent-isolated *Rb. sphaeroides* reaction centers.[8]

The experimental data [F(0)/F(E), filled circles] agree well with the superexchange predictions for the change in the rate of charge separation in the *Rb. sphaeroides* reaction center. A quadratic fit to the experimental data is also shown in Figure 4.27 (solid curve). The best fit between the experimental data and the superexchange theoretical model was obtained for a ∂E of 250 meV; fits were attempted for ∂E values between 110 meV and 300 meV.

The experimental data provide an excellent fit to the superexchange model, especially since the only parameter in the theoretical model that was allowed to vary was the energy of the virtual state P^+B^-H relative to the initial state P*BH (∂E).

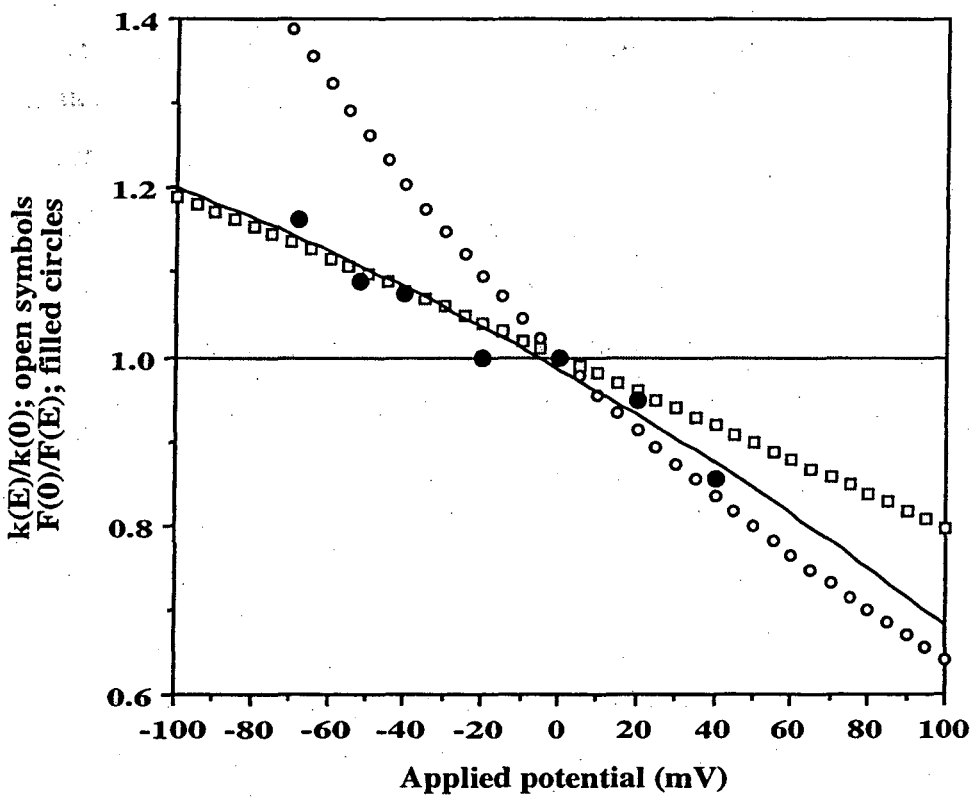

Figure 4.27: Comparison of the superexchange theory for the effect of an applied electric field on *Rb. sphaeroides* reaction centers (open symbols) and the experimental results on the change in fluorescence caused by an electric-field effect on *Rb. sphaeroides* reaction centers (closed symbols). Open squares, $\partial E = 250$ meV. Open circles, $\partial E = 110$ meV. $\Delta G_o = 250$ meV for both cases. See text for details.

Conclusions

Externally applied electric fields do influence the fluorescence emission of *Rb. sphaeroides* chromatophores. However, the fluorescence changes do not reflect a simple electric-field effect only on the rate of charge separation in the reaction center. Instead, our results are consistent with an additional electric-field effect directly on the fluorescence emission of LH1 and LH2 antenna complexes. The electric-field effect on the antenna complexes is observed most clearly in the Fm state of *Rb. sphaeroides*, when the probability of charge separation in the reaction center is minimal. In the Fm state, the fluorescence change is best fit as a quadratic function for all accessible voltages (+40 mV to -68 mV); the fluorescence emission increases for negative potentials and decreases for positive potentials. The change in fluorescence from the antenna complexes under conditions of an externally applied electric field is approximately 15% per 100 mV.

Support for the hypothesis of an electric-field effect directly on the antenna complexes of *Rb. sphaeroides* is provided by an electric field-induced change in the fluorescence emission of LM1.1, a mutant *Rb. sphaeroides* strain which expresses LH1 and LH2 but does not express functional reaction centers. Additional support for this hypothesis is found in the published literature; isolated antenna complexes from *Rb. sphaeroides* and *Rb. capsulatus* display strong fluorescence quenching under applied electric-field conditions which cannot be modeled by a Stark effect on the fluorescence.[17]

Our model for the observed fluorescence changes in *Rb. sphaeroides* chromatophores (see Figure 4.24) postulates that the electric-field effect on the antenna fluorescence is separate from the electric-field effect on charge separation in the reaction center. Thus, the electric-field effect on the charge separation rate in the

reaction center can be extracted from the observed data in the Fo state by subtraction of the electric-field effect on the antenna complexes in the Fm state.

The change in the fluorescence caused by an electric-field effect on the reaction center extracted from the Fo and Fm state data is estimated to be 11% per 100 mV. The fluorescence change shows an asymmetric, quadratic relation between the change in charge separation rate and the transmembrane potential difference. Comparison with theoretical predictions about the mechanism of charge separation in the reaction center show good agreement with the superexchange model of charge separation. Based on this model, the value of ∂E is estimated to be 250 meV from our experimental results.

References for Chapter Four

[1]Allen, J.P., Feher, G., Yeates, T.O., Komiya, H. & Rees, D.C. (1987) *Proc. Natl. Acad. Sci. USA* 84: 5730-5734.

[2]McDermott, G., Prince, S.M., Freer, A.A., Hawthornthwaite-Lawless, A.M., Papiz, M.Z., Cogdell, R.J. & Isaacs, N.W. (1995) *Nature (UK)* 374: 517-521.

[3]Martin, J.-L., Breton, J., Hoff, A.J., Migus, A. & Antonetti, A. (1986) *Proc. Natl. Acad. Sci. USA* 83: 957-961.

[4]Prince, R.C., Baccarini-Melandri, A., Hauska, G.A., Melandri, B.A. & Crofts, A.R. (1975) *Biochim. Biophys. Acta* 387: 212-227.

[5]Bixon, M. & Jortner, J. (1988) *J. Phys. Chem.* 92: 7148-7156.

[6]Marcus, R.A. (1956) *J. Chem. Phys.* 24: 966-979.

[7]Bixon, M., Michel-Beyerle, M.E. & Jortner, J. (1988) *Isr. J. Chem.* 28: 155-168.

[8]Moser, J.E. & Gratzel, M. (1993) *Chemical Physics* 176: 493-500.

[9]Ogrodnik, A. (1990) *Biochim. Biophys. Acta* 1020: 65-91.

[10]Dau, H. & Sauer, K. (1991) *Biochim. Biophys. Acta* 1098: 49-60.

[11]Bixon, M., Jortner, J., Michel-Beyerle, M.E. & Ogrodnik, A. (1989) *Biochim. Biophys. Acta* 977: 273-286.

[12]Lockhart, D.J. & Boxer, S.G. (1988) *Proc. Natl. Acad. Sci. USA* 85: 107-111.

[13]Lockhart, D.J. & Boxer, S.G. (1988) *Chem. Phys. Lett.* 144: 243-250.

[14]Lockhart, D.J., Hammes, S.L., Franzen, S. & Boxer, S.G. (1991) *J. Phys. Chem.* 95: 2217-2226.

[15]Ogrodnik, A., Langenbacher, T., Bieser, G., Siegl, J., Eberl, U., Volk, M. & Michel-Beyerle, M.E. (1992) *Chem. Phys. Lett.* 198: 653-658.

[16]Popovic, Z.D., Kovacs, G.J., Vincett, P.S., Alegria, G. & Dutton, P.L. (1986) *Biochim. Biophys. Acta* 851: 38-48.

[17]Moser, C., Alegria, G., Gunner, M.R. & Dutton, P.L. (1988) *Isr. J. Chem.* 28: 133-139.

[18]Gottfried, D.S., Stocker, J.W. & Boxer, S.G. (1991) *Biochim. Biophys. Acta* 1059: 63-75.

[19]Dau, H. & Sauer, K. (1992) *Biochim. Biophys. Acta* 1102: 91-106.

[20]Zankel, K. L.; Reed, D.W. & Clayton, R.K. (1968) *Proc. Natl. Acad. Sci. USA* 61: 1243-1247.

[21]De Grooth, B.G. & Amesz, J. (1977) *Biochim. Biophys. Acta* 462: 237-258.

[22]Crielaard, W., Hellingwerf, K.J. & Konigs, W.N. (1989) *Biochim. Biophys. Acta* 973: 205-211.

[23]Godik, V.I. & Borisov, A.Y. (1980) *Biochim. Biophys. Acta* 590: 182-193.

[24]Parson, W.W., Clayton, R.K. & Cogdell, R.J (1975) *Biochim. Biophys. Acta* 387: 265-278.

[25]Zannoni, D. & Marrs, B.L. (1981) *Biochim.Biophys.Acta* 637: 96-106.

[26]Armitage, J.P. & Evans, M.C. (1981) *FEBS Lett* 126: 98-102.

[27]Jackson, J.B. & Goodwin, M.G. (1993) *Biochim. Biophys. Acta* 1144: 199-203.

[28]Bixon, M. & Jortner, J. (1991) *J. Phys. Chem.* 95: 1941-1944.

[29]Wasielewski, M.R. & Tiede, D.M. (1986) *FEBS Lett.* 204: 368-372.

[30]Timpmann, K., Zhang, F.G., Freiberg, A. & Sundström, V. (1993) *Biochim. Biophys. Acta* 1183: 185-193.

[31]Freer, A.A., Prince, S.M., Sauer, K., Papiz, M.Z., Hawthornthwaite-Lawless, A.M., McDermott, G., Cogdell, R.J. & Isaacs, N.W. (1996) *Structure* 4: 449-462.

[32]Novoderezhkin, V.I. & Razjivin, A.P. (1995) *Biophys. J.* 68: 1089-1100.

[33]Arlt, T., Schmidt, S., Kaiser, W., Lauterwasser, C., Meyer, M., Scheer, H. & Zinth, W. (1993) *Proc. Natl. Acad. Sci.* 90: 11757-11761.

[34]Arlt, T., Dohse, B., Schmidt, S., Wachtveitl, J., Laussermair, E., Zinth, W. & Oesterhelt, D. (1996) *Biochemistry* 28: 9235-44.

Chapter Five:

The Kennard-Stepanov relation applied to *Rb. sphaeroides* wild type and mutant strains

Introduction:

The Kennard-Stepanov relation is a useful means of examining energy transfer and equilibration processes in a variety of systems.[1,2] Because the energy transfer and equilibration processes in *Rb. sphaeroides* are not yet fully understood, we will use the Kennard-Stepanov relation to examine these processes in *Rb. sphaeroides* wild type, as well as in several *Rb. sphaeroides* mutants. The availability of *Rb. sphaeroides* mutants provides a unique opportunity to investigate excitation equilibration in greater depth for this photosynthetic system. The mutants used in this study are lacking parts of the photosynthetic apparatus; one of the light harvesting complexes (LH1 or LH2), and/or the reaction center. These *Rb. sphaeroides* mutants selectively remove components from the photosynthetic apparatus. We can then investigate the effect of removing that photosynthetic component on the excitation transfer and equilibration among the remaining components. Deconstructing the photosynthetic system in this way will give us insights as to how the different components of the *Rb. sphaeroides* photosynthetic system function in the process of excitation transfer and energy equilibration.

The Kennard-Stepanov (KS) relation is derived from the Einstein coefficients for absorption and spontaneous emission.[3,4] There are several key assumptions which form the foundation of the Kennard-Stepanov relation, and these assumptions must be met by the experimental system for the KS relation to be valid for that system. These assumptions include: the system is homogenous,[5] the Franck-Condon principle is

obeyed, the absorption and fluorescence transitions are strongly allowed, and the excited state is completely thermally relaxed before fluorescence emission occurs. When these conditions are met, the KS relation describes a linear relationship between the absorption and fluorescence spectra.

The Kennard-Stepanov temperature, T*, can be deduced from the slope of the KS relation. If all the assumptions underlying the KS relation are valid, T* should match the ambient temperature T. Strictly speaking, all of the assumptions hold only for very simple systems, such as the absorption and fluorescence of single atoms. Even for relatively simple systems, such as fluorescent dyes, the KS relation is not always valid.[6,7] Despite this fact, the Kennard-Stepanov relation has been applied to much more complicated systems including chlorophyll,[8] bacteriochlorophyll,[9] and pigment-protein complexes such as phycobilisomes,[10] photosystem I (PSI)[11] and photosystem II (PSII).[12] These are complex, non-homogenous systems which do not fit all of the assumptions of the KS relation. Nevertheless, these systems frequently do display a linear relation between absorption and fluorescence as predicted by the KS relation. In addition, the calculated KS temperature T* is often close to the ambient temperature at which the measurements are taken. Close agreement with the KS relation is generally taken as an indication that the excitation in the system has reached a thermally relaxed equilibrium before fluorescence emission occurs: that excitation equilibration throughout the entire system is rapid on the time scale of fluorescence emission.

The Kennard-Stepanov relation itself may be expressed in various forms. A useful representation of the relation is:

$$F(\nu) = \ln [hc\, I(\nu) / 8\pi\nu^4\sigma(\nu)] = - hc\nu / k_B T^* + D(T) \qquad [5.1]$$

where h is Planck's constant, c is the velocity of light, k_B is Boltzmann's constant, T* is the Kennard-Stepanov temperature, D(T) is a term that depends only on temperature,

$\sigma(\nu)$ is the absorption spectrum on a frequency scale, and $I(\nu)$ is the fluorescence spectrum in photons / [second (nm bandwidth)] on a frequency scale. A plot of $F(\nu)$ versus ν will give a slope of $- hc / k_B T^*$. Since h, c and k_B are constants, the Kennard-Stepanov temperature, T*, can be extracted from the slope. If all the assumptions that are used in the derivation of the KS relation are valid, T* will be the ambient temperature.

The calculated T* is an average value over the slope of the line derived from the overlapping portion of the absorption and fluorescence emission spectra $\sigma(\nu)$ and $I(\nu)$. Of course, the slope derived from the KS relation is most accurate over the regions of highest signal-to-noise in the experimental absorption and fluorescence spectra. This is the Stokes region. Away from the maxima of the spectra, where the absorption or fluorescence are near zero, $F(\nu)$ becomes unreliable.

Deviations from the Kennard-Stepanov relation in the Stokes region can be instructive. There are several possible reasons for such deviations. One reason is that the excitation has not reached thermal relaxation before fluorescence emission occurs. This is known as warm fluorescence. A characteristic of warm fluorescence is that the apparent temperature given by the KS relation increases with increasing excitation energy.

Another possible reason for deviation from the KS relation is an inhomogeneity in the system. This may be caused by an impurity or multiple species in the system. Inhomogenous broadening of a pure system will also cause deviations from the ideal KS relation. Inhomogenous broadening may be caused by solvent-pigment interactions, protein-pigment interactions, or multiple configurational states of the system either in the ground or excited states.

A third possibility is the presence of non-equilibrated subsystems within the system. In this case, two or more subsystems within the system may not come to full

equilibrium with each other before fluorescence emission occurs. Each individual subsystem, however, may obey the KS relation independently.

Extended Kennard-Stepanov theory:

More information can be extracted from the absorption and fluorescence spectra of a system by looking at the local slope of the Kennard-Stepanov relation as it varies across the frequency ν. This is called the extended KS theory as developed by Sawicki and Knox.[13] This local slope of F(ν) often reveals interesting structure, such as flat plateaus which correspond to spectral regions where the T*(ν) is a constant value. The local slope can also show peaks or valleys, where the T*(ν) changes sometimes dramatically in a particular spectral region. Sawicki and Knox have proposed one model to explain some of the peaks that may be seen in the T*(ν) plots. We will briefly review this model.

The Sawicki-Knox model[11] is composed of two or more subsystems which independently obey the KS relation, but which have not reached complete equilibrium between themselves before fluorescence occurs. These subsystems may represent distinct molecular species, or may represent two states of a single unimolecular system. Their model calculations have shown that the position and magnitude of the peak in T*(ν) depends on the relative position of the subsystems' absorption and fluorescence, the oscillator strength of each component, and the rate of excitation transfer (k) between the subsystems. Of course, as the rate of excitation transfer between the two subsystems increases, the subsystems come closer to excitation equilibration and the magnitude of the T*(ν) peak decreases. Their model requires a rate constant for excitation transfer between the two subsystems less than 10 times the fluorescence rate constant to produce a noticeable peak in T*(ν).

We will apply the Sawicki-Knox method of extended Kennard-Stepanov analysis to the absorption and fluorescence spectra of intracytoplasmic membrane preparations from *Rb. sphaeroides* mutants and wild type.

Kennard-Stepanov applied to photosynthetic systems:

Before presenting our data, however, it will be instructive to review the results of applying the KS relation to related systems. The *Rb. sphaeroides* system is complex and inhomogenous. Because even single molecules can produce complicated T*(ν) plots, it may seem ambitious to apply the KS analysis to inhomogenous pigment-protein complexes. However, interesting information can be extracted even from complex systems, such as *Rb. sphaeroides.*

Bacteriochlorophyll a (BChl), the bacteriochlorophyll pigment that is found in *Rb. sphaeroides* wild type as well in the mutant strains, has been investigated as a single molecule in a variety of organic solvents. Becker *et al.*[7] examined the absorption and fluorescence spectra of BChl in five polar solvents and found that the KS temperatures are higher than the ambient temperature (296 K) by 20 to 40 degrees Kelvin. Becker *et al.* also examined bacteriopheophytin a (BPheo), another pigment which is found in the reaction center of *Rb. sphaeroides* wild type, in two polar solvents. BPheo also had a KS temperature elevated above ambient temperature by 20 to 40 degrees Kelvin. The elevated KS temperatures are explained as being caused by inhomogenous broadening and vibronic mixing in the excited state.

Bellacchio and Sauer[14] have also investigated the spectral properties of BChl in several organic solvents. At low temperatures, they find that the Kennard-Stepanov relation breaks down dramatically in hydrogen-bond donating solvents such as 1-propanol. At room temperature, the calculated KS temperature in a variety of organic solvents is only slightly elevated from the ambient temperature (296 K) by about 10 to 30 K. The measurements at room temperature are most relevant to the following

discussion because our Kennard-Stepanov measurements on *Rb. sphaeroides* wild type and mutants are all performed at room temperature. Bellacchio and Sauer also calculate the local slope of the KS relation, T*(ν). The local slope of T* calculated for BChl in 1-propanol at room temperature (296 K) is flat across the region of maximum overlap between the absorption and fluorescence spectra, but elevated at the red and blue edges of the spectra up to 400 K (100 K above ambient temperature).

Chlorophyll a (Chl a) has also been investigated through application of the Kennard-Stepanov relation.[15] Most recently, Knox et al.[16] have examined the absorption and fluorescence spectra of Chl a in various polar organic solvents, as well as in peridinin - Chl a protein complexes. They find that the T*(ν) deviates significantly from the ambient temperature on the red edge of the fluorescence spectra for Chl a in a variety of solvents. The local slope of the KS temperature in this region is extremely elevated above ambient temperature, into the thousands of Kelvins. The increase of T*(ν) on the red edge of the fluorescence spectrum is also present in the peridinin-Chl a protein complexes. The maximum of the elevated T* occurs near an energy of 1.8 eV, in a region where the absorption intensity is very low. However, a significant increase in KS temperature is evident even at higher energy, in a spectral region where there is still appreciable absorption. Knox et al. hypothesize an electronic triplet state below the S_1-S_0 fluorescence transition which contributes to fluorescence emission on the red edge. This electronic state is proposed to explain the elevated T* on the red edge of the fluorescence emission.

Chlorophyll has also been investigated through the KS relation in Photosystem II (PSII). Dau and Sauer have studied exciton equilibration in PS II using membrane particles from spinach.[10] These membrane particles contain Chl b as well as Chl a in a large pigment-protein complex. There are approximately 200-300 chlorophyll molecules per PS II complex, and there are at least six distinct spectral species of chlorophyll evident from gaussian deconvolution of the absorption and fluorescence

bands. The PS II system is spectrally heterogeneous and complex. However, PS II is in good agreement with the predicted Kennard-Stepanov relation. At room temperature, Dau and Sauer find that the KS temperature matches very closely the ambient temperature (295 K) over the entire wavelength range of the chlorophyll absorption (700 to 645 nm). Dau and Sauer also note that the fluorescence emission spectra of PS II are identical regardless of the wavelength of the excitation light. Because PS II fluorescence is insensitive to excitation wavelength, and because PS II obeys the Kennard-Stepanov relation closely at room temperature, Dau and Sauer conclude that excitation in PS II reaches a complete equilibrium across all spectral components before fluorescence emission occurs.

Chlorophyll has also been studied through application of the KS relation to Photosystem I (PS I). Croce *et al.*[11] examined detergent-isolated PS I with a full antenna complement (LHCI), which has a total of about 210 Chl per P700 (P700 is the primary donor species in PS I). Croce *et al.* use the KS relation to calculate the "ideal" fluorescence emission from the absorption spectrum. This ideal fluorescence is that which would be observed if the KS relation were valid for the PSI - LHCI complex. The fluorescence spectrum calculated from the KS relation at room temperature is in very close agreement with the experimental room temperature fluorescence emission of the PS I - LHCI complex. Therefore, at room temperature the KS relation describes the system well, and Croce *et al.* conclude that the PSI - LHCI complex did reach complete thermal equilibrium before fluorescence emission occurred. In contrast, at temperatures below about 200 K, the agreement with the calculated KS fluorescence emission is lost. The authors postulate that at low temperatures, thermal equilibration of excitation in the antenna and core complex of PSI is not attained on the time scale of fluorescence emission.

In conclusion, KS analysis provides valuable information about even complex photosynthetic systems. Although these systems are inhomogenous, many

photosynthetic systems show good agreement with the Kennard-Stepanov predictions. These systems have very rapid excitation equilibration among all the photosynthetic components on the timescale of fluorescence emission.

Kennard-Stepanov applied to *Rb. sphaeroides* strains:

Next we will turn our attention to the Kennard-Stepanov relation at room temperature as applied to wild-type and mutant strains of *Rb. sphaeroides.* In order to make these measurements, chromatophores are isolated from the different *Rb. sphaeroides* strains as described in Chapter Two. The buffer used for washing and resuspension of the chromatophore membranes is Buffer A as described in Chapter Two: 5 mM $MgCl_2$, 5 mM HEPES, 800 mM sucrose and 100 mM KCl at pH 7.5. However, the concentration of the chromatophore solution is much more dilute than the solution used for the electric-field experiments described in Chapter Three. The absorption of the chromatophore solution is approximately $A_{880} = 0.01$. This low concentration is used to prevent self-absorption of the fluorescence emission, which could produce artifacts in the KS relation. Because of the very low concentrations used in the KS experiments, it is necessary to average the absorption and fluorescence emission for relatively long periods of time. Several scans are summed to improve the signal-to-noise.

Absorption measurements are performed on an AVIV UV-vis-IR spectrophotometer model 14-DS, with a fixed bandpass of 0.25 nm, in the configuration described in Chapter Two. Measurements are made every 1 nm, averaged for 1 second per nm, in a polystyrene cell of cross-section 1 cm^2. Eight to ten scans are summed together to generate the final absorption spectrum. A sample cell containing buffer only is measured before each scan as a background correction. The buffer scan is subtracted from each absorption scan.

Fluorescence measurements are made on a Spex Fluorolog 1680 double monochromator, in the configuration described in Chapter Two. Measurements are made every 1 nm, averaged for 5 seconds per nm, in a polystyrene cell of cross-section 1 cm^2. Five to ten scans are summed together to generate the final fluorescence spectrum. Both excitation and emission slits are set at or below 2 nm FWHM for both excitation and emission. The wavelength dependence of the fluorimeter emission path and photomultiplier tube is corrected with a standard lamp calibration, as described in Chapter Two. The background counts, averaging between 30 and 90 counts per second, are subtracted from the fluorescence emission spectra as a baseline correction.

The ambient temperature is determined with a mercury thermometer inside the sample compartment of the fluorimeter and absorption spectrophotometer. The ambient temperature is 23 °C ± 2 °C, or approximately 296 K.

The Kennard-Stepanov relation is calculated from the areas of maximum overlap between the absorption and fluorescence spectra. The edges of the spectra, less than 5% of the intensity of the maximum, are not used in the KS calculations.

RC-1A results (LH1 only):

The mutant RC-1A expresses LH1 complexes, without LH2 or reaction centers. Fluorescence emission can be generated by excitation at various wavelengths. Excitation at 510 nm excites electronic transitions primarily in the carotenoid molecules associated with LH1 (and LH2 if present). These carotenoid molecules transfer excitation energy efficiently to BChl in LH1. Excitation at 375 nm is primarily into the Soret absorption band, consisting of both the Bx and By bands of BChl. Excitation at 590 nm is primarily into the Qx band of BChl. These excitation wavelengths (510, 375, or 590 nm) all generate nearly identical fluorescence spectra in the long-wavelength region, between 800 and 1000 nm. The long-wavelength fluorescence emission in this region arises from the Qy transition of BChl. Over almost all of this

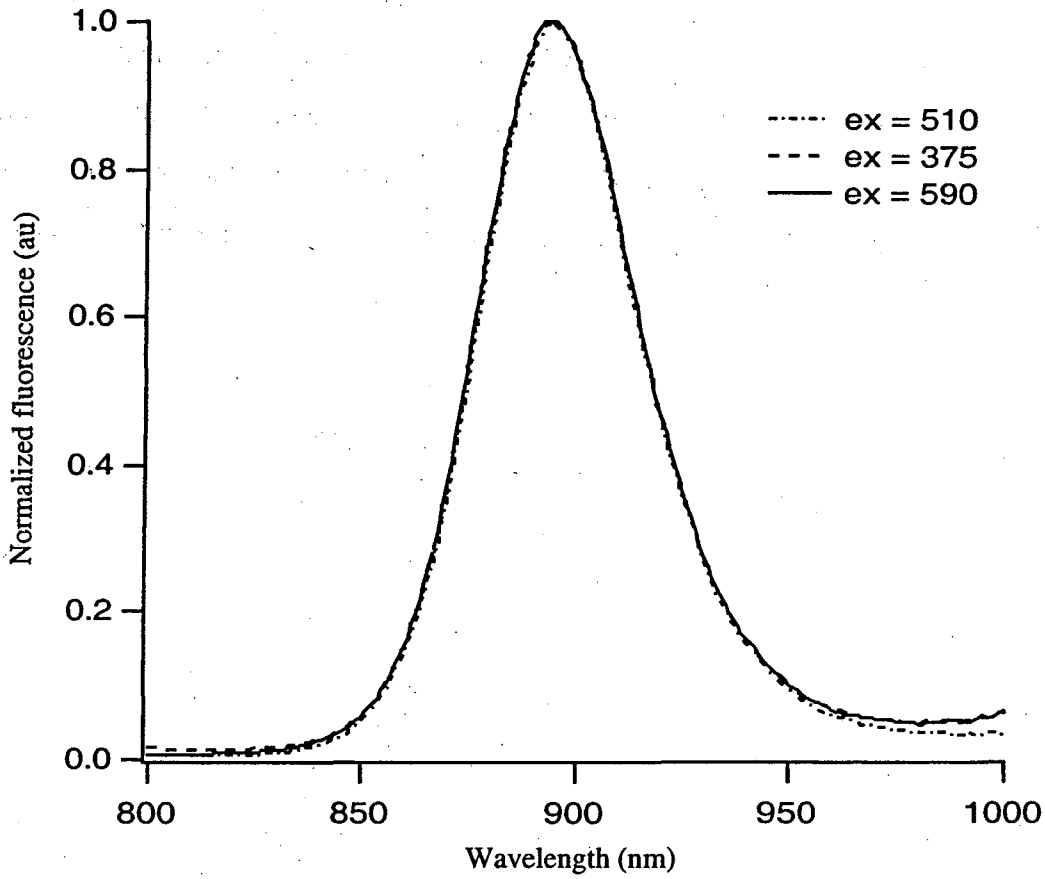

Figure 5.1: Fluorescence emission of RC-1A (expressing LHI) excited by three different excitation wavelengths. Excitation at 375 nm (dashed line), 510 nm (dash/dot line) and 590 nm (solid line). The spectra are all taken at room temperature and normalized at the maxima. The same sample is used for all excitation wavelengths. See the text for details of the fluorimeter configuration, buffer and concentration.

long-wavelength region, the fluorescence spectra generated by different excitation wavelengths are indistinguishable within the detection limits of our equipment (Figure 5.1). There is a slight deviation at very long wavelength (greater than 950 nm) where the intensity of the fluorescence emission is low; deviation in this region does not affect the KS calculations. The fact that the spectra are so very well matched for different

excitation wavelengths is one indication that, before fluorescence emission occurs, the excitation in the LH1 complex of RC-1A has reached an equilibrium distribution.

Both the fluorescence emission and absorption spectra of RC-1A are shown in Figure 5.2, as a function of frequency rather than wavelength. Excitation at 375 nm is used to generate this fluorescence emission. The fluorescence spectrum represented as

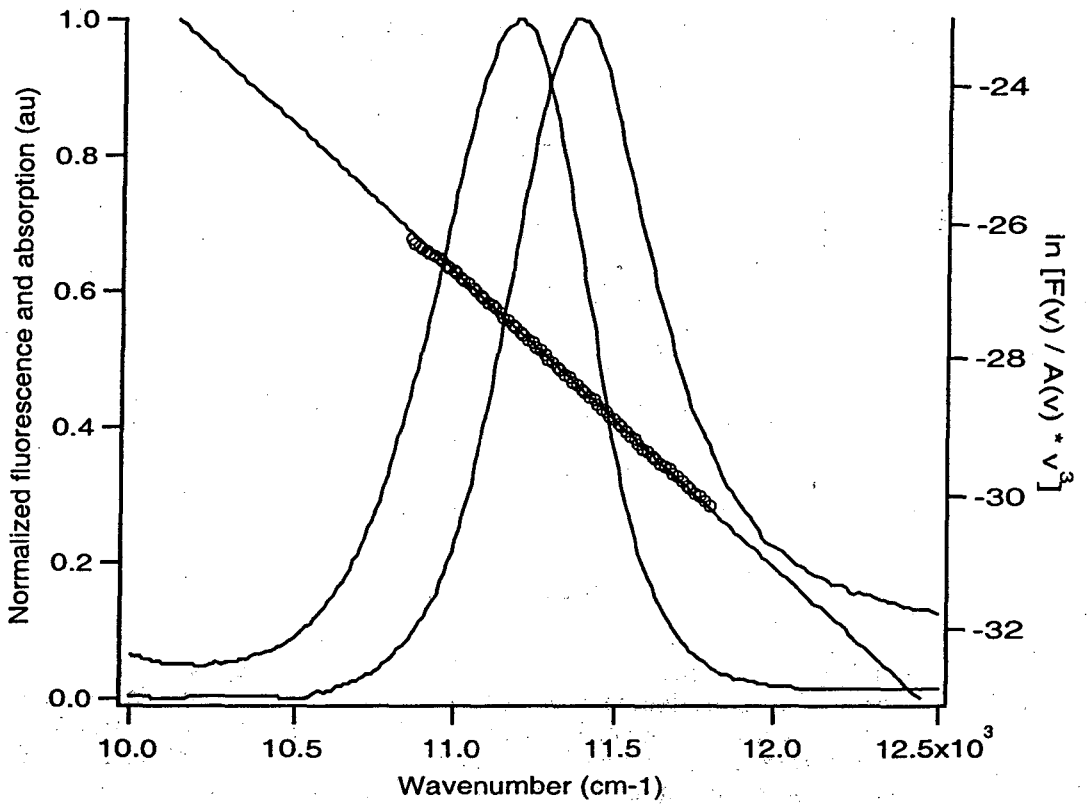

Figure 5.2: The fluorescence and absorption spectra of RC-1A, plotted as a function of frequency and normalized at the maxima. This fluorescence spectrum was generated with excitation at 375 nm. The fluorescence spectrum has been divided by a correction factor of ν^2 as described in the text. The Kennard-Stepanov relation for RC-1A is plotted against the right axis (open circles). The straight line is a least-squares fit to the Kennard-Stepanov relation in the Stokes region. The slope of the line corresponds to a T* value of 330 K; the spectra were taken at 296 K.

a function of frequency has been divided by a factor of ν^2; $F(\nu) = F(\lambda) / \nu^2$. This correction is necessary because the fluorescence spectrum is recorded on an instrument as a function of wavelength, with a fixed bandpass, but the bandpass is variable with frequency. This correction factor converts the fluorescence measurement from photons per wavelength interval to energy per frequency interval. The correction is applied to all fluorescence spectra in this chapter which are presented as a function of frequency. The absorption and fluorescence spectra have both been normalized at their maxima to a value of 1.00. The area of maximum overlap between the two spectra lies approximately between 10,750 cm^{-1} and 11,750 cm^{-1}. At higher frequency, the intensity of the fluorescence spectrum is very low; at lower frequency, the intensity of the absorption spectrum is small.

Figure 5.2 also shows the Kennard-Stepanov relation calculated for RC-1A, plotted against the right axis, as a function of frequency (open circles). Within the area of maximum overlap between the two spectra, to first approximation the KS relation represents a straight line. A least-squares fitting of the KS relation in the region of maximum spectral overlap yields a slope corresponding to a KS temperature of 330 K. Both the fluorescence and absorption spectra are taken at 296 K. The calculated KS temperature is about 30 K higher than predicted from the ideal KS relation.

The local slope of the KS relation, $T^*(\nu)$, is plotted in Figure 5.3 as a function of frequency for all three excitation wavelengths. For all $T^*(\nu)$ spectra, the window used to calculate the local derivative is nine data points. At the edges of the spectra, where either the absorption or fluorescence intensity is very low, the calculated $T^*(\nu)$ has been truncated. This is because in regions of low spectral intensity the KS relation becomes unreliable, which leads to large fluctuations in the $T^*(\nu)$ plot.

The three $T^*(\nu)$ spectra generated by the three different excitation wavelengths show many similarities. The three fluorescence spectra which are generated by three

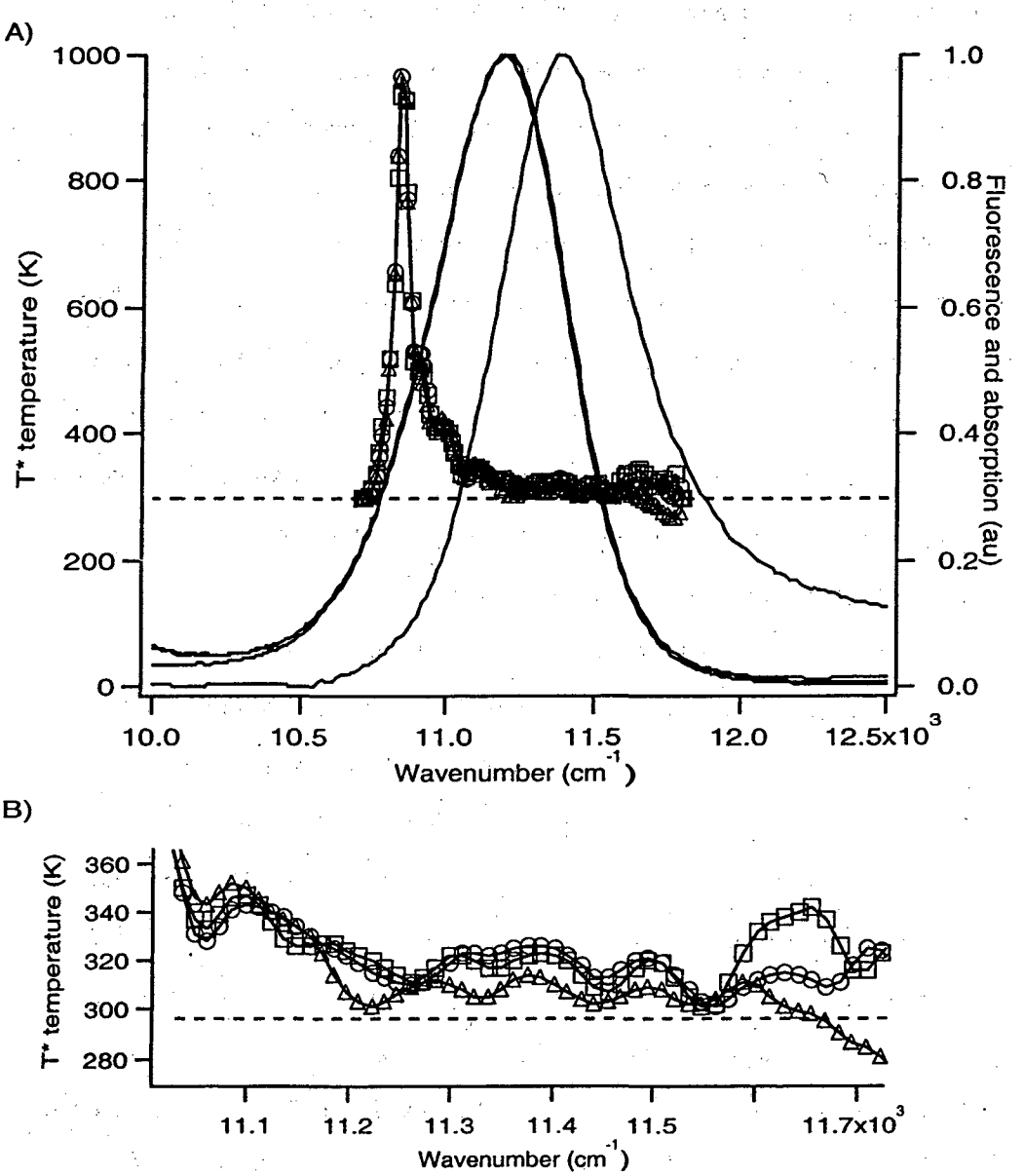

Figure 5.3: A) The local slope of the Kennard-Stepanov relation, T*(ν), for RC-1A shown on a temperature scale. Three different T*(ν) are shown, corresponding to three excitation wavelengths. Circles, excitation at 590 nm; squares, excitation at 375 nm; triangles, excitation at 510 nm. The absorption and the three fluorescence spectra generated by those three excitation wavelengths are plotted against the right axis. The horizontal line indicates ambient temperature, 296 K.

B) An expanded view of T*(ν) for RC-1A from 11,000 cm^{-1} to 11,750 cm^{-1}. The horizontal line indicates ambient temperature, 296 K.

different excitation wavelengths (375, 510, and 590 nm) are displayed together in Figure 5.3. Across the midrange of frequency values (11,000 cm^{-1} to 11,500 cm^{-1}), T*(ν) is mostly flat and featureless and is just slightly elevated above the room temperature value of 296 K (dashed line). However, on the red edge of the spectra below 11,000 cm^{-1}, T*(ν) shows a definite and strong peak of nearly 1000 K. The peak at the red edge is very reproducible for all the excitation wavelengths. In this region the fluorescence and absorption spectra intensity are both quite significant, and therefore the peak in the T*(ν) plot is not due to fluctuations in the KS relation arising from low spectral intensities. There is also a small feature on the blue edge of the spectra. The feature on the blue edge is not reproducible. There is a small peak present for excitation at 375 which is less prominent for 590 nm excitation, and is replaced by a small red-shifted negative feature with 510 nm excitation.

It is possible to generate an ideal KS fluorescence spectrum, I*, based on the absorption spectrum and the ideal KS relation. This I* fluorescence spectrum is the fluorescence that would be generated if the experimental system fully obeyed all the assumptions used in the derivation of the Kennard-Stepanov theory. The KS theory predicts a mirror-image relationship between the absorption and fluorescence spectra. The calculated I* fluorescence emission for RC-1A is shown in Figure 5.4. The experimentally observed absorption and fluorescence (dotted lines) are also displayed in Figure 5.4. The I* fluorescence spectrum is truncated at 10,600 cm^{-1}, because at lower frequency the absorption intensity is low and the KS relation becomes unreliable.

The I* fluorescence of RC-1A is slightly red-shifted from the experimentally observed fluorescence and broader on the red edge. The largest difference from the experimental fluorescence is on the red edge of the fluorescence, in the region where the large T*(ν) peak is observed. On the red edge of the emission, the experimental fluorescence has a much lower intensity than is calculated from the ideal KS relation.

This may indicate that a long-wavelength component in that red-edge region is not as highly fluorescent as predicted by the ideal KS relation.

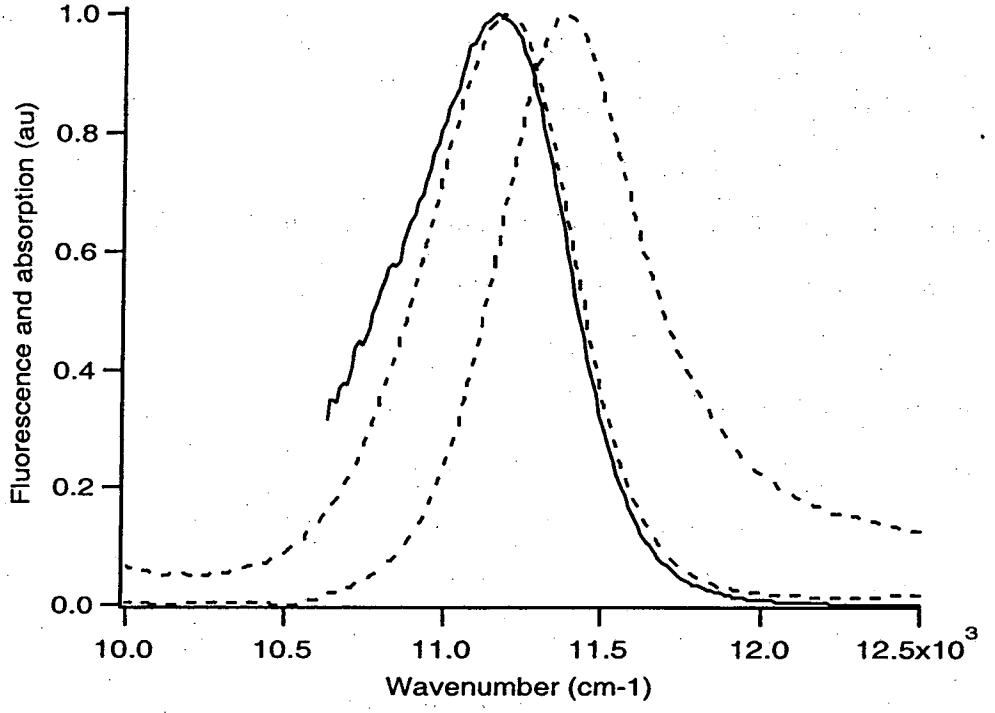

Figure 5.4: Experimental absorption and fluorescence of RC-1A (dotted lines), and the I* fluorescence calculated from the experimental absorption and the ideal Kennard-Stepanov relation at 296 K (solid line).

BALM/LH2 results (LH2 only):

The mutant BALM/LH2 contains LH2 complexes, without LH1 or reaction centers. Four wavelengths (375, 510, 590, and 800 nm) are used to generate fluorescence emission, shown in Figure 5.5. Absorption at 375 nm, 510 nm, and 590 nm are into absorption bands as described in the previous section. Excitation at 800 nm is in one of the Qy transition bands of LH2 BChl absorption. Each of these four excitation wavelengths produces nearly identical fluorescence emission from

BALM/LH2 in the long-wavelength region (800-1000 nm). On the very low-intensity blue edge below 825 nm there is a slight variation in the fluorescence emission; this is outside the range used for the KS calculations. Over the majority of the spectrum, fluorescence produced by different excitation wavelengths is indistinguishable within the limits of our detection. This is one indication that before fluorescence emission occurs in the *Rb. sphaeroides* mutant BALM/LH2, the excitation in the LH2 complex has reached an equilibrium distribution.

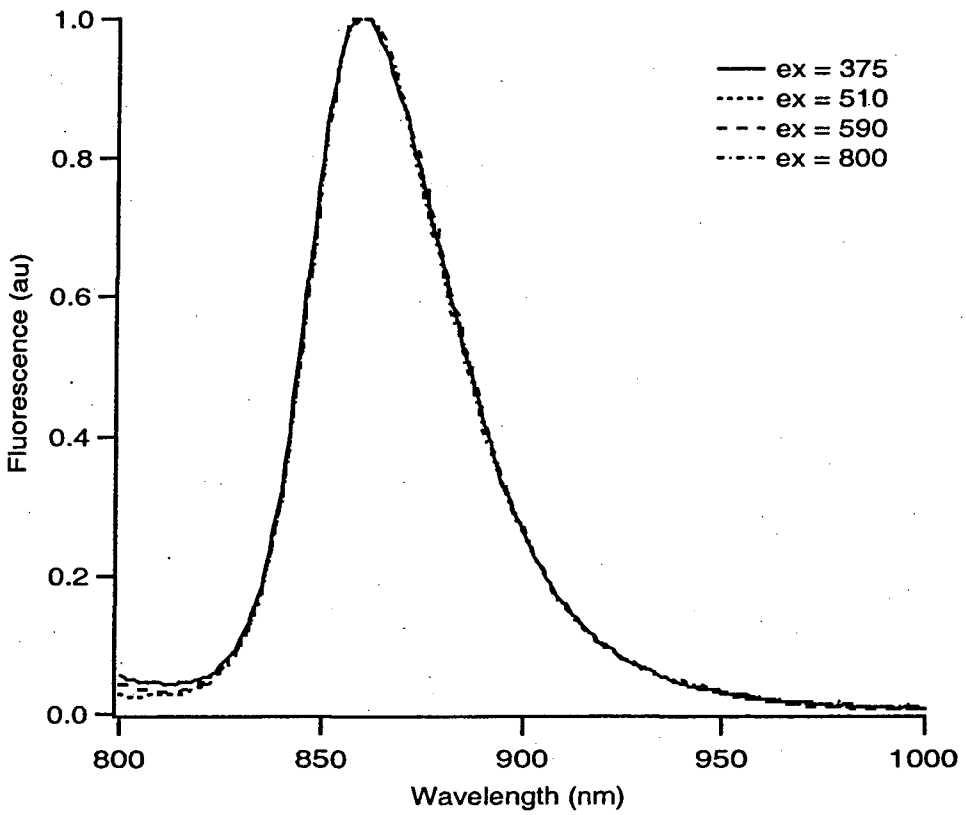

Figure 5.5: Fluorescence emission of BALM/LH2 (expressing LH2) excited by four different excitation wavelengths. Excitation is at 375 nm (solid line), 510 nm (dotted line), 590 nm (dashed line) and 800 nm (dash-dot line). The spectra are all taken on the same sample preparation at room temperature, and normalized at the maxima.

The KS relation for BALM/LH2 is plotted in Figure 5.6, together with the absorption and the fluorescence spectra for excitation at 510 nm. The KS temperature T*, calculated from the slope of the least-squares fit to the most linear central region of the KS relation, is 340 K; the KS temperature is approximately 40 K higher than the experimental ambient temperature.

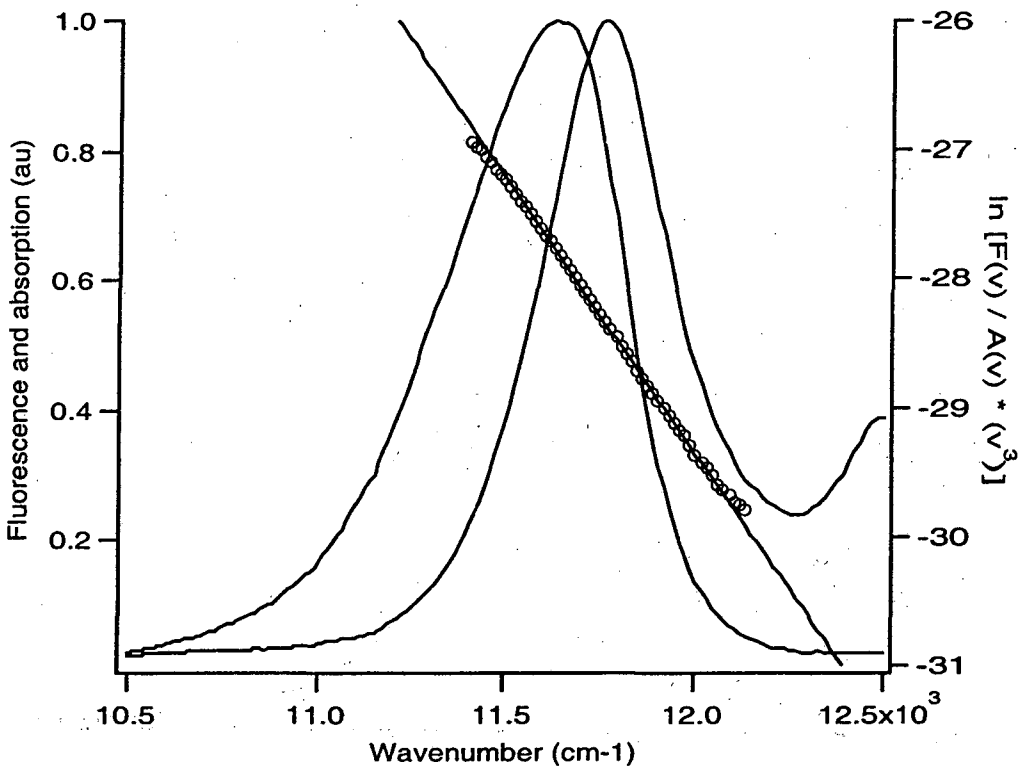

Figure 5.6: The fluorescence and absorption spectra of BALM/LH2, plotted as a function of frequency and normalized at the maxima. This fluorescence spectrum was generated with excitation at 510 nm. The Kennard-Stepanov relation for BALM/LH2 is plotted against the right axis (open circles). The straight line is a least-squares fit to the Kennard-Stepanov relation in the Stokes region. The slope of the line corresponds to a value of 340 K. The spectra were taken at ambient temperature, 296 K.

The T*(ν) plots for all four excitation wavelengths (375, 510, 590 and 800 nm) are shown in Figure 5.7. Similar to the results from RC-1A, a peak in T*(ν) appears on the red edge of the spectra where the absorption intensity is significant. The peak seen for BALM/LH2 ranges between 1500 K (for excitation at 375 nm) and 3000 K (for excitation at 590 nm). The variation in the magnitude of the T*(ν) peak is within the predicted error for the T*(ν) plot. As we will discuss in the section on error estimation, the error bars for the T*(ν) function increase at the edges of the fluorescence and absorption spectra. The position of the red edge T*(ν) peak is very reproducible for all of the excitation wavelengths.

There is a smaller peak in T*(ν) on the blue edge of the spectra, ranging between 450 K (for excitation into the carotenoid absorption band at 510 nm) and 900 K (for excitation into BChl absorption at 375 or 800 nm). This blue edge peak is also reproducible in its position. This blue edge T*(ν) peak may be due to contributions from a second absorption band. In BALM/LH2, there are two absorption bands associated with LH2; one band is at 800 nm, and the other is at 850 nm. In the region of the blue edge T*(ν) peak, the tail of the 800 nm absorption band overlaps with the 850 nm absorption band. This overlapping absorption band may be responsible for the deviation from the ideal behavior of the KS relation in this spectral region.

The calculated I* fluorescence spectrum of BALM/LH2 is slightly red-shifted and broadened compared to the experimental BALM/LH2 fluorescence spectrum (Figure 5.8). This is similar to the I* fluorescence calculated for RC-1A (Figure 5.4), which is also red-shifted and broadened from the experimental fluorescence. Again, the largest deviation from the experimental fluorescence spectrum is on the red edge; the region of the large T*(ν) peak. The experimental fluorescence on the red edge is not so intense as that predicted by the ideal KS relation. The I* fluorescence is truncated at

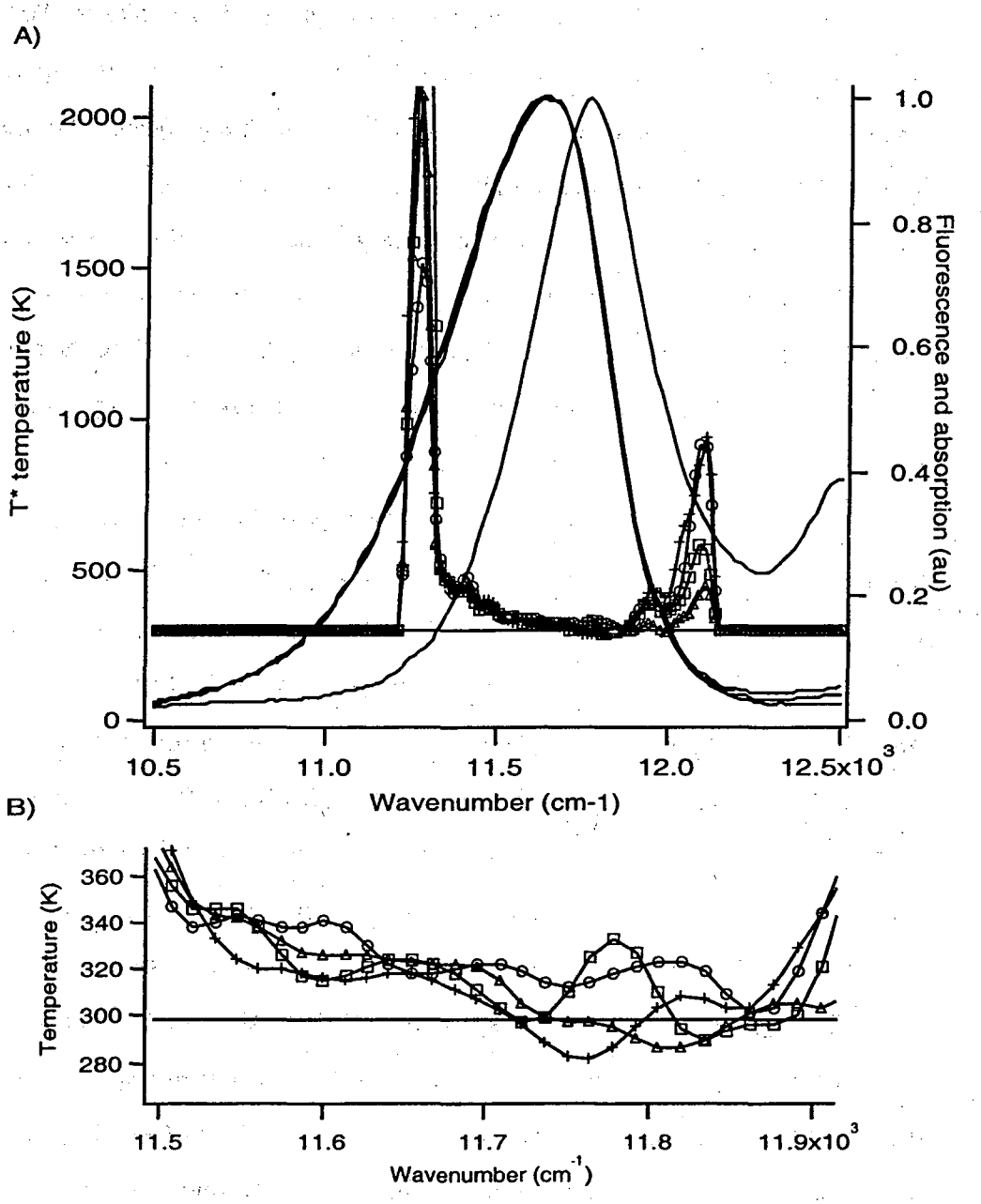

Figure 5.7: A) The local slope of the Kennard-Stepanov relation, T*(ν), for BALM/LH2 shown on a temperature scale. Four different T*(ν) are shown, corresponding to four excitation wavelengths. Circles, excitation at 375 nm; triangles, excitation at 510 nm; squares, excitation at 347 nm; plus signs, excitation at 800 nm. The absorption spectrum and the four fluorescence spectra generated by those four excitation wavelengths are plotted against the right axis. The horizontal line indicates ambient temperature, 298 K.

B) An expanded view of T*(ν) for BALM/LH2 from 11,500 cm^{-1} to 11,900 cm^{-1}. The horizontal line indicates ambient temperature, 298 K.

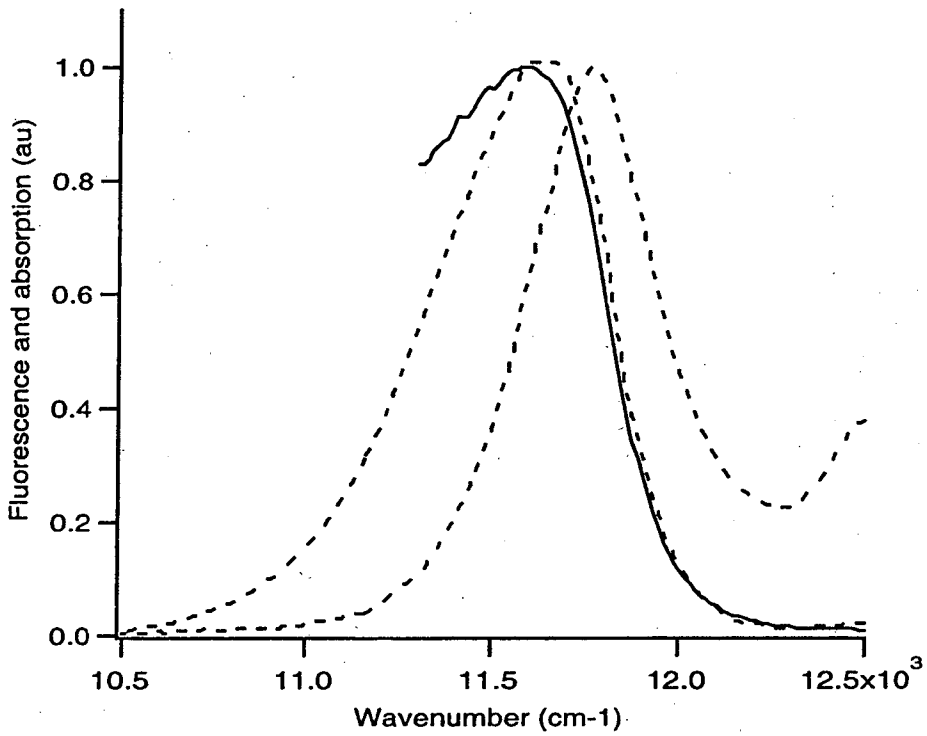

Figure 5.8: The experimental absorption and fluorescence emission (excitation at 510 nm) of BALM/LH2 (dashed lines), and the I* fluorescence (solid line), which is calculated from the experimental absorption and the ideal Kennard-Stepanov relation at 298 K. The I* spectrum is truncated at 11,300 cm^{-1} because at lower frequency the absorption intensities are very low.

11,300 cm^{-1} because at very low absorption intensities the KS relation is no longer accurate.

LM1.1 results (LH1 and LH2):

The mutant LM1.1 contains both antenna complexes LH1 and LH2, but lacks reaction centers. Excitation at 800 nm, into the Qy band of LH2 BChl absorption, produces a fluorescence spectrum different from that excited at 590 nm, into the Qx BChl absorption band (Figure 5.9). The two different spectra are normalized at their

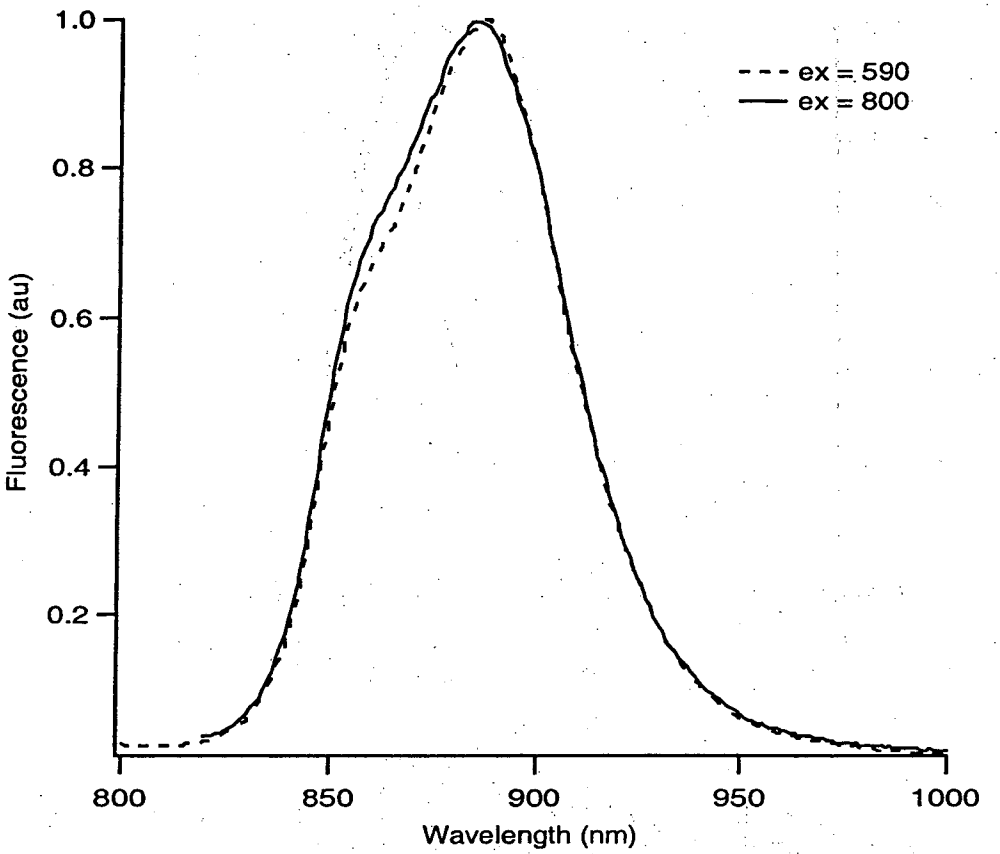

Figure 5.9: Fluorescence emission of LM1.1 (expressing LH1 and LH2) excited by two different excitation wavelengths. Excitation is at 590 nm (dashed line) and 800 nm (solid line). Excitation at 800 nm produces greater emission intensity at 860 nm than excitation at 590 nm, when the two spectra are normalized at their maxima. The same sample is used for both excitation wavelengths, and spectra are taken at room temperature. Excitation at 375 nm or 510 nm produce identical spectra as excitation at 590 nm within the detection limits of the instrumentation; for clarity these spectra are not included.

fluorescence emission maxima at 890 nm. This is the first example in this chapter of a *Rb. sphaeroides* mutant which has a change in the fluorescence emission spectrum as a function of the excitation wavelength.

Excitation at 800 nm (into the LH2 BChl absorption) produces a more pronounced shoulder at 860 nm (which corresponds to emission from LH2) than does excitation at 590 nm (Figure 5.9). Excitation at 375 nm and 510 nm produce fluorescence spectra identical to that resulting from excitation at 590 nm. The difference in fluorescence emission spectra as a function of excitation wavelength is one indication that the excitation has not reached a complete equilibrium distribution in LM1.1 before emission occurs.

For clarity, only 800 nm and 590 nm excitation are presented in the KS plot of LM1.1 (Figure 5.10). Both excitation wavelengths result in similar KS temperatures from a least-squares fitting of the central linear region. Excitation at 800 nm results in a T* of 325 K, and 590 nm excitation results in a T* of 320 K. Despite the difference in the shoulder region of the fluorescence spectra (around 11,600 cm^{-1}), both excitation wavelengths also produce similar T*(ν) plots (Figure 5.11). Over most of the central region of the spectra, the T*(ν) values are in excellent agreement with ambient temperature (296 K). The T*(ν) plot generated from 800 nm excitation is slightly below ambient temperature in the shoulder region of the fluorescence emission. At the red edge, at 11,000 cm^{-1}, there is a large peak in T*(ν) for both excitation wavelengths. The peak is approximately 1000 K for 800 nm excitation and 2200 K for 590 nm excitation. There is a small peak on the blue edge, which may be caused by the tail of the 800 nm absorption band in that region, similar to the case for BALM/LH2.

The calculated I* fluorescence for LM1.1 is once again slightly red-shifted and broadened compared to the experimental fluorescence generated from either excitation wavelength (Figure 5.12). These are the same trends as seen in the I* fluorescence of RC-1A and BALM/LH2. The I* fluorescence is truncated in Figure 5.12 below 10,900 cm^{-1} because of low absorption intensities at lower frequency.

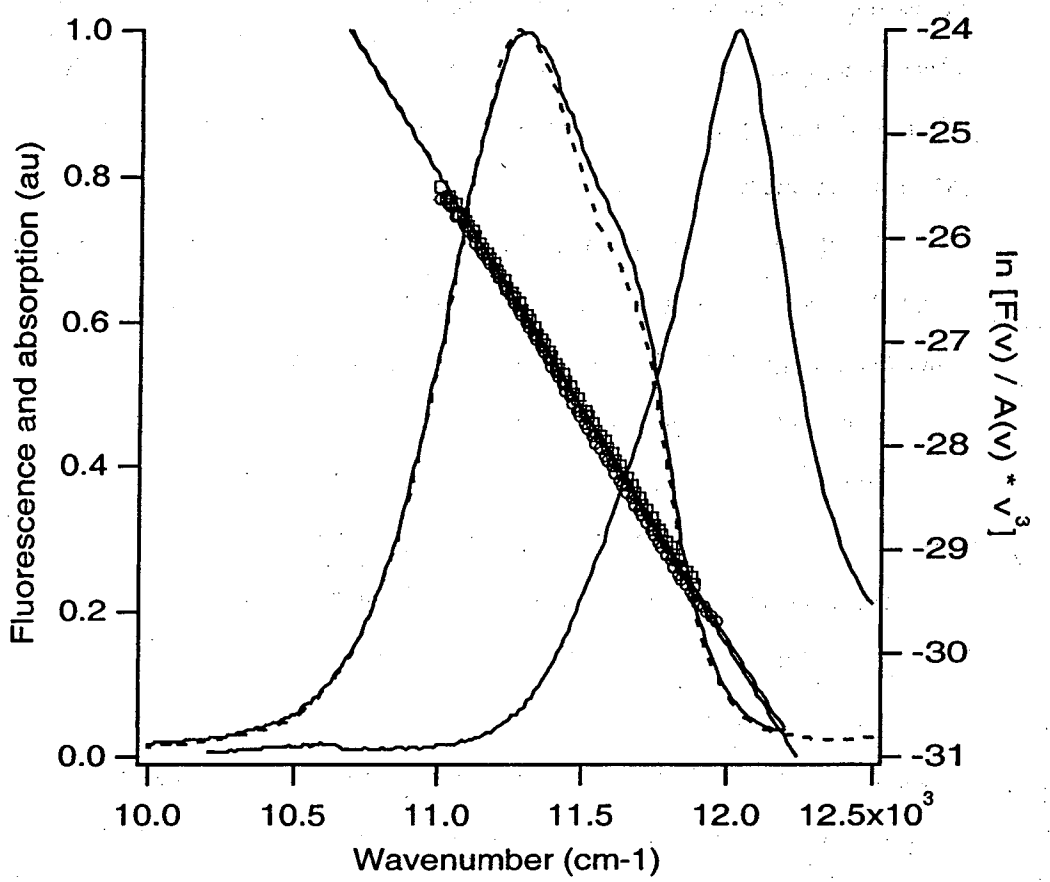

Figure 5.10: The fluorescence and absorption of LM1.1, plotted as a function of frequency and normalized at the maxima. These fluorescence spectra were generated with excitation at 590 nm (dashed line) and 800 nm (solid line). The Kennard-Stepanov relation for LM1.1 is plotted against the right axis for both fluorescence emission spectra; open circles for excitation at 800 nm and open squares for excitation at 590 nm. The two straight lines are least-squares fits to both Kennard-Stepanov plots in the Stokes region. The slope of the fit for excitation at 800 nm corresponds to a T* value of 325 K, and for excitation at 590 nm the slope of the fit corresponds to a T* value of 320 K. All spectra were taken at 296 K.

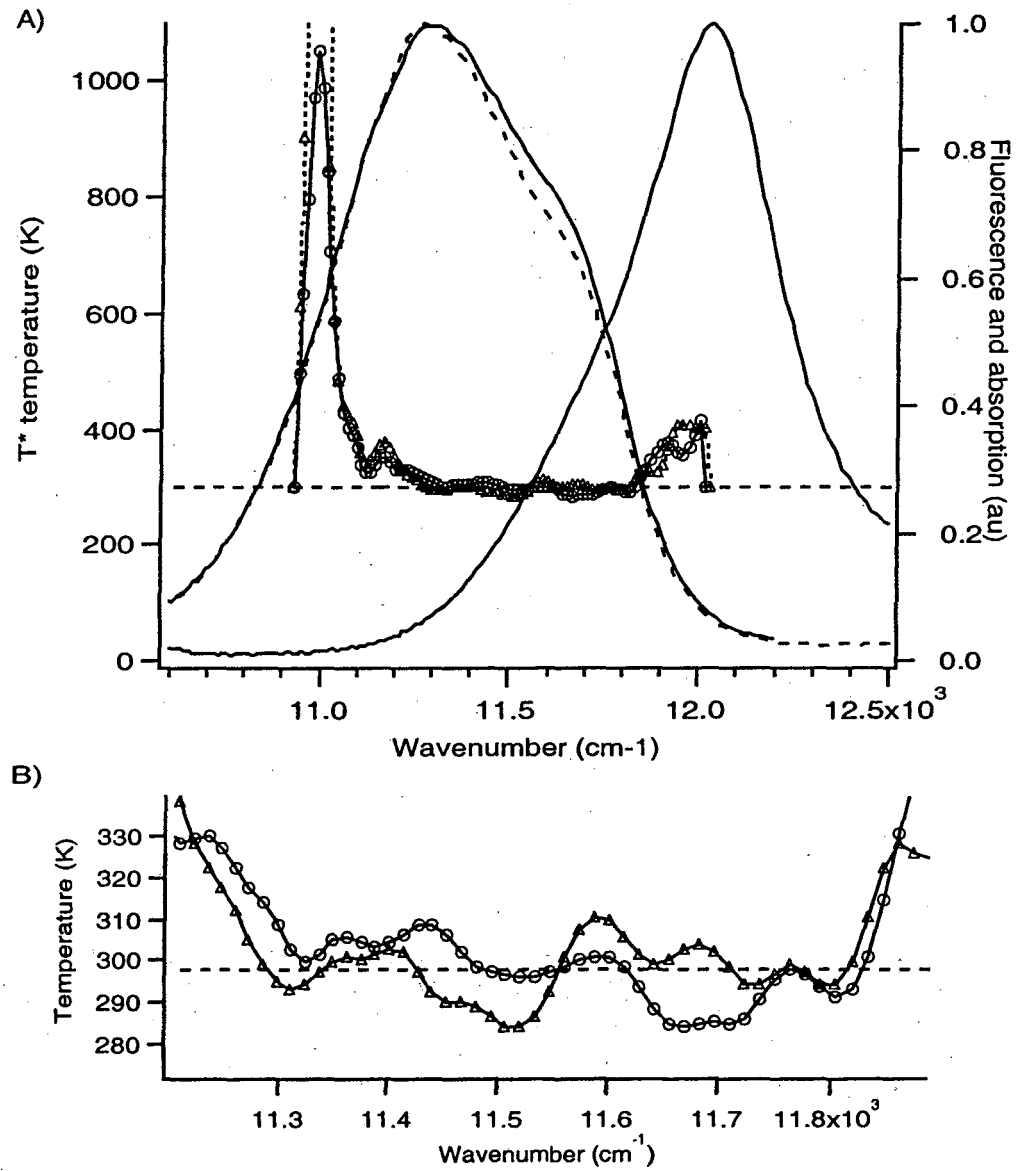

Figure 5.11: A) The local slope of the Kennard-Stepanov relation, T*(ν), for LM1.1 shown on a temperature scale. Two different T*(ν) are shown, corresponding to two excitation wavelengths. Circles, excitation at 800 nm, and triangles, excitation at 590 nm. The absorption spectra and the two fluorescence spectra generated by those excitation wavelengths are plotted against the right axis; 800 nm excitation, solid line, and 590 nm excitation, dashed line. The horizontal line indicates ambient temperature, 296 K.

B) An expanded view of T*(ν) for LM1.1 from 11,200 cm^{-1} to 11,900 cm^{-1}. The horizontal line indicates ambient temperature, 296 K.

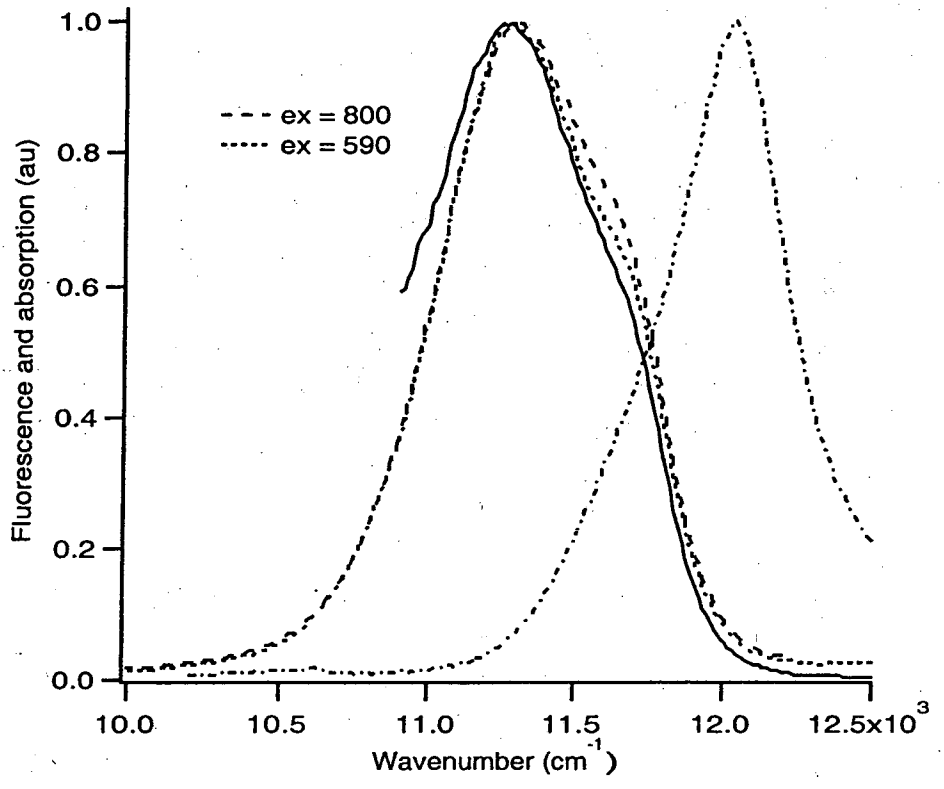

Figure 5.12: The experimental absorption (dash-dot line) and fluorescence spectra of LM1.1. For the fluorescence spectra of LM1.1, excitation is shown at both 800 nm (dashed line) and 590 nm (dotted line), together with the I* fluorescence (solid line), which is calculated from the experimental absorption and the ideal Kennard-Stepanov relation at 296 K. The I* spectrum is truncated at 10,900 cm^{-1}, because at lower frequency the absorption intensity is very low.

Wild-type results (LH1, LH2 and RC):

Wild-type *Rb. sphaeroides* contains both antenna complexes LH1 and LH2, as well as the reaction center. The wild-type sample that will be investigated in this section has a relatively high content of LH1 relative to LH2; the absorption of the two bands is approximately equal (Figure 5.14). The ratio of LH1 to LH2 in *Rb. sphaeroides* depends on growth conditions, light intensity and age of the culture. While the high

LH1 to LH2 ratio is not typical for every sample, identical experimental results are obtained for other wild-type preparations with a lower ratio of LH1 to LH2.

In wild-type *Rb. sphaeroides*, the reaction center functions as an excitation sink. Excitation is energetically funneled from the antenna to the reaction center where the excitation is used in charge separation if the reaction center is open, the Fo state. Alternatively, the excitation is quenched by the reaction center if the reaction center cannot perform charge separation, for example if the reaction center is in the Fm state (see Chapter Three). The quenching of excitation in the Fm state is less efficient than excitation quenching in the Fo state. These two states of the reaction center, Fm and Fo, result in two configurations of the wild type that must be considered separately.

The Fm state

First we will address the Fm state. In the wild type, as in LM1.1, different excitation wavelengths produce different emission spectra. Excitation at 800 nm results in an increase in the shoulder of the fluorescence emission at 860 nm, compared to excitation at 375 nm, when the spectra are normalized at the maxima (Figure 5.13). This is identical to what is seen in LM1.1; excitation into an LH2 absorption band produces an increased fluorescence emission from LH2 relative to fluorescence emission from LH1. Excitation at 510 nm and 590 nm produce the same fluorescence spectra as excitation at 375 nm. For clarity we present only the data from 375 nm and 800 nm excitation. The difference in fluorescence emission as a function of excitation wavelength is one indication that the excitation has not fully equilibrated in the Fm state of wild-type *Rb. sphaeroides* before fluorescence emission occurs.

In the Fm state, excitation at 375 nm leads to an average calculated T* of 372 K, about 75 K higher than ambient temperature (Figure 5.14). It is apparent on first examination that the KS relation deviates significantly from a single value in the region of maximum overlap between the fluorescence and absorption spectra. In contrast to

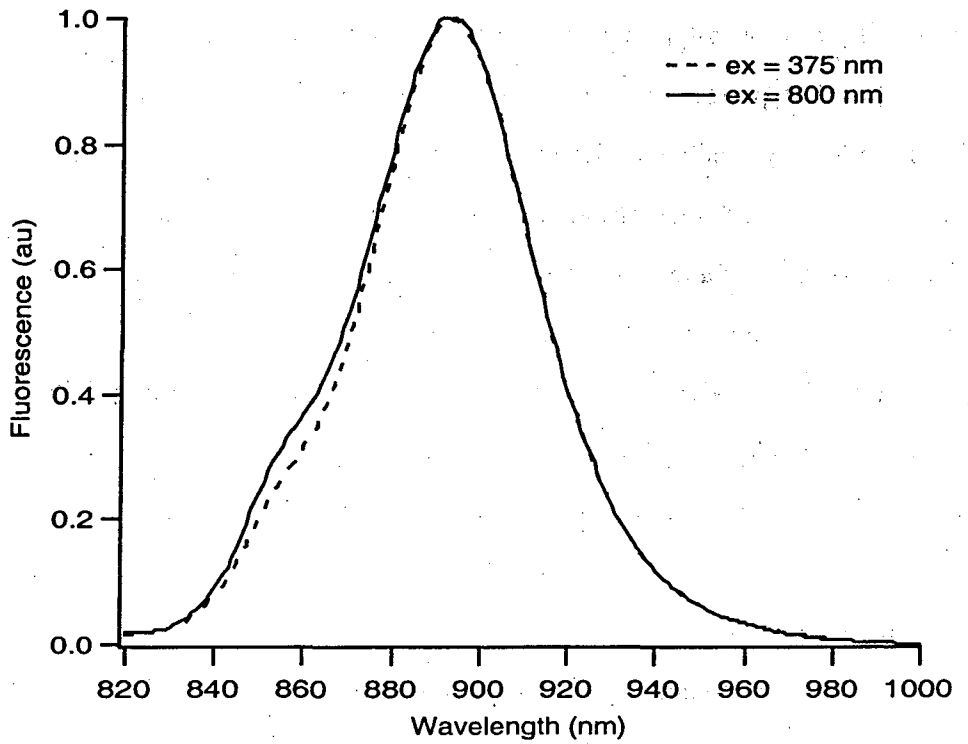

Figure 5.13: Fluorescence emission of wild type *Rb. sphaeroides* (expressing LH1, LH2, and reaction centers) in the Fm state, excited at two wavelengths; 375 nm (dashed line) and 800 nm (solid line). The two spectra are different in the shoulder region at 860 nm, which corresponds to emission from LH2. Excitation at 800 nm produces more emission at 860 nm relative to 890 nm than excitation at 375 nm. The fluorescence spectra are taken at room temperature on the same sample and normalized at the maxima.

the mutants of *Rb. sphaeroides* that we have discussed, the wild type appears to have two separate linear regions in the KS plot, with a transition around 11,600 cm^{-1}. Least-squares fitting to the low-energy region (11,000 cm^{-1} to 11,400 cm^{-1}) results in a T* of 340 K. Fitting to the linear high-energy region (11,800 cm^{-1} to 12,000 cm^{-1}) results in a T* of 362 K. These two separate values of T* indicate that there may be incomplete energy equilibration in the wild type before fluorescence emission occurs. Two separate linear regions in the KS plot are present for all excitation wavelengths used,

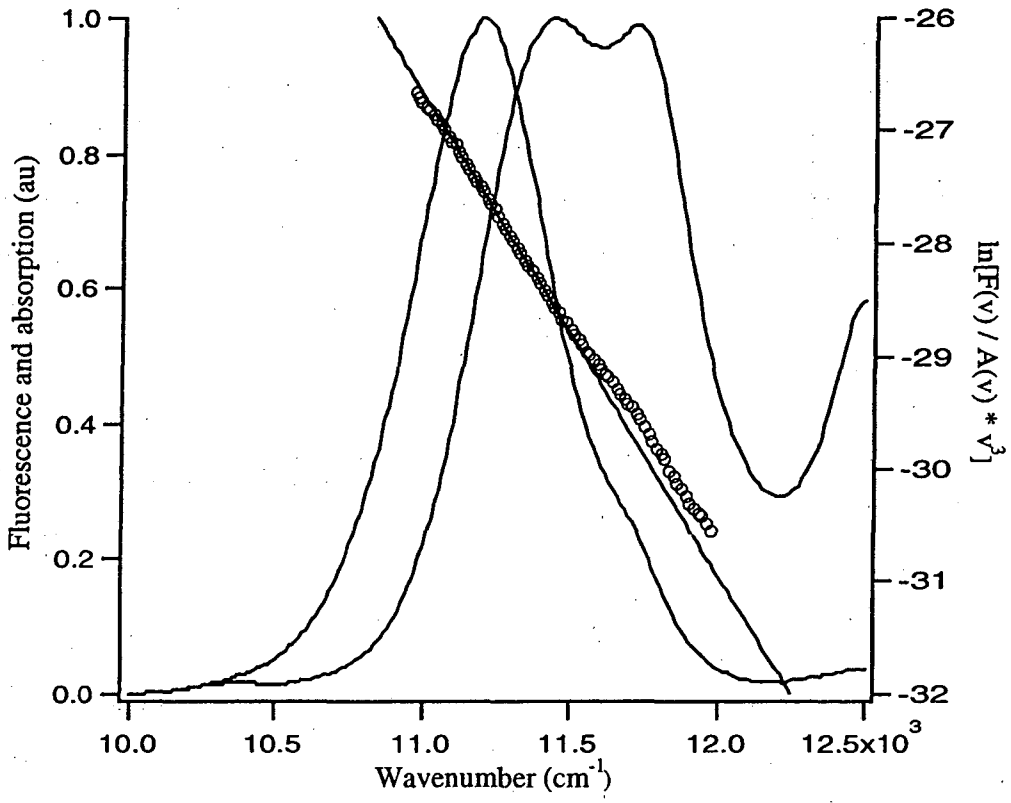

Figure 5.14: Absorption and fluorescence (excitation at 375 nm) of wild type *Rb. sphaeroides* in the Fm state, plotted as a function of frequency and normalized at the maxima. The Kennard-Stepanov relation for the wild type is plotted against the right axis (open circles). There are two linear regions in the Kennard-Stepanov plot, with a transition between them in the region of 11,600 cm^{-1}.

including 510 nm, 590 nm, and 800 nm as well as 375 nm. The two separate linear regions in the KS plot are also present in four distinct preparations of wild-type *Rb. sphaeroides* chromatophores, and they are present regardless of the ratio of LH1 to LH2 in the absorption spectrum of the preparation.

The T*(v) plot (Figure 5.15) of wild-type *Rb. sphaeroides* chromatophores in the Fm state shows a large peak on the red edge of the spectra, identical to the T*(v) plots of the mutant *Rb. sphaeroides* strains. The maximum of the red-edge peak is in a

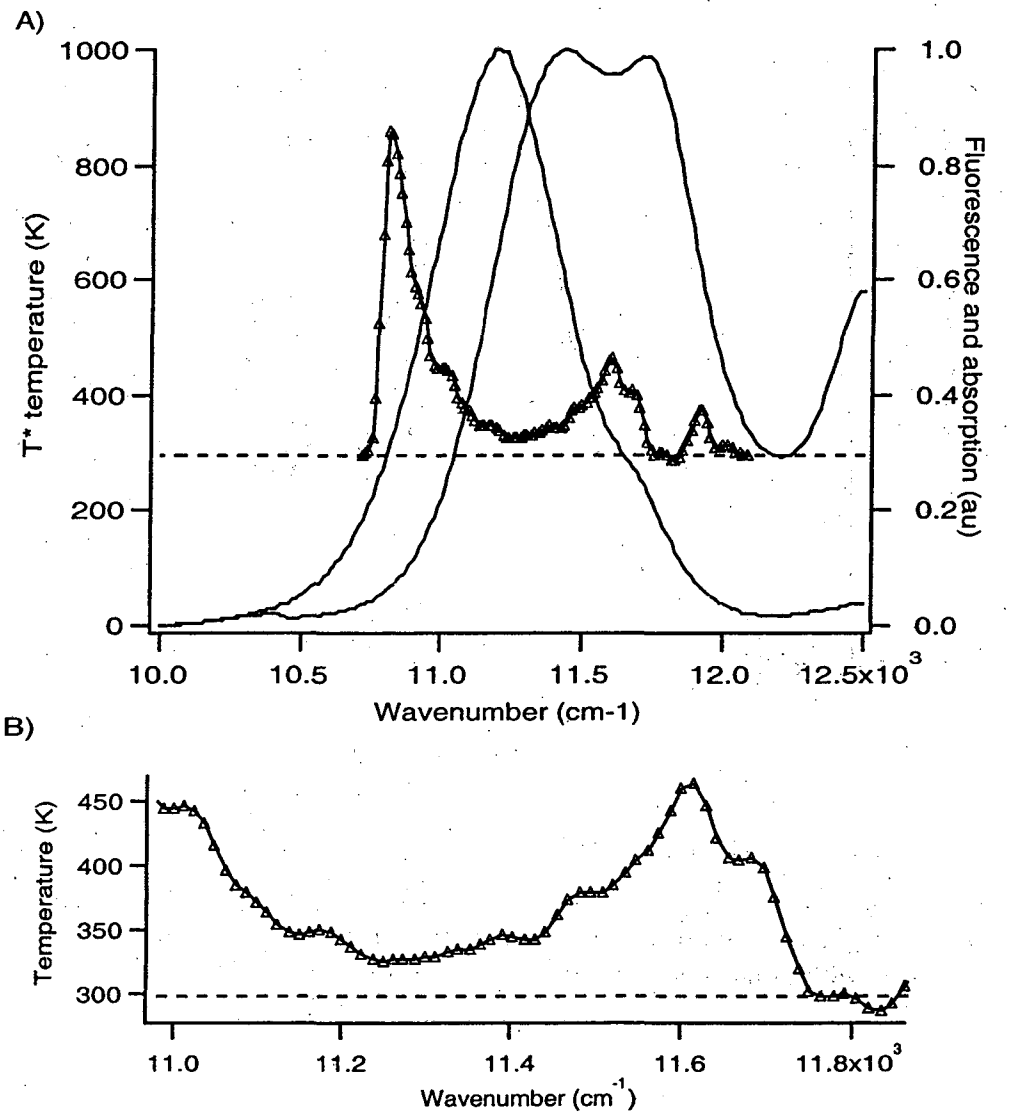

Figure 5.15: A) The local slope of the Kennard-Stepanov relation, T*(ν), for wild type *Rb. sphaeroides* in the Fm state, shown on a temperature scale. The absorption spectrum and fluorescence spectrum for excitation at 375 nm are plotted against the right axis. The horizontal line indicates ambient temperature, 296 K. B) An expanded view of T*(ν) for the wild type from 11,000 cm^{-1} to 11,850 cm^{-1}. The horizontal line indicates ambient temperature, 296 K.

region of the spectra where the absorption has significant intensity, at 10,850 cm^{-1}. In addition to the red-edge peak, there is a second peak in the Stokes region at 11,600 cm^{-1}. This peak is not observed in any of the T*(ν) plots from the mutant strains of *Rb. sphaeroides*, including strain LM1.1 which contains both LH1 and LH2. The maximum of the Stokes region peak in the T*(ν) is approximately 450 K. This peak occurs in the region of transition between the two linear components in the wild-type T* plot.

We have presented results of the KS analysis for excitation at 375 nm in the Fm state. Excitation at 800 nm in the Fm state produces a fluorescence emission spectrum different from that produced by excitation at 375 nm, with a higher fluorescence emission ratio of LH2 to LH1. Despite the different fluorescence spectrum generated by excitation at 800 nm, the results of the KS analysis (Figure 5.16) are similar to those obtained for excitation at 375 nm. Again, there are two separate linear regions in the KS plot, which correspond to different T* temperatures. Least squares fitting to the low energy linear region results in a T* of 348 K, and the high energy region produces a T* of 312 K. The T*(ν) plot (Figure 5.17) shows a peak on the red edge of the spectra at 10,850 cm^{-1}, and a second peak in the Stokes region at 11,600 cm^{-1}. The height of the second T*(ν) peak for excitation at 800 nm is approximately 525 K, about 75 K higher than the peak generated by excitation at 375 nm.

The Fo state

In the Fo state charge separation in the reaction center is very efficient, so the Fo state reaction center is a more efficient drain of excitation than the Fm state reaction center. The Fo state of the reaction center also produces a fluorescence emission spectrum from *Rb. sphaeroides* chromatophores which is distinct from the fluorescence emission of *Rb. sphaeroides* in the Fm state, when the same excitation wavelength is used. Figure 5.18 shows the Fo and Fm state fluorescence spectra, normalized at the

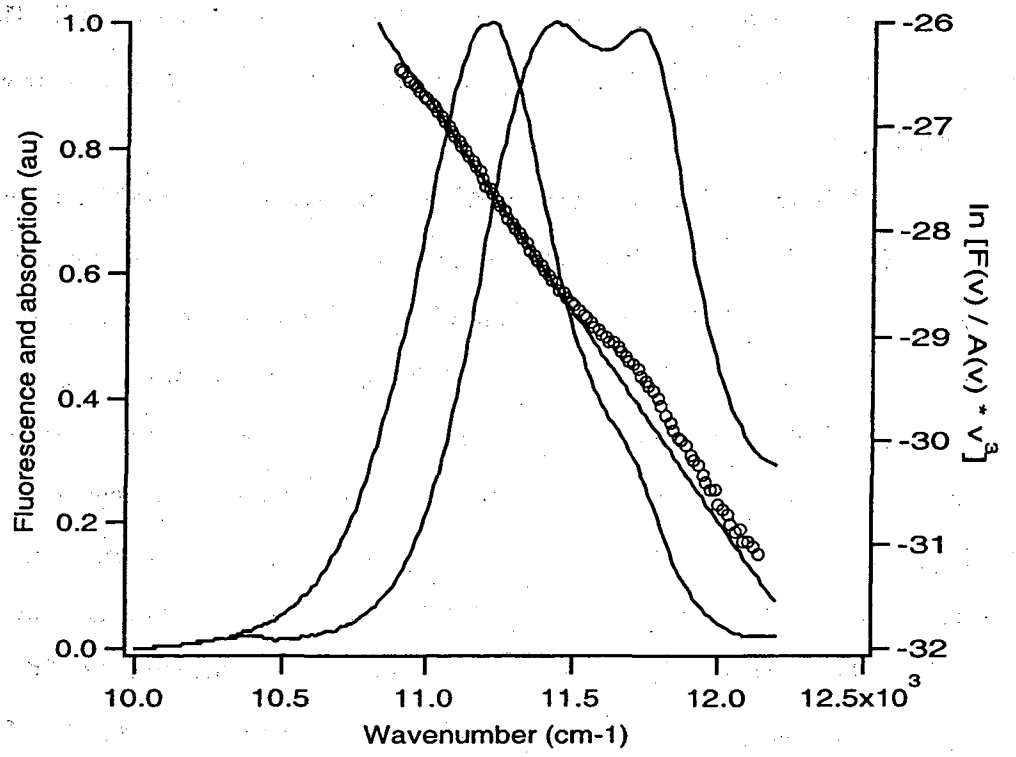

Figure 5.16: The fluorescence and absorption spectra of wild type *Rb. sphaeroides* in the Fm state, plotted as a function of frequency and normalized at the maxima. This fluorescence spectrum was generated with excitation at 800 nm. The Kennard-Stepanov relation for the wild type is plotted against the right axis (open circles). The straight line is a least-squares fit to the Kennard-Stepanov relation in the low - energy Stokes region. The slope of the line corresponds to a value of 348 K. The spectra were taken at 296 K.

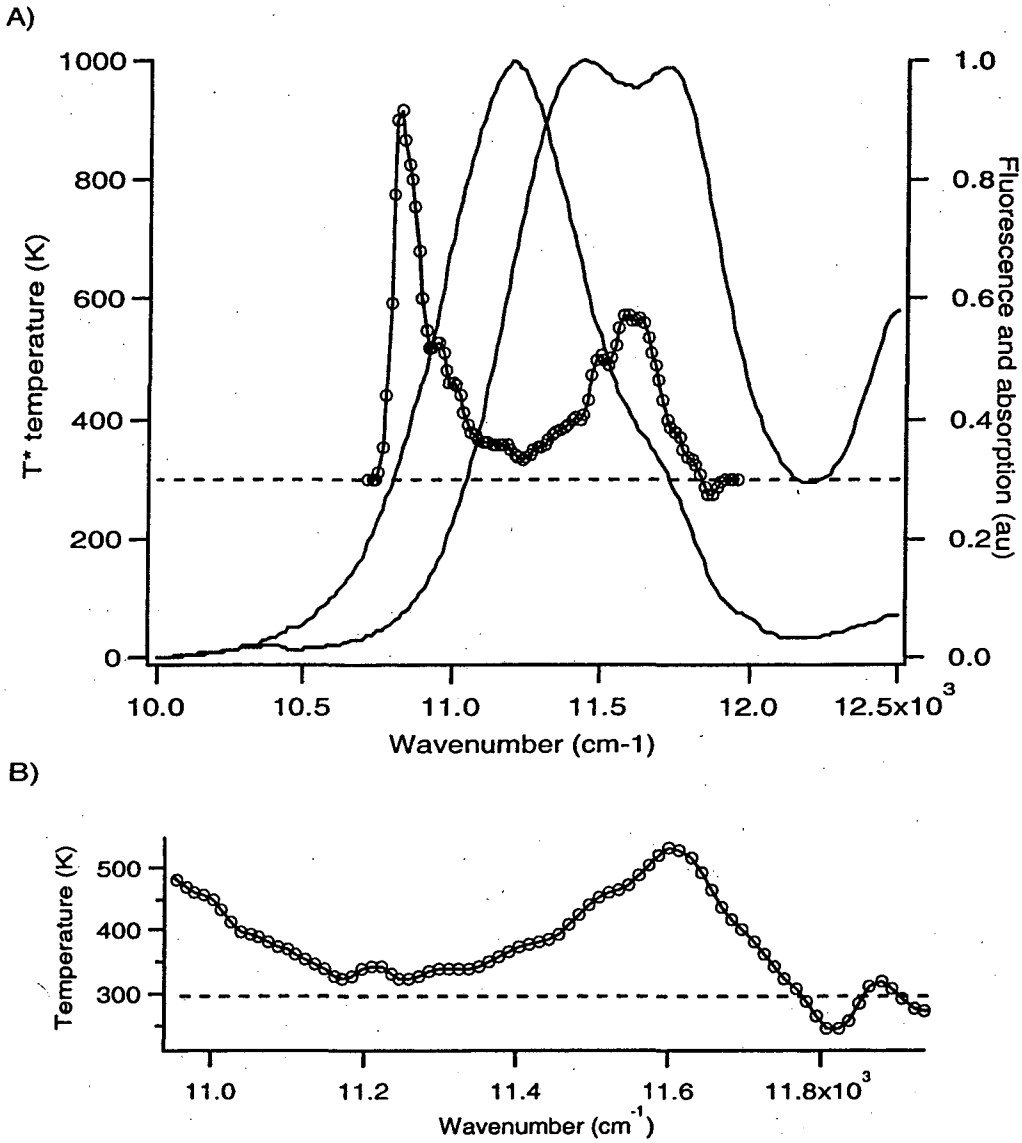

Figure 5.17: A) The local slope of the Kennard-Stepanov relation, T*(ν), for wild type *Rb. sphaeroides* in the Fm state shown on a temperature scale. The absorption spectrum and fluorescence spectrum for excitation at 800 nm are plotted against the right axis. The horizontal line indicates ambient temperature, 296 K.

B) An expanded view of T*(ν) for the wild type from 11,000 cm^{-1} to 11,850 cm^{-1}. The horizontal line indicates ambient temperature, 296 K.

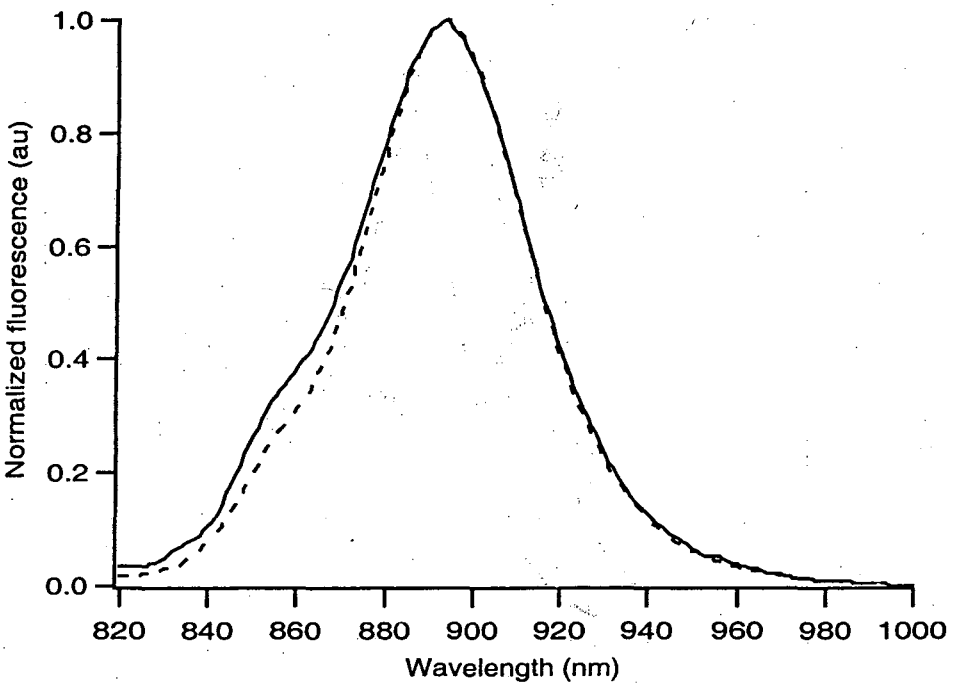

Figure 5.18: Fluorescence emission of wild type *Rb. sphaeroides* in the Fm state (dashed line) and Fo state(solid line). Excitation is at 375 nm. The fluorescence spectra are normalized at the maxima. The same sample is used for both the Fo and Fm state, and spectra are taken at room temperature.

maximum, both for excitation at 375 nm. In the Fo state, the ratio of emission at 860 nm to 890 nm is greater than in the Fm state; the same trend holds for excitation at any other wavelength. Compared with the Fm state, in the Fo state a greater relative amount of fluorescence arises from LH2 (860 nm) compared to LH1 (890 nm). The order of increasing 860 nm to 890 nm fluorescence ratio is: Fm 375 nm excitation, Fm 800 nm excitation, Fo 375 nm excitation, Fo 800 nm excitation. As we will see, the larger the ratio of 860 nm to 890 nm fluorescence, the larger the Stokes region peak becomes in the T*(ν) plots.

Figure 5.19 shows the KS relation for the Fo state of wild-type *Rb. sphaeroides* with excitation at 375 nm and 800 nm. The KS analysis produces similar results as for

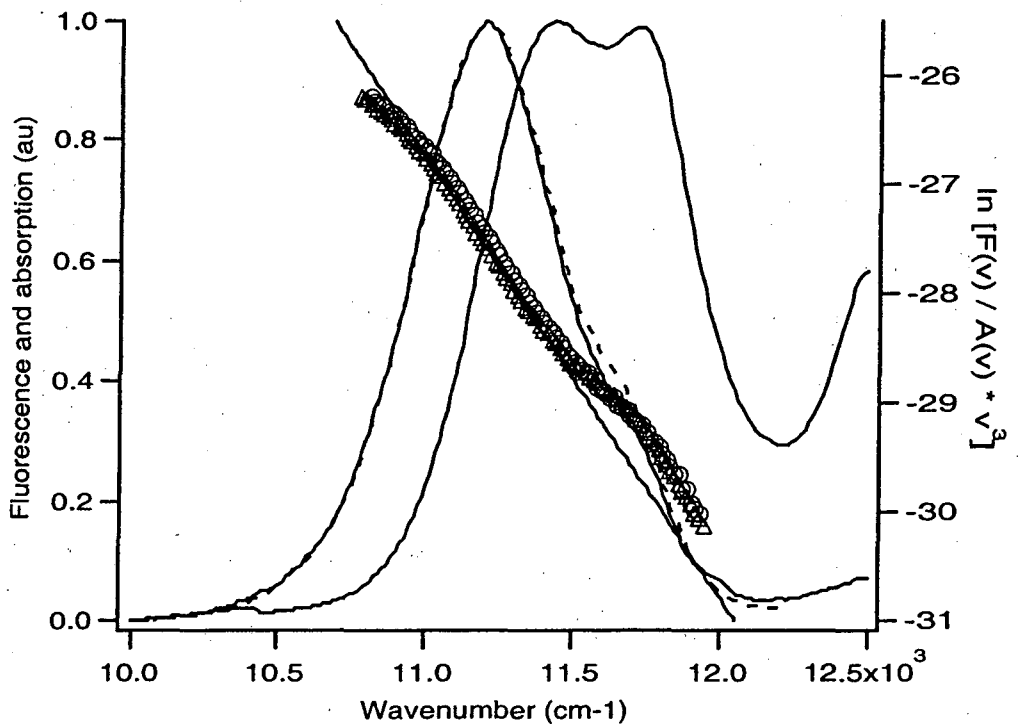

Figure 5.19: The fluorescence and absorption spectra of wild type *Rb. sphaeroides* in the Fo state, plotted as a function of frequency and normalized at the maxima. Two fluorescence spectra are shown, with excitation at 800 nm (dashed line) and 375 nm (solid line). The Kennard-Stepanov relation for both excitation wavelengths is shown for the wild type in the Fo state, plotted against the right axis; circles, excitation at 375 nm, and triangles, excitation at 800 nm.

the Fm state calculations, and shows two separate linear regions for each excitation wavelength. For excitation at 375 nm, the low-energy region T* is 358 K and the high energy region T* is 367 K. For excitation at 800 nm, the low energy region T* is 370 K and the high energy region T* is 310 K.

The T*(v) plot for both excitation wavelengths in the Fo state (Figure 5.20) reveals the same red-edge peak at 10,850 cm^{-1} and a second peak in the Stokes region at 11,600 cm^{-1}. For excitation at 375 nm, the Stokes region peak has a maximum of 550 K, and for excitation at 800 nm, the Stokes region peak has a maximum of 700 K.

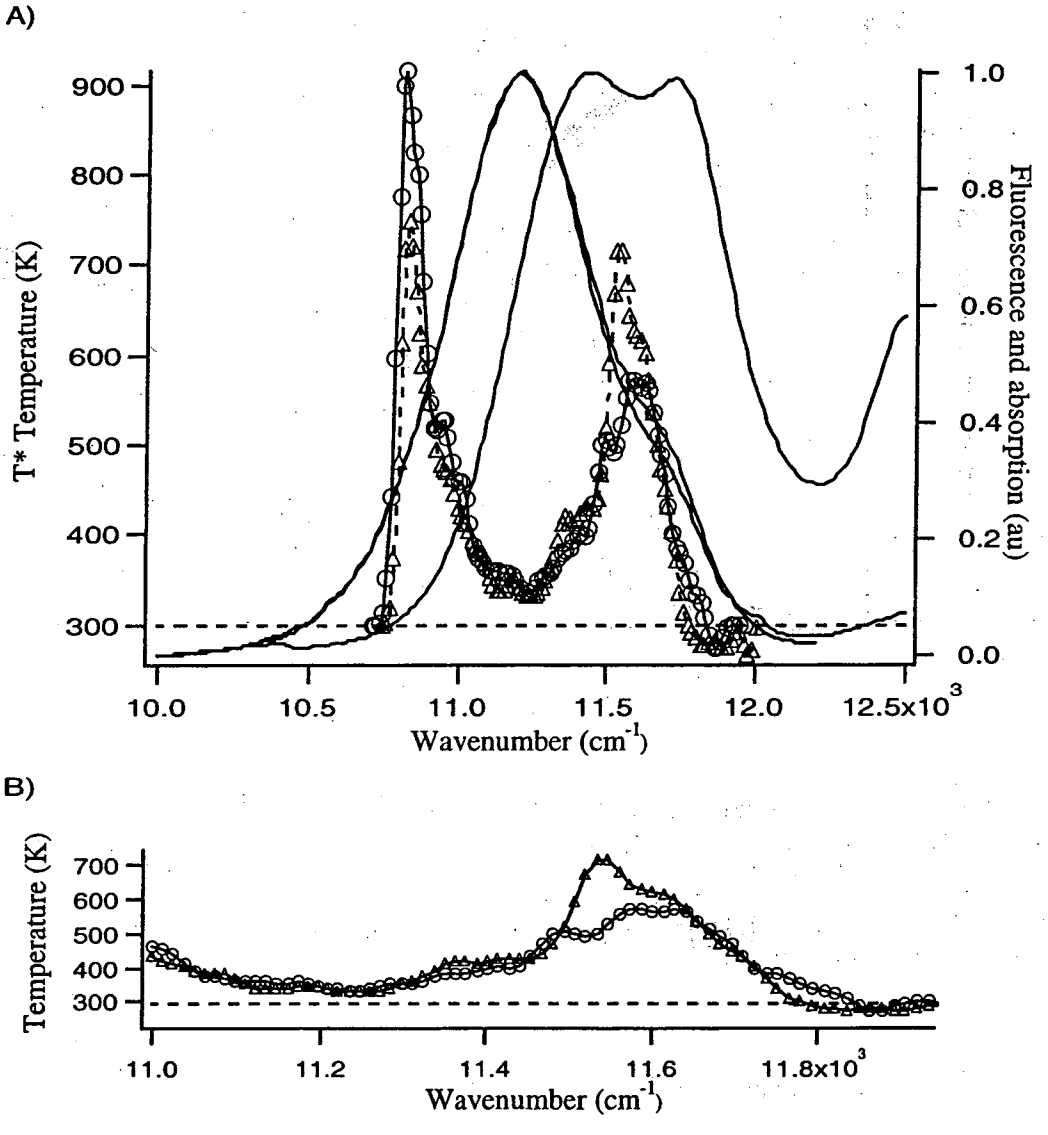

Figure 5.20: A) The local slope of the Kennard-Stepanov relation, T*(ν), for wild type *Rb. sphaeroides* in the Fo state shown on a temperature scale. T*(ν) is shown for both excitation at 800 nm (triangles) and 375 nm (circles). The absorption spectrum and fluorescence spectrum for excitation at 800 nm (dashed line) and excitation at 375 nm (solid line) are plotted against the right axis. The horizontal line indicates ambient temperature, 296 K.

B) An expanded view of T*(ν) for the wild type from 11,000 cm^{-1} to 11,900 cm^{-1}. The horizontal line indicates ambient temperature, 296 K.

Figure 5.21 shows the I* calculated fluorescence spectrum together with the experimental fluorescence for excitation at 375 nm in the Fo and Fm states. The calculated fluorescence spectrum for the wild type is slightly red-shifted from the experimental fluorescence in either the Fo or Fm state. The I* spectrum has a much lower intensity than the experimental fluorescence in the shoulder region of the fluorescence emission, near 11,750 cm^{-1}.

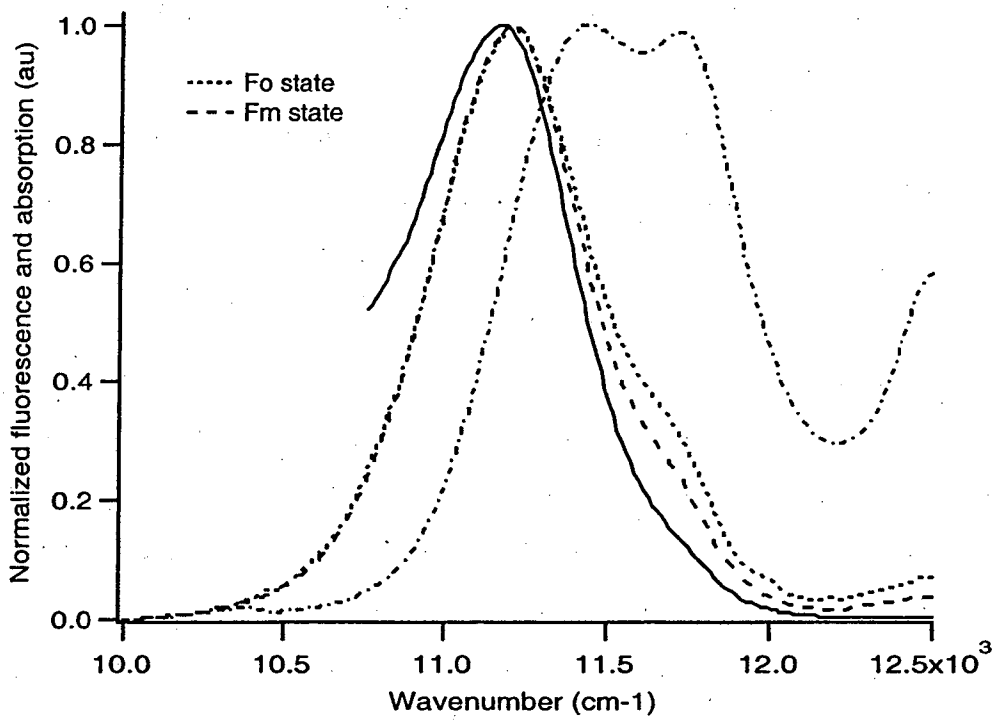

Figure 5.21: The I* fluorescence spectrum of wild type *Rb. sphaeroides* (solid line), calculated from the absorption spectrum (dash-dot line) and the ideal Kennard-Stepanov relation at 296 K. Two experimental fluorescence spectra are also shown for comparison with the I* spectrum, both with excitation at 375 nm; Fo state (dotted line) and Fm state (dashed line). The I* spectrum is truncated at 10,700 cm^{-1}, because at lower frequency the absorption intensity is very low.

In summary, in both the Fo and Fm state of wild-type *Rb. sphaeroides*, the KS analysis presents a structure that is more complex than that of the mutant *Rb. sphaeroides* strains. For all excitation wavelengths, in addition to the peak on the red edge of the T*(ν) spectra that is seen in mutant strains lacking a reaction center, there is also, in the wild type, a second peak in the Stokes region at 11,600 cm^{-1}. The peak in the Stokes region increases in magnitude with an increasing ratio of fluorescence emission of 860 nm to 890 nm; the ratio of LH2 to LH1 fluorescence. The highest magnitude for the second peak is in the Fo, open reaction center state, with excitation at 800 nm into an absorption band of LH2 (T* = 700 K); this state has the highest 860 : 890 nm ratio of fluorescence. The ideal KS calculated fluorescence spectrum is red-shifted from the experimental fluorescence, and has a lower intensity than the experimental fluorescence in the shoulder region.

Error Analysis:

There are a variety of factors that contribute to error in the absorption and fluorescence spectra. These factors are difficult to estimate precisely and to propagate through the KS calculations. Alternatively, we have employed an empirical method for estimation of errors in the KS spectra, through estimation of the error in the absorption and fluorescence spectra used in the KS analysis. The errors in the KS spectra are calculated from the variation in the data sets used to generate the fluorescence and absorption spectra. An envelope around the data is calculated, which corresponds to the scatter of the data points collected during each experiment. The maximum and minimum spectra of the fluorescence and absorption are created from the envelope around the data sets. As a representative data sample, we will present the error analysis for RC-1A. Figure 5.22 shows a detail of the absorption and fluorescence raw data of RC-1A together with the error bars used to generate the maximum and minimum spectra. These spectra are then used together in combinations to produce four

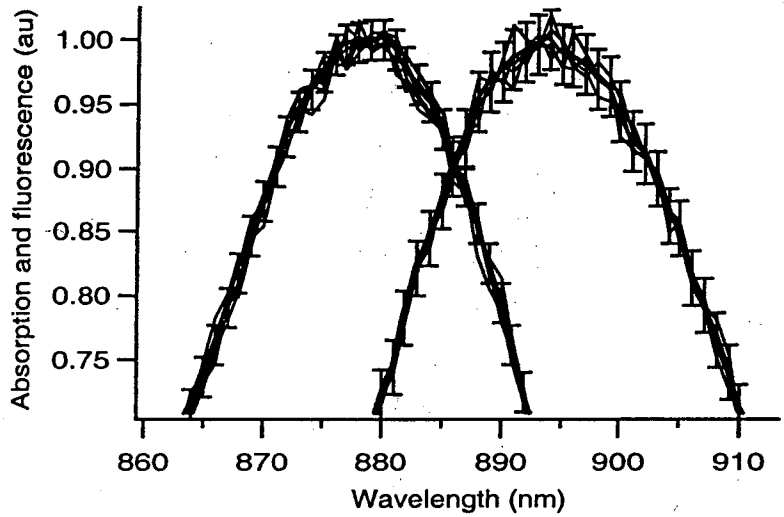

Figure 5.22: A detail of the RC-1A fluorescence and absorbtion raw data (light lines) and averaged spectra (heavy lines), together with error bars empirically estimated from the scatter in the raw data. The envelopes created around the error bars are used to generate the maximum and minimum spectra of the absorption and fluorescence as seen in Figure 5.23.

alternative KS error spectra, shown for RC-1A in Figure 5.23. In the regions where the fluorescence or absorption are very low, the KS error spectra (solid lines) deviate most extremely from the experimental KS spectrum (dots). Least-squares fitting to the linear region of each KS error spectra produces T* values ranging from 310 K to 347 K. T* for the KS experimental spectrum of RC-1A is 330 K; thus the error estimation gives a T* value of 330 +/- 20 K.

In the T*(v) spectra, the error analysis produces values that deviate most from the experimental value at the edges of the spectra (Figure 5.24). Possible structure on the blue edge of the RC-1A spectra is not reproduced in the error spectra. However, the red-edge spectral peak is reproduced in all of the error spectra and varies in magnitude from 550 K to 1900 K. The error analysis of RC-1A is representative of the errors found in all data sets.

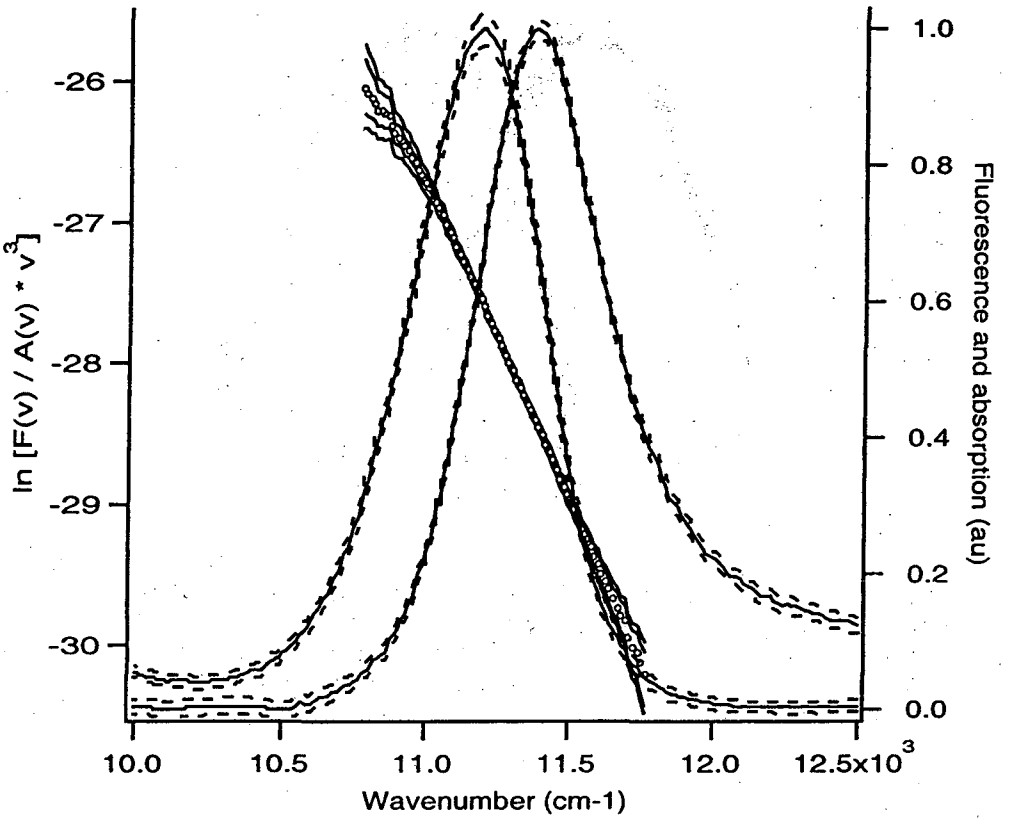

Figure 5.23: Four Kennard-Stepanov error spectra (solid lines) for RC-1A, together with the experimental Kennard-Stepanov spectrum (open dots) for RC-1A. The maximum and minimum absorption and fluorescence spectra used to generate the Kennard-Stepanov error spectra are plotted against the right axis (dashed lines). A least-squares fit to the linear central region of the four Kennard-Stepanov error spectra give T* values ranging between 310 K and 347 K.

The slit width of the fluorimeter is an important factor in the error analysis. Larger slit widths lead to greater uncertainty in the position of the fluorescence spectra as a function of frequency. Any slit width greater than 2 nm FWHM produced variations in the fluorescence data sets that resulted in large distortions in the measurement. All data sets used in these experiments are taken with slit widths less than 2 nm FWHM.

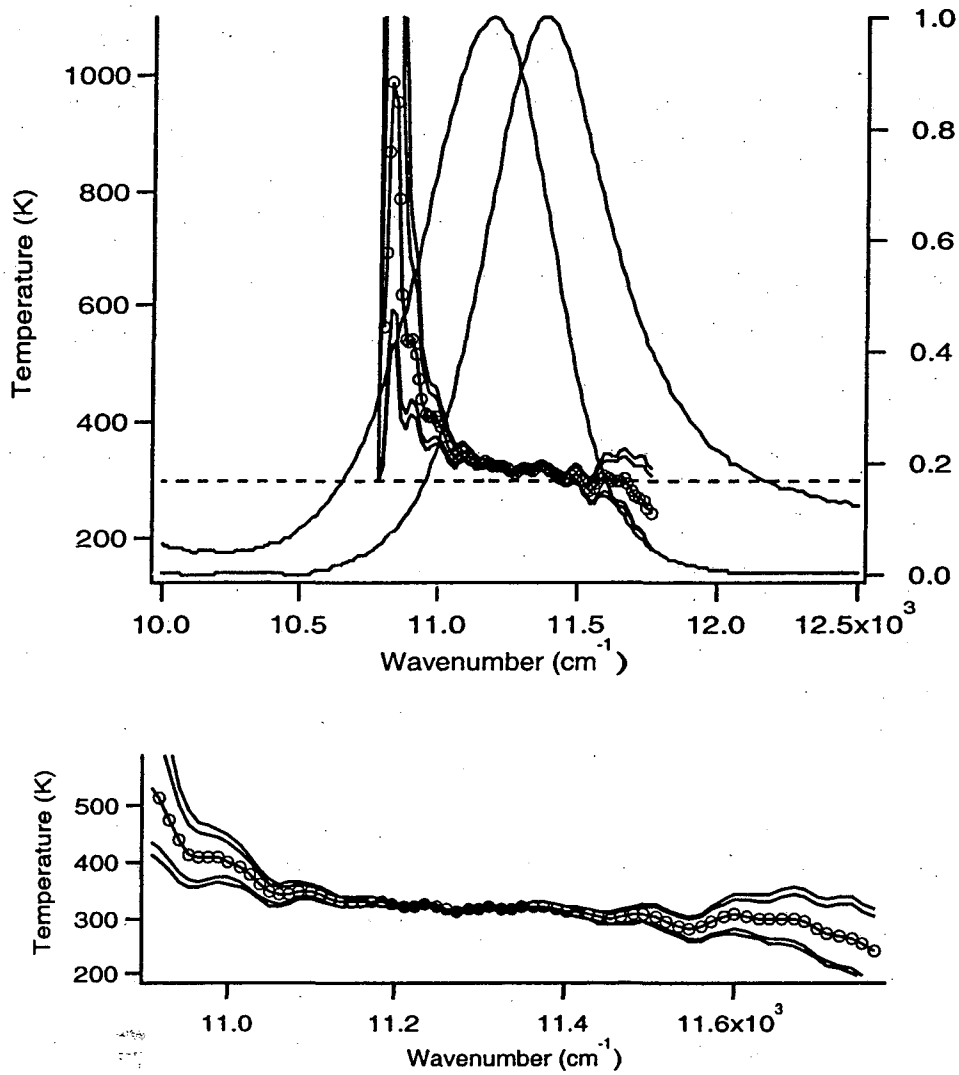

Figure 5.24: A) The local slope of the four Kennard-Stepanov error functions shown in figure 5.23 (solid lines), T*(ν) for RC-1A, together with the experimental Kennard-Stepanov function for RC-1A (open dots), shown on a temperature scale. The absorption spectrum and fluorescence spectrum for excitation at 375 nm are plotted against the right axis. The horizontal line indicates ambient temperature, 296 K. B) An expanded view of T*(ν) for RC-1A from 10,800 cm^{-1} to 11,800 cm^{-1}. The horizontal line indicates ambient temperature, 296 K.

Discussion:

First we will present a model of the photosynthetic components in *Rb. sphaeroides* to facilitate the interpretation of the experimental results. The LH2 antenna complex from *Rps. acidophila* has been crystallized, and its structure is known to high resolution.[17] This LH2 complex is closely related to the LH2 complex of *Rb. sphaeroides*; therefore, we will take the *Rps. acidophila* LH2 structure as a template for *Rb. sphaeroides* LH2. Based on this structure, LH2 is a torus-shaped protein, circular with a hole in the center. Within the protein, two rings of BChl are densely packed together in a ninefold symmetrical arrangement. The close packing of BChl within the LH2 protein results in very rapid excitation transfer between BChl molecules, with a time constant on the order of 100 fs for excitation transfer within the B850 ring,[18] and 0.9 ps for excitation transfer from the B800 ring to the B850 ring.[19] Theoretical calculations for the rates of excitation transfer have also been made using Förster theory and the known atomic structures of the antenna complexes and the reaction center.[20] The distribution of excitation in the B850 ring is modeled well by strong Coulombic, or exciton, coupling of the BChl molecules.[21,22] This causes delocalization of the excitation in the antenna over multiple pigments, although delocalization is not complete over the entire antenna because of static and dynamic disorder.[23] Excitonic coupling within the antenna will not affect the validity of the KS analysis, so long as the excitation reaches a complete equilibration between all of the excitonic bands prior to fluorescence emission.

While the LH1 antenna complex has not yet been crystallized, low-resolution electron density mapping indicates that it also has a torus-shaped protein structure and closely packed BChl.[24] Excitation transfer within LH1 is also rapid, on the order of 80 ps.[18] Exciation in LH1 is also well modeled by excitonic delocalization.[25] The hole in the center of LH1 is large enough to accommodate the reaction center. Our working model for the arrangement of the complexes is a reaction center surrounded by LH1,

with rings of LH2 on the periphery of the LH1 ring. This model is based on that of Papiz *et al.*[26] There are two measured time constants for excitation transfer from LH2 to LH1; 4.6 ps and 26.3 ps.[27] The first time constant is interpreted as direct excitation transfer from LH2 to LH1, and the second time constant is interpreted as excitation migration within LH2 prior to transfer to LH1. In this study, it was also noted that "a significant fraction of excitation remained in B850 (LH2) for considerably longer times."[26]

The rate of energy transfer from LH1 to the reaction center is not known at room temperature, because the measurement is complicated by the thermal equilibration of excitation in the antenna complexes. However, at 77 K, the time constant of energy transfer from LH1 to the reaction center can be measured in *Rb. sphaeroides* as 35 ps.[28] As a first approximation, 35 ps can be considered to be the time constant for excitation transfer from LH1 to the reaction center (RC) at room temperature.

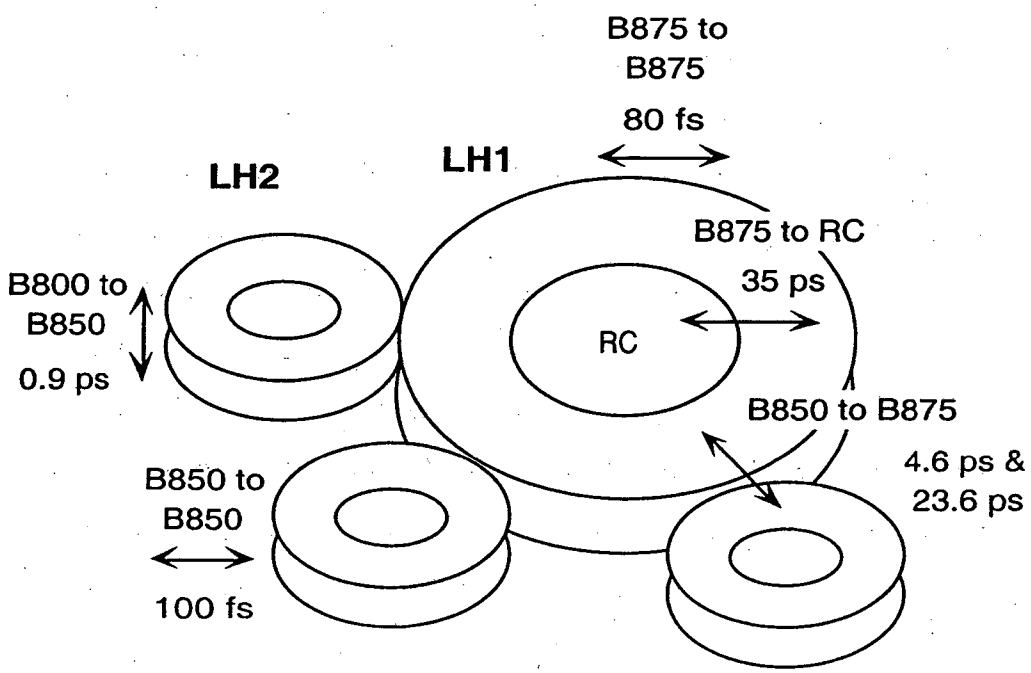

In this model, excitation transfer within antenna complexes, both LH1 and LH2, is very rapid, on the fs timescale. Direct excitation transfer from LH2 to LH1 occurs with a time constant of 4.6 ps; however, a longer time constant of 26.3 ps is also associated with excitation transfer, and even on that timescale excitation transfer from LH2 to LH1 is not complete. The time constant for excitation transfer from LH1 to the RC is estimated to be 35 ps.

The T* of the mutant strains:

We consider first the results from the three mutant strains of *Rb. sphaeroides*. The three mutants RC-1A, BALM/LH2 and LM1.1 represent the light harvesting complexes LH1, LH2, and both LH1 and LH2, respectively. The overall T* values for these strains have been determined. It is clear that a single averaged number such as T* extracted from the Kennard-Stepanov analysis is an oversimplification, and that more information may be obtained from the local slope of T*(ν). However, the single T* values are included here for comparison with previous KS analyses on photosynthetic systems. The T* values calculated from least-squares fitting to the linear region of the KS plots of the *Rb. sphaeroides* mutants are elevated above ambient temperature by 20 to 40 K. There is no systematic variation in the T* value as a function of excitation wavelength. Higher excitation energies did not lead to higher T* values; thus the warm fluorescence phenomenon is not observed in the *Rb. sphaeroides* mutant strains.

The elevation of T* by 20 to 40 K is in good agreement with the T* values calculated for isolated BChl molecules in a variety of organic solvents.[7] Such close agreement with results obtained from isolated BChl may seem at first surprising, because BChl in the light harvesting complexes have various complex pigment-protein interactions not found for isolated BChl molecules. Pigment-protein interactions may cause inhomogenous broadening, which is a cause of elevated T* temperatures.[6] Inhomogenous broadening can be modeled as a distribution of energetically distinct

species, each with individual absorption and fluorescence spectra. The KS relation is then an integrated function over the distribution of spectra.[6] From this treatment, the KS temperature T* becomes:

$$T^* = [(a^2 + b^2) / a^2]\ T \qquad [5.2]$$

Where a is the gaussian width parameter of the homogenous absorption, b is the distribution of the electronic energy of the distinct species, and $(a^2 + b^2)^{1/2}$ is the gaussian width parameter of the observed absorption.[6] Therefore, in the case of inhomogenous broadening, the observed KS temperature T* is greater than the ambient temperature T.

The relatively low KS temperature of the mutant strains indicates that the various chromophores in the light harvesting complexes transfer excitation very rapidly among themselves. Such rapid excitation sharing allows the complex to appear functionally as a single chromophore in the KS analysis. Rapid transfer of excitation within the light harvesting complexes supports the model of *Rb. sphaeroides* presented above. The lifetime of fluorescence emission for the mutant strains lacking reaction centers is approximately 650 ps.[29] Therefore, excitation equilibration processes within (on a fs timescale) and between (on a 4.6 - 23.6 ps timescale) the light harvesting complexes are very rapid on the timescale of fluorescence emission. In this way, the antenna systems of the mutant *Rb. sphaeroides* strains are similar to other photosynthetic systems such as PSII, which also show good experimental agreement with the Kennard-Stepanov relation.[10]

The T*(ν) of the mutant strains:

The T*(ν) plots reveal the structure of T* as a function of frequency. All three *Rb. sphaeroides* mutant strains produced a T*(ν) near the ambient temperature over the majority of the spectral range. Again, there is little variation observed in the T*(ν) as a function of excitation wavelength, ruling out a warm fluorescence. This result is

somewhat surprising for LM1.1, which has a different fluorescence spectrum depending on excitation wavelength. Despite the difference in fluorescence emission, all T*(ν) of LM1.1 were similar. The reason for this similarity is not known.

On the red edge of all three mutant strain spectra, for all excitation wavelengths, there is a strong peak in the T*(ν) plot. This peak differs in magnitude but is very reproducible in position, approximately 300 cm^{-1} to the red of the fluorescence emission maximum. This is near the edge of the absorption spectrum intensity. At the edges of the spectra, where the intensity is low, the error analysis reveals that the T*(ν) is very sensitive to small changes in the absorption and fluorescence spectra. However, while the magnitude of the red-edge peak fluctuates, it is always present in the same position in the error analysis.

What is the origin of the red-edge peak that is seen in all of the *Rb. sphaeroides* mutant strains?

One possibility is the presence of subsystems that have not reached complete equilibrium within the light harvesting complexes. The modeling studies of Sawicki and Knox show that two systems with incomplete equilibration between them do produce a sharp peak in the T*(ν) plot.[13] The position and magnitude of the peak depend on the relative spectral positions of the two systems and the rate of excitation transfer between them. One possible cause for the observed red-edge peak is a subset of extreme red-shifted BChl within the light harvesting complexes. The existence of such a subset, such as B896, has been postulated based on time-resolved anisotropy studies and modeling of exciton dynamics in both light harvesting complexes.[30] A related explanation for ultrafast relaxation data in B850 of LH2 of *Rb. sphaeroides* postulates a low energy exciton band, arising from exciton splitting of delocalized energy in the BChl ring.[31] A low energy red edge exciton band has also been proposed on the basis of hole-burning experiments in LH2.[32] This low lying exciton band may appear functionally in the Kennard-Stepanov analysis as a distinct red-shifted subset.

If a low energy, red edge population of BChl has an incomplete equilibrium with the majority of the BChl in the light harvesting complexes, the system would show a peak in the $T^*(\nu)$ according to the modeling simulations of Sawicki and Knox. Alternately, if the red edge subset has an altered or diminished fluorescence such that it is not in agreement with the KS prediction, a peak in the $T^*(\nu)$ may result. The low energy exciton band invoked in the analysis of ultrafast relaxation of B850 is proposed to be "dark", *i.e.*, to have a diminished fluorescence.[26]

A red-edge peak in the $T^*(\nu)$ similar to that which we observe in the light harvesting complexes has also been observed in chlorophyll molecules in organic solvents.[14] In the case of Chl a, the red-edge peak is ascribed to low-lying triplet states below the 0-1 transition band of Chl a. In isolated BChl studies in organic solvents, at room temperature there is not an intense peak observed on the red edge in the $T^*(\nu)$ as there is in Chl a. However, there is a broad increase in the $T^*(\nu)$ of BChl on the red edge of the spectra, reaching approximately 400 K (about 100 K above ambient temperature).[14] This red-edge rise in the $T^*(\nu)$ of BChl may possibly have the same origin as the red-edge peak seen in Chl a. Thus it is possible that the red-edge peak observed in the $T^*(\nu)$ of the light harvesting complexes is an intrinsic feature to BChl and Chl a, and that this is the same feature we observe in the light harvesting complexes. The specific origin of the red-edge peak in the isolated molecules has not yet been conclusively determined.

Inhomogenous broadening is another factor that can lead to elevated T^* values. However, the modeling studies of Sawicki and Knox show that inhomogenous broadening in test systems causes an increase in $T^*(\nu)$ over the entire range, rather than a sharp peak.[13]

The ideal fluorescence (I*) for the mutant strains:

I* is the fluorescence calculated from the experimental absorption spectrum and the ideal KS relation. The I* spectra for the *Rb. sphaeroides* mutant strains show a distinct trend; *i.e.*, a slight red-shift and a broadening on the red edge of the spectra, relative to the experimental fluorescence spectra. The experimental fluorescence spectrum is narrower and blue-shifted from the ideal fluorescence predicted by the KS relation. This data may be viewed as a deficiency of fluorescence emission on the red edge; that states which are absorbing light on the red edge of the absorption spectrum are not fully contributing to the fluorescence emission. This may be caused by a quenching of fluorescence on the red edge, or an efficient non-radiative excitation decay path on the red edge. Alternatively, these red edge states in the absorption spectrum may not receive excitation energy efficiently from higher energy states, and thus do not fluoresce efficiently. In this case, the red edge low energy states are not in full equilibrium with the higher energy states. These data are consistent with a red edge subset or low energy red edge exciton band in the light harvesting complexes which is not so highly fluorescent as predicted by the ideal Kennard-Stepanov relation.

The wild-type T*:

The wild-type *Rb. sphaeroides* differs from all the mutant strains previously discussed because it contains a functional reaction center. This reaction center quenches excitation energy in the antenna both in the Fo and the Fm states. In the Fo state, the fluorescence lifetime in the antenna is 60 ps.[33] In the Fo state, part of the excitation energy in the antenna is used for charge separation in the reaction center. In the Fm state, the antenna fluorescence lifetime is 250 ps.[17] The Fm state still quenches excitation energy in the antenna effectively. In the absence of functional reaction centers, the antenna fluorescence lifetime is approximately 650 ps,[34] much longer than

in the presence of even closed reaction centers which do not undergo charge separation (the Fm state).

A single T* value in the linear region in the KS plot for the wild-type *Rb. sphaeroides* is a particularly poor fit. For all excitation wavelengths, and in both the Fo and the Fm states, wild-type *Rb. sphaeroides* displays a split T* plot with two separate linear regions in the area of maximum overlap between the fluorescence and absorption spectra. Forcing a fit to a single T* value in this region gives very high values, about 80 to 200 K above room temperature. The reason for this poor fit and the lack of agreement with ambient temperature becomes obvious in the T*(ν) plot.

The wild-type T*(ν):

The T*(ν) plot of the wild type reveals the same red-edge peak as is present in the analysis of the mutant strains. It is also approximately 300 cm^{-1} to the red of the fluorescence emission maximum, as in the mutant strains. The height of the red edge T*(ν) peak varies between 700 and 900 K, but is always present in the same position. The presence of a reaction center therefore does not correct this deviation from the ideal Kennard-Stepanov relation on the red edge. The origin of the red-edge peak in the wild-type *Rb. sphaeroides* is probably the same as the origin of the red-edge peak seen in the mutant *Rb. sphaeroides* strains (see previous discussion).

In addition to the red-edge peak, there is also a second peak in the Stokes region of the wild-type *Rb. sphaeroides* T*(ν) plot. This second peak is the reason for the elevated T* value when a single value is extracted from the KS analysis. On either side of the second peak, the T*(ν) approaches closely to the ambient temperature. The presence of the T*(ν) peak indicates that the absorbing and fluorescing components have not reached an equilibrated state before fluorescence occurs. The magnitude of the T*(ν) peak in the Stokes region is directly related to the intensity of fluorescence

emission at 860 nm compared to 890 nm (F_{860} : F_{890}); that is, the ratio of LH2 to LH1 fluorescence.

What is the origin of the Stokes region peak in the wild type? Our model postulates that the RC is surrounded by LH1, and that LH2 is more distant from the reaction center than LH1. In this model, the reaction center is draining excitation more efficiently from LH1 than from LH2. The timescale of energy transfer from LH1 to the RC is approximately 35 ps, while energy transfer from LH2 to LH1 is occurring on a similar timescale (26.3 ps). Therefore, the presence of the reaction center energy siphon prevents complete excitation equilibration within *Rb. sphaeroides* and increases the relative fluorescence emission from LH2 compared with LH1.

Excitation wavelength has a direct effect on the magnitude of the T*(ν) peak (Table 5.1). Excitation at 800 nm (into LH2) produces a higher F_{860} : F_{890} ratio than excitation at 375 nm (into the Qx band of both LH1 and LH2). Direct excitation into LH2 increases the extent of excitation in LH2 that is not transferred completely to LH1 prior to fluorescence. That lack of equilibration is reflected in an increase in the magnitude of the T*(ν) peak, from 450K at 375 nm excitation to 525 K at 800 nm excitation (in the Fm state).

The state of the reaction center also has an effect on the magnitude of the T*(ν) peak. In the Fo state, the reaction center drains excitation more efficiently than in the Fm state. The lifetime of fluorescence in the wild type is 60 ps in the Fo state as opposed to 250 ps in the Fm state. Therefore, the increased rate of excitation drain in the Fo state causes an increased lack of equilibration, which is evident in the higher F_{860} : F_{890} ratio in the Fo state relative to the Fm state. This lack of equilibration is reflected in an increase in the magnitude of the T*(ν) peak, from 450 K in the Fm state to 550 K in the Fo state (for 375 nm excitation). The magnitude of the T*(ν) peak in the Stokes region of wild-type *Rb. sphaeroides* is a direct indication of the extent of non-equilibration between LH1 and LH2.

	Fm; ex=375nm	Fm; ex=800nm	Fo; ex=375nm	Fo; ex=800nm
Stokes T*(ν) magnitude	450 K	525 K	550 K	700 K
Red edge T*(ν) magnitude	900 K	700 K	900 K	750 K

Table 5.1: The magnitude of the peaks in the T*(ν) spectra for wild-type *Rb. sphaeroides* in Kelvins. The top row shows the magnitude of the T*(ν) peak in the Stokes region, and the bottom row shows the magnitude of the T*(ν) peak at the red edge for comparison. The magnitudes of the peaks are shown for the Fm and Fo state, and for excitation at 375 nm and 800 nm.

The ideal fluorescence (I*) for the wild type:

The ideal fluorescence (I*), calculated from the absorption of *Rb. sphaeroides* wild type and the ideal KS relation at 296 K, is slightly red-shifted from the experimental fluorescence and also has a much lower intensity in the shoulder region of the emission. The difference on the red edge of the spectrum is similar to that seen for the mutant strains, and is consistent with a diminished fluorescence from a red edge BChl subset or low energy exciton band.

The difference in the shoulder region of the I* in the wild type is not seen in the I* spectrum for the mutant LM1.1, which also has both LH1 and LH2. The shoulder region corresponds to the maximum of emission from LH2. Thus, in the wild type, the experimental emission from LH2 is higher than what is predicted by the ideal Kennard-Stepanov relation. This is consistent with our model in which the reaction center siphons energy from LH1 on the same timescale as excitation transfer from LH2 to LH1, resulting in an incomplete excitation equilibration in wild-type *Rb. sphaeroides*.

Conclusions:

The Kennard-Stepanov relation is a useful means of examining energy transfer and equilibration processes, even in complex photosynthetic systems. We have described the Kennard-Stepanov analysis as applied to *Rb. sphaeroides* wild type and several strains of *Rb. sphaeroides* mutants.

None of the mutant strains that we have examined in this study expresses reaction centers. The Kennard-Stepanov analysis of these mutant strains shows that each of these photosynthetic systems has very rapid excitation equilibration across the majority of the spectral range of the light harvesting complexes, showing excellent agreement with the KS relation. However, on the red edge of the fluorescence emission there is a peak in the $T^*(\nu)$ for all strains at all excitation wavelengths. This peak is consistent with a subsystem, such as a red-shifted pool of BChl or a low energy exciton band, that is not in complete equilibrium with the bulk BChl. There is other evidence for such a red edge subsystem from hole burning[27] and time resolved experiments[26] on antenna complexes of *Rb. sphaeroides*. The experimental fluorescence has a lower intensity on the red edge of the emission than the I^* fluorescence calculated from the absorption spectrum and the ideal KS relation. This is consistent with a diminished fluorescence or "dark" state for the red-shifted component.

The wild-type *Rb. sphaeroides* also has a peak on the red edge of the $T^*(\nu)$ spectrum, like the mutant strains. However, the wild type also shows a second peak in the Stokes region. The presence of a reaction center in the wild type dramatically changes the excitation equilibration processes in the *Rb. sphaeroides* photosynthetic system. Wild-type *Rb. sphaeroides* at room temperature does not show good agreement with the Kennard-Stepanov predictions; in this way it behaves quite differently from other heterogeneous photosynthetic systems with reaction centers, such as PSI[11] and PSII.[12]

On the basis of our working model, the reaction center functions as an efficient excitation sink, siphoning excitation from LH1 more efficiently than LH2 and disrupting equilibration in the system. The extent of the disruption of excitation equilibration depends on the excitation wavelength (whether excitation is only into LH2 or both LH1 and LH2) and the state of the reaction center (Fo or Fm, which affect the degree of excitation drain by the reaction center). Notably, the reaction centers in PSI and PSII do not have such an effect on the excitation equilibration in those systems.

It is clear that the relatively "simple" photosynthetic system *Rb. sphaeroides* is not actually simple. In some ways, *Rb. sphaeroides* is more complex than the more highly heterogeneous PSI and PSII systems. The individual components of the *Rb. sphaeroides* photosynthetic system, LH1 and LH2, are in very good agreement with the Kennard-Stepanov relation, with the exception of a deviation on the red edge of fluorescence emission. However, wild-type *Rb. sphaeroides* is more complex and presents a picture of a system which has not reached complete equilibration, in spite of very rapid excitation transfer within and between components of the system. It is evident that time resolved studies showing rapid excitation transfer are not sufficient evidence for complete excitation equilibration within a complex system such as *Rb. sphaeroides*.

References for Chapter Five

[1]Bowen, E.J. & Metcalf, W.S. (1951) *Proc. Roy. Soc. London* A206: 437-445.

[2]Kozma, L., Szalay, L. & Hevesi, J. (1964) *Acta Phys. Chem. Szeged* 10: 67-74.

[3]Kennard, E.H. (1918) *Phys. Rev.* 11: 29-38.

[4]Stepanov, B.I. (1957) *Sov. Phys.-Dokl.* 2: 81-84.

[5]A homogenous system contains only one absorbing and fluorescing component.

[6]Van Metter, R.L. & Knox, R.S. (1976) *Chemical Physics* 12: 333-340.

[7]Strickler, S.J. & Berg, R.A. (1962) *J. Chem. Phys.* 37: 814-822.

[8]Knox, R.S., Laible, P.D., Sawicki, D.A. & Talbot, M.F.J. (1997) *Journal of Luminescence* 72-74: 580-581.

[9]Becker, M., Nagarajan, V. & Parson, W.W. (1991) *J. Am. Chem. Soc.* 113: 6840-6848.

[10]Bjorn, L.O. & Bjorn, G.S. (1986) *Photochem. and Photobiol.* 44 (4): 535-542.

[11]Croce, R., Zucchelli, G., Garlaschi, F.M., Bassi, R. & Jennings, R.C. (1996) *Biochem.* 35: 8572-8579.

[12]Dau, H. & Sauer, K. (1996) *Biochim. et Biophys. Acta* 1273: 175-190.

[13]Sawicki, D.A. & Knox, R.S. (1996) *Phys. Rev. A* 54: 4837-4841.

[14]Bellacchio, E. & Sauer, K. (1999) *J. Phys. Chem. B* 103: 2279-2290.

[15]Hevesi, J. & Singhas, G.S. (1969) *Spectrochim. Acta A* 25: 1751-1758.

[16]Knox, R.S., Brown, J.S., Laible, P.D. & Talbot, M.F.J. (1999) *Photosynth. Res.* 60: 165-177.

[17]McDermott, G., Prince, S. M., Freer, A. A., Hawthornthwaite-Lawless, A. M., Papiz, M. Z., Cogdell, R. J. & Isaacs, N. W. (1995) *Nature (UK)* 374: 517-521.

[18]Fleming, G.R. & van Grondelle, R. (1997) *Current Opinion in Structural Biology* 7: 738-748.

[19]Herek, J.L., Fraser, N.J. Pullerits, T., Martinsson. P,. Polivka, T., Scheer. H., Cogdell, R.J. & Sundström, V. (2000) *Biophysical Journal* 78: 2590-2596.

[20] Ritz, T., Sanghyun, S. & Schulten, K. (2001) *J. Phys. Chem. B* 105: 8259-8267.

[21] Sauer, K., Cogdell, R.J., Prince, S.M., Freer, A.A., Isaacs, N.W. & Scheer, H. (1996) *Photochem. Photobiol.* 64: 564-576.

[22] Freer, A., Prince, S., Sauer, K., Papiz, M., Hawthornthwaite-Lawless, A., McDermott, G., Cogdell, R. & Isaacs, N. (1996) *Structure* 4: 449-462.

[23]Krueger, B.P., Scholes, G. D., Yu, J.-Y. & Fleming, G.R. (1999) *Acta Physica Polonica A.*, 95: 63-83.

[24]Karrasch, S., Bullough, P.A. & Ghosh, R. (1995) *EMBO J.* 14: 631-638.

[25] Sundström, V. (2000) *Progress in Quantum Electronics* 24: 187-238.

[26]Papiz, M.Z., Prince, S.M., Hawthornthwaite-Lawless, A.M., McDermott, G., Freer, A.A., Isaacs, N.W. & Cogdell, R.J. (1996) *Trends in Plant Science* 6: 198-206.

[27]Nagarajan, V. & Parson, W.W. (1997) *Biochemistry* 36: 2300-2306.

[28]Visscher, K.J., Bergström, H., Sundström, V., Hunter, C.N. and van Grondelle, R. (1989) *Photosynth. Res.* 22: 211-217.

[29]Sebban, P. and Moya, I. (1983) *Biochim. et Biophys. Acta* 722: 436-442.

[30]Novoderezhkin, V.I. & Razjivin, A.P. (1995) *Biophysical Journal* 68: 1089-1100.

[31]Nagarajan, V., Alden, R.G., Williams, J.C. & Parson, W.W. (1996) *Proc. Natl. Acad. Sci. USA* 93(24): 13774-13779.

[32]Reddy, N.R.S., Picorel, R. & Small, G.J. (1992) *J. Phys. Chem.* 96: 6458-6464.

[33]Borisov, A.Yu., Freiberg, A.M., Godik, V.I., Rebane, K.K., and Timpmann, K.E. (1985) *Biochim. et Biophys. Acta* 807: 221-229.

[34]Sebban, P. (1985) *Physiol. Veg.* 23: 449-462.

Blank

Appendix A: Growth media

RCV (2 Liters)

Distilled water	1750 ml
10% $(NH_2)SO_4$ [50g/500ml]	20 ml
10% malic acid/NaOH [50g malic acid; 30 g NaOH]	80 ml
super salts [see below]	100 ml
phosphates [20g KH_2PO_4; 30gK_2HPO_4 anhyd.]	30 ml

add phosphates last to prevent precipitation
adjust pH to 6.8

super salts:

1% EDTA [1g/100ml]	20 ml
20% $MgSO_4 \cdot 7H_2O$ [20g/100ml]	10 ml
7.5% $CaCl_2 \cdot 2H_2O$ [7.5g/100ml]	10 ml
0.5% $FeSO_4$ [0.15g/25ml]	25 ml
trace elements	10 ml

trace elements:

Distilled water	250 ml
$MnSO_4$	0.40 g
H_3BO_3	0.70 g
$Cu(NO_3)_2$	0.01 g
$ZnSO_4 \cdot 7H_2O$	0.06 g
$Na_2MoO_4 \cdot 2H_2O$	0.20 g

Vitamin supplements:
50 ml distilled water
100 mg thiamin
50 mg biotin
100 mg niacin (add niacin last)
Adjust pH to 6.8 with NaOH

Sterile-filter vitamin solution and add after autoclaving RCV
2 ml vitamin solution per liter of RCV

For DMSO cultures:

Use RCV recipe with triple-distilled water
Add:

$Na_2MoO_4 \cdot 2H_2O$	0.20 g/l
Fructose	6 g/l
Pyruvate	6 g/l

YCC+ (1 Liter)

940 ml distilled water
20 ml phosphate buffer
30 ml ammonium succinate
5 ml metals 44
5 g yeast extract
6 g casamino acids
pH = 6.8 with NaOH

Phosphate buffer
- one liter distilled water
- 115 g K_2HPO_4
- 45 g KH_2PO_4

Ammonium succinate
- 118 g succinic acid
- 750 ml distilled water
- pH = 6.8 with about 140 ml NH_4OH
- bring final volume to one liter

Metals 44
- four liters distilled water
- 28.4 g tetrasodium EDTA
- 4.0 g $ZnSO_4 \cdot 7H_2O$
- 0.16 g $CuSO_4 \cdot 5H_2O$
- 0.08 g $NaB_4O_7 \cdot 10H_2O$
- 0.12 g $CoCl_2 \cdot 6H_2O$
- 10.0 g nitrilotriacetic acid
- 0.08 g $Na_2MoO_4 \cdot 2H_2O$
- 27.6 g $Ca(NO_3)_2 \cdot 4H_2O$
- 160 g $MgSO_4 \cdot 7H_2O$
- 3.0 g $FeSO_4 \cdot 7H_2O$

Add biotin vitamins and antibiotics after autoclaving YCC+ media

2 ml biotin vitamin per liter of YCC+
Biotin vitamins
- 100 ml distilled water
- 100 mg niacin
- 50 mg thiamine-HCl
- 2 ml of 1mg/ml biotin in 50% ethanol:H_2O

sterile-filter vitamins before adding to YCC+ media

Antibiotics
- 2.5 µg/ml tetracycline
- 25 µg/ml kanamycin

Appendix B:
Genotypes and Phenotypes of *Rb. sphaeroides* Mutant Strains

Introduction:

The mutant strains of *Rb. sphaeroides* used in these studies were generous gifts from Dr. JoAnne Williams at Arizona State University. All development and construction of the mutant strains was accomplished by Dr. Williams' lab at ASU. This appendix is a brief summary of some of the most important considerations in the construction of the mutant strains that have a bearing on the experiments discussed in this dissertation.

The genetics of purple photosynthetic bacteria:

The genes expressing the photosynthetic components of *Rb. sphaeroides* are located on the largest chromosome (chromosome I). Sequencing of the *Rb. sphaeroides* chromosome has been aided by homology to a similar region in *Rb. capsulatus*. In 1976 Yen and Marrs[1] discovered a grouping of pigment biosynthesis genes on the chromosome of *Rb. capsulatus* that was later found to also contain genes coding for the reaction center and LH1 polypeptides. It is now called the photosynthesis gene cluster.

The sequence of the 46 kB photosynthesis gene cluster in *Rb. capsulatus* has been determined.[2] Knowledge of this sequence, and the high degree of homology between purple photosynthetic bacteria, has allowed for oligonucleotide-directed mutagenesis of *Rb. sphaeroides* which permits the insertion of restriction sites at desired positions (see Figure B.1). These restriction sites enable digestion of the DNA

by restriction enzymes at novel positions and deletion or modification of genetic material in the photosynthesis gene cluster.

The *puf* operon

Refer to Figure B.1 for illustration of the following discussion. There are two regions of the *Rb. sphaeroides* chromosome relevant to the mutant strain development, the *puf* operon and the *puc* operon. The puf operon contains genes which express the reaction center polypeptides L and M, and the LH1 polypeptides α and β. Digestion by restriction enzymes enables the replacement of the genes coding for the LH1 β and α polypeptides (*pufBA*) and/or the reaction center L and M polypeptides (*pufLM*) with antibiotic resistance markers. The products are known as deletion mutants. In addition to these genes, other genes are present on the *puf* operon which are essential to photosynthetic growth.

The *pufQ* gene is located at the 5' end of the *puf* operon, upstream of *pufBA*. *PufQ* codes for a hydrophobic 77-amino acid protein which is believed to stimulate bacteriochlorophyll synthesis, possibly very early in the biosynthetic pathway.[3] In the absence of *pufQ*, normal wild type levels of light harvesting complexes do not assemble.

Another gene present on the *puf* operon is *pufX*, located downstream at the 3' end of the operon. The *pufX* gene product has an M(r) of 8-10,000 Da and copurifies with the RC/LH1 complex.[4] Copurification with RC/LH1 suggests an affiliation with PufX *in vivo*.[5] Hydropathy plots indicate a single transmembrane helix structure, similar in dimension to the α or β subunit of LH1, but which binds no pigments.[6] One PufX polypeptide is estimated to associate with each LH1/RC complex.[7] In the absence of PufX, *Rb. sphaeroides* with functional reaction centers and LH1 is reported to be photosynthetically incompetent, although *pufX* deletion is not lethal.[8] Photosynthetic growth capability is restored by a variety of secondary suppressor

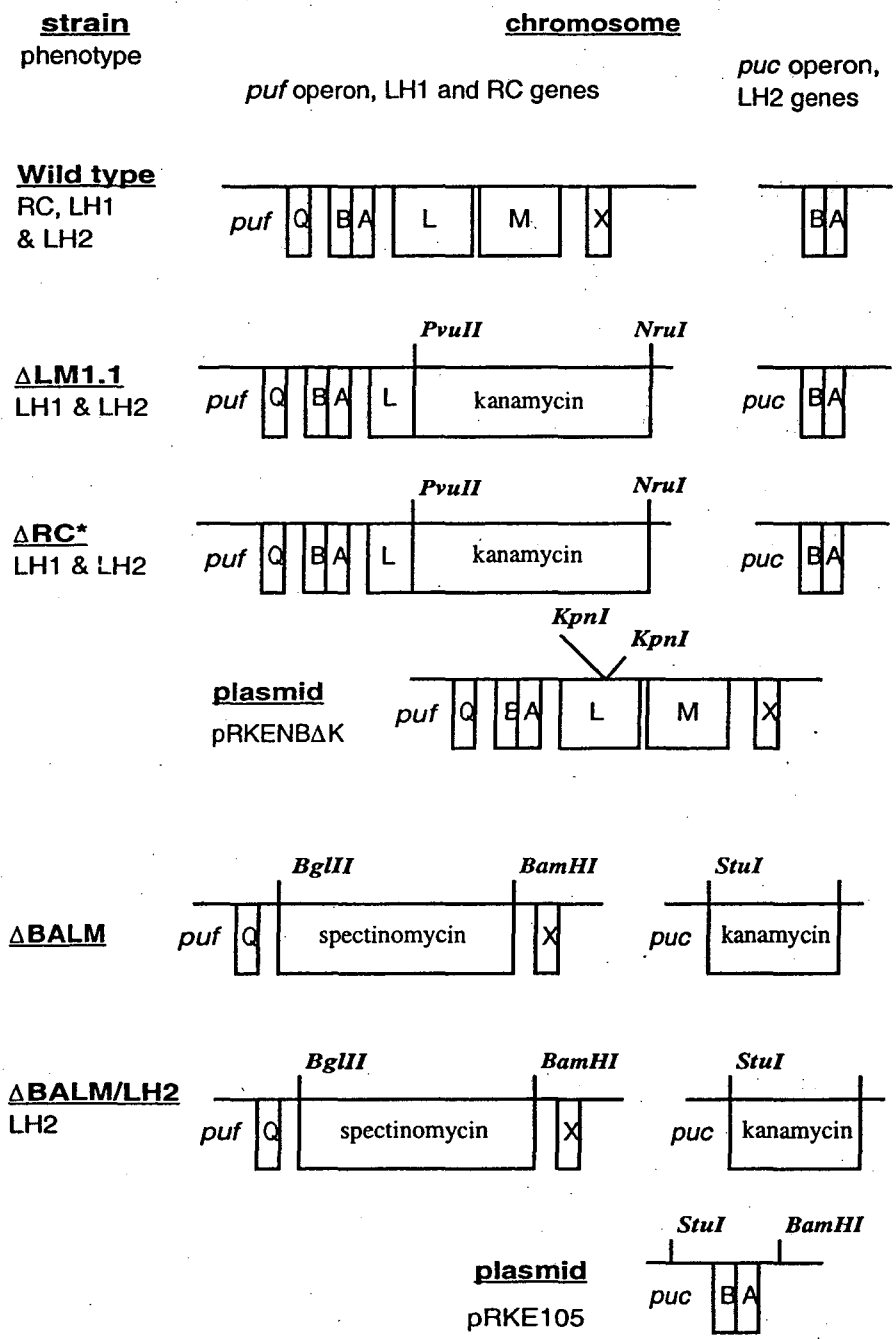

Figure B.1: A schematic presenting the genetic alterations in mutant strains of *Rb. sphaeroides*. Modifications are shown within the *puf* and *puc* operons, together with any supplemental plasmids which contain genetic material. Restriction sites are shown in bold. Note that all plasmids also express tetracycline resistance. See reference 16, Williams and Taguchi, for further details. Figure B.1 continues on the next page.

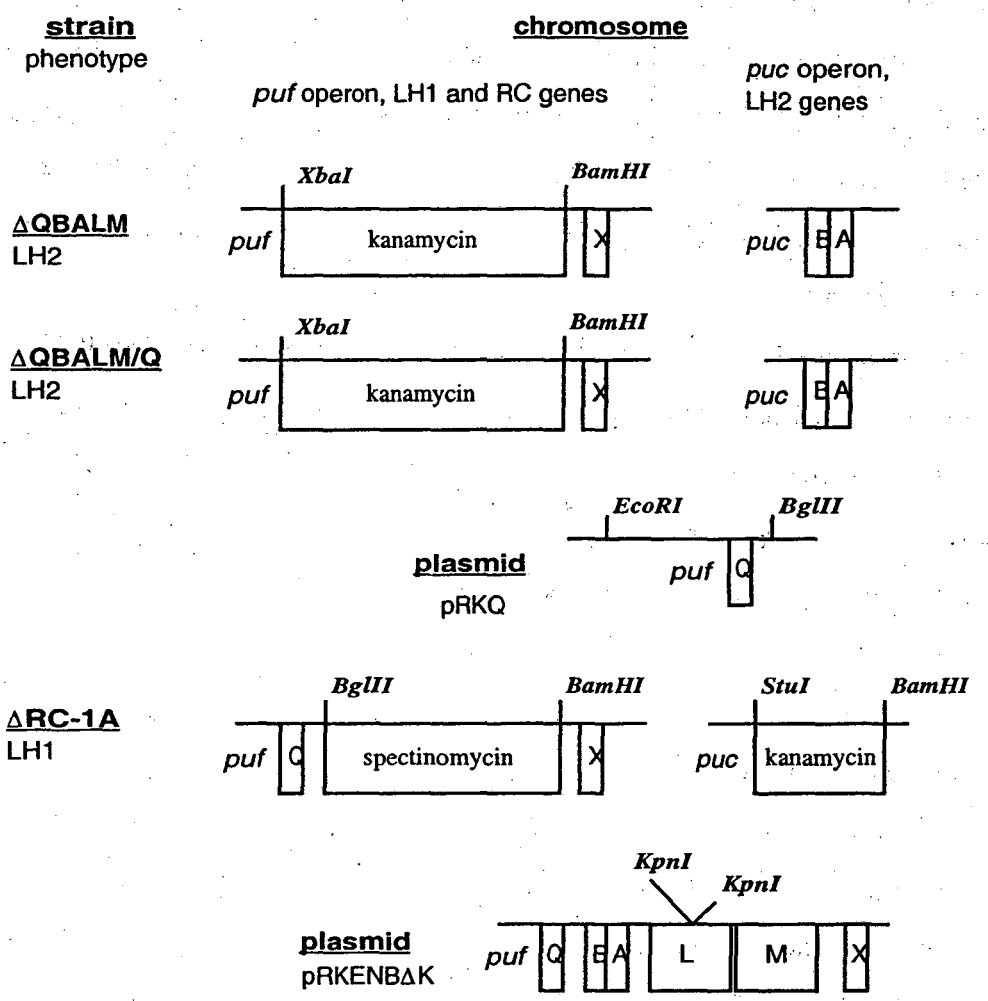

Figure B.1, continued: A schematic presenting the genetic alterations in mutant strains of *Rb. sphaeroides*. Modifications are shown within the *puf* and *puc* operons, together with any supplemental plasmids which contain genetic material. Restriction sites are shown in bold. Note that all plasmids also express tetracycline resistance. See reference 16, Williams and Taguchi, for further details. Figure B.1 begins on the previous page.

mutations acting on LH1, including mutations which prevent the assembly of LH1. Strains without *pufX* (*pufX*- mutants) express higher levels of LH1 than wild type, and electron flow to the cytochrome bc1 complex is inhibited under multiple flash conditions.[9] *PufX*- mutants have a lower turnover rate of Q/QH_2 exchange at the Q_B site,[10] possibly indicating a role for PufX in mediating the accessibility of that site by permitting diffusion of the quinol. PufX may also be involved with the dimerization of LH1/RC complexes.[7]

Another effect of *pufX* deletion is a change in the morphology of the ICM. It has been reported that certain *pufX*- mutants have ICM 50% larger than wild type,[11] and that the chromatophores obtained from *pufX*- mutants are not sealed vesicles,[12] or have a decreased degree of orientation. These factors are of course crucial to our study which relies on differential salt gradients across oriented sealed vesicles for producing an electric field across the membrane.

The *puc* operon

Physically distant from the *puf* operon is the *puc* operon, which codes for the polypeptides in LH2. In *Rb. sphaeroides*, the *puc* operon consists of *pucBAC*, which code for the β and α subunits of LH2, as well as PucC, which appears to be involved with the stable assembly of LH2.[13] Deletion of the *puc* operon can also lead to changes in membrane morphology, although the relation is not definitive. Some mutants missing *pucBA* or *pucBAC* show extended tubes or sheets[14] in the ICM rather than vesiculation, but not all *pucBAC*- mutants follow this pattern. Some *pucBAC* mutants appear normal.[15] Some mutants missing only *pucC* may have an altered morphology. It should be noted that *Rs. rubrum*, which lacks *pucBAC* and does not express any LH2, does form vesicular intracytoplasmic membrane structure and intact sealed chromatophores.

Plasmids

Besides deletion strains lacking *puf* or *puc* operons, additional genetic manipulations can be achieved through incorporation of plasmids which contain supplementary or altered genetic material. For *Rb. sphaeroides*, a broad-host-range plasmid called pRK serves as a convenient vector for gene insertion. The number of plasmids present in any given bacterial cell depends on the specific bacterial strain as well as the type of plasmid, and is known as the copy number. For *Rb. sphaeroides* there are typically 4-6 pRK plasmids per cell, while for *Rs. rubrum* the copy number for the same plasmid can be as high as 14.[16] A high copy number may sometimes, but not always, result in overexpression of the gene product on the plasmid relative to wild type. The plasmids used in the construction of the *Rb. sphaeroides* mutants contain an antibiotic resistance marker which insures the plasmid presence in the host cell under conditions of selection; *i.e.*, when the cells are grown in the presence of the specific antibiotic. In the absence of antibiotic or other selection, up to 50% of *Rb. sphaeroides* cells lose all pRK plasmids in just six to eight doublings; this process of plasmid loss is known as "curing the strain".

Three plasmids have been used in development of the strains that will be discussed here. The first, pRKENBΔK, contains the entire *puf* operon coding for LH1 and the reaction center, as well as *pufQ* and *pufX*. The reaction center L subunit has been modified by a deletion of 172 base pairs, and as a result the plasmid does not assemble functional reaction centers (assayed by absorption spectroscopy and bleaching experiments). The second plasmid, pRKQ, contains only the supplementary gene *pufQ*. The third plasmid, pRKE105, contains the LH2 genes on the *puc* operon, *pucBAC*. All three plasmids express tetracycline resistance. Tetracycline is unstable when exposed to light and decomposes to a toxic form. Since loss of plasmids occurs without antibiotic selection, maintenance of these strains therefore requires growing the strains with plasmids in the absence of light.

Mutant strain genotypes and phenotypes:

Following is a discussion of the genotypes of the individual mutant strains which are used in this study. Refer to Figure B.1 for illustration. Note that none of these mutants express functional reaction centers.

ΔLM1.1[17] is a deletion mutant which contains *pufQ, pufBA*, and *pucBA* on the chromosome, and thus expresses normal wild type levels of LH1 and LH2. It has a kanamycin resistance marker in place of *pufL*, *pufM* and *pufX*; therefore it will not express a functional reaction center. The absence of *pufX* may cause morphological changes in the ICM and lead to chromatophores different from the wild type as discussed above.

ΔRC* is based on ΔLM1.1 and supplemented with plasmid pRKENBΔK, expressing *pufQBAMX*. *PufL* is not expressed in its wild type form from this plasmid due to a deletion of 172 base pairs at residue 58, and functional reaction centers do not assemble. This strain expresses LH1 and LH2 genes from the chromosome. ΔRC* also has a supplemental copy of LH1 on the plasmid, and overproduces LH1 relative to the wild type.

ΔBALM[16] is a deletion mutant which has a spectinomycin resistance marker in place of the *pufBALM* gene sequence, and thus is incapable of producing reaction centers or LH1. *PufQ* and *pufX* are present on the gene; however, the spectinomycin resistance marker ends with a stop codon so *pufX* is probably not expressed, and this strain may have an altered membrane morphology as discussed above. ΔBALM also has a kanamycin resistance marker in place of the *pucBA* genes and so cannot express LH2 polypeptides, making it a "blank" in terms of light harvesting complexes.

ΔBALM/LH2[18] is based on the ΔBALM deletion mutant and in addition contains the plasmid pRKE105, which codes for the LH2 α and β polypeptides. This is an LH2-only mutant which probably does not express *pufX* due to a stop codon

terminator in the spectinomycin resistance marker. Therefore ΔBALM/LH2 may have an altered intracytoplasmic membrane morphology as discussed above.

ΔRC-1A is also derived from ΔBALM and is complemented with the plasmid pRKENBΔK, expressing *pufQBAMX*. *PufL* is not expressed in its wild type form from this plasmid due to a deletion of 172 base pairs at residue 58, and functional reaction centers do not assemble. This strain produces LH1 as well as the *pufQ* and *pufX* gene products from the plasmid.

ΔQBALM is a deletion strain which carries a kanamycin resistance marker in place of *pufQBALM*. *PucBA* is unaltered on the chromosome, and therefore this strain should express LH2 polypeptides as well as the *pufX* gene product. However, the absence of *pufQ* inhibits formation of wild type levels of LH2.

ΔQBALM/Q is derived from ΔQBALM and supplemented with pRKQ, a plasmid which expresses *pufQ*. *PucBA* is expressed from the chromosome as well as *pufX*. This strain produces LH2.

In summary, the genotypes and phenotypes of seven reaction centerless mutants of *Rb. sphaeroides* bacteria have been presented. One is a blank, expressing no antenna complexes (ΔBALM), one expresses only LH1 (ΔRC1A), and two express LH1 and LH2 (ΔLM1.1 and ΔRC*). ΔRC* also overexpresses LH1. The remaining three mutants express LH2 only (ΔBALM/LH2, ΔQBALM, and ΔQBALM/Q), although ΔQBALM does not synthesize wild type levels of bacteriochlorophyll because of the loss of *pufQ*.

References for Appendix B

[1]Yen, H.C. & Marrs, B. (1976) *J. Bacteriol.* 126: 619-629.

[2]Alberti, M., Burke, D. & Hearst, J. (1995) in *Anoxygenic Photosynthetic Bacteria* (Blankenship, R.E., Madigan, M. & Bauer, C.E., eds.) pp. 1083-1106, Kluwer Academic Publishers, Boston, MA.

[3]Fidai, S., Dahl, J.A. & Richards, W.R. (1995) *FEBS Lett.* 372: 264-268.

[4]Farchaus, J.W., Barz, W.T., Grunberg, H. & Oesterhelt, D. (1992) *EMBO J.* 11: 2779-2788.

[5]Pugh, R.J., McGlynn, P., Jones, M.R. & Hunter, C.N. (1998) *Biochim. Biophys. Acta* 1366: 301-316.

[6]Lilburn, T.G., Prince, R.C. & Beatty, J.T. (1995) *J. Bacteriol.* 177: 4593-4600.

[7]Francia, F., Wang, J., Venturoli, G., Melandri, B.A., Barz, W.P. & Oesterhelt, D. (1999) *Biochemistry* 38: 6834-6845.

[8]Barz, W.P. & Oesterhelt, D. (1994) *Biochemistry* 33: 9741-9752.

[9]Lilburn, T.G., Haith, C.E., Prince, R.C. & Beatty, J.T. (1992) *Biochim. Biophys. Acta* 1100: 160-170.

[10]Barz, W.P., Vermeglio, A., Francia, F., Venturoli, G., Melandri, B.A. & Oesterhelt, D. (1995) *Biochemistry* 34: 15248-15258.

[11]Lilburn, T.G, Haith, C.E., Prince, R.C. & Beatty, J.T. (1992) *Biochim. Biophys. Acta* 1100: 160-170.

[12]Barz, W.P., Fancia, F., Venturoli, G., Melandri, B.A., Vermeglio, A. & Oesterhelt, D. (1995) *Biochemistry* 34: 15235-15247.

[13]Gibson, L.C.D., McGlynn, P., Chaidhri, M. & Hunter, C.N. (1992) *Molec. Microbiol.* 6: 3171-3186.

[14]Sturgis, J.N. & Niederman, R.A. (1996) *Arch. Microbiol.* 165: 235-242.

[15]Golecki, J.R., Tadros, M.H., Ventura, S. & Oelze, J. (1989) *FEMS Microbiol. Lett.* 65: 315-318.

[16]Williams, J.C., Taguchi, A.K.W. (1995) in *Anoxygenic Photosynthetic Bacteria* (Blankenship, R.E., Madigan, M.T & Bauer, C.E., eds) pp. 1030-1065, Kluwer Academic Publishers, Boston, MA.

[17]Paddock, M.L., Rongey, S.H., Feher, G. & Okamura, M.Y. (1989) *Proc. Natl. Acad. Sci. USA* 86: 6602-6606.

[18]Lee, J.K., Kiley, P.J. & Kaplan, S. (1989) *J. Bacteriol.* 171: 3391-3405.

Appendix C

The effect of ferricyanide on the fluorescence emission of *Rb. sphaeroides* wild-type and mutant membrane preparations

Ferricyanide is a chemical oxidant. Addition of ferricyanide has been frequently cited in the literature as a means of oxidizing the primary electron donor (the special pair, P) of various species of purple photosynthetic bacteria.[1,2] Under these oxidized conditions (P^+BHQ_A), the special pair can no longer initiate charge separation. The chemically oxidized state of the special pair is identical to the state which occurs under conditions of prolonged continuous illumination (P^+BHQ_A). In this state, because excitation is not being used for charge separation, the fluorescence has a maximum value. This state is called the Fm state (see Chapter Two). Oxidizing the special pair is of interest for our experiments on the rate of charge separation in the reaction center of *Rb. sphaeroides* (Chapter Four), because the Fm state is the control state in which charge separation cannot occur.

However, in our hands, the addition of potassium ferricyanide to chromatophores of *Rb. sphaeroides* does not produce a state of maximum fluorescence emission. Instead, addition of ferricyanide results in a strong quenching of the fluorescence emission of *Rb. sphaeroides* chromatophores (in the Fm state) across the entire emission wavelength range (Figure C.1a). The maximum extent of quenching is at 890 nm, which is also the emission maximum of LH1 (Figure C.1b).

The addition of ferricyanide, which causes strong fluorescence quenching, does not have a large effect on the *Rb. sphaeroides* absorption in the near-IR region (Figure C.2). Small decreases in absorption are evident at 800 nm and 865 nm, consistent with the oxidation of the reaction center pigments.[3] However, the maximum absorption

change is only approximately 2%, while the fluorescence emission change is approximately 85% at 890 nm.

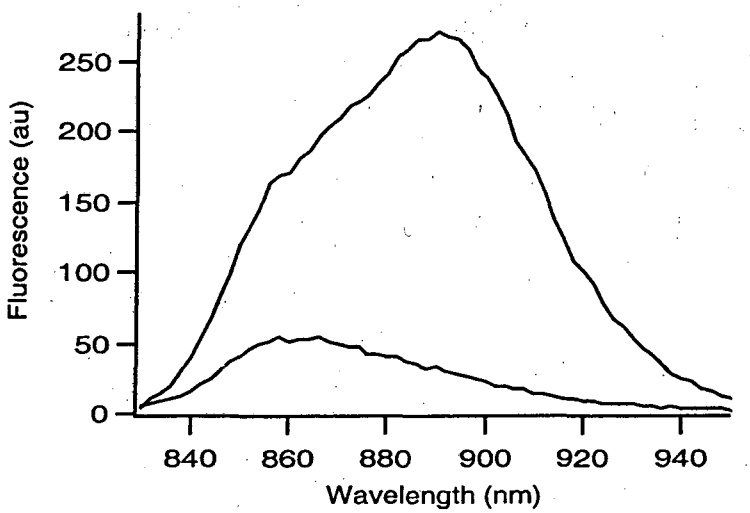

Figure C.1a: Fluorescence emission of *Rb. sphaeroides* wild-type chromatophores before (top curve) and after (bottom curve) addition of potassium ferricyanide (final concentration 3.5 mM). Excitation at 800 nm.

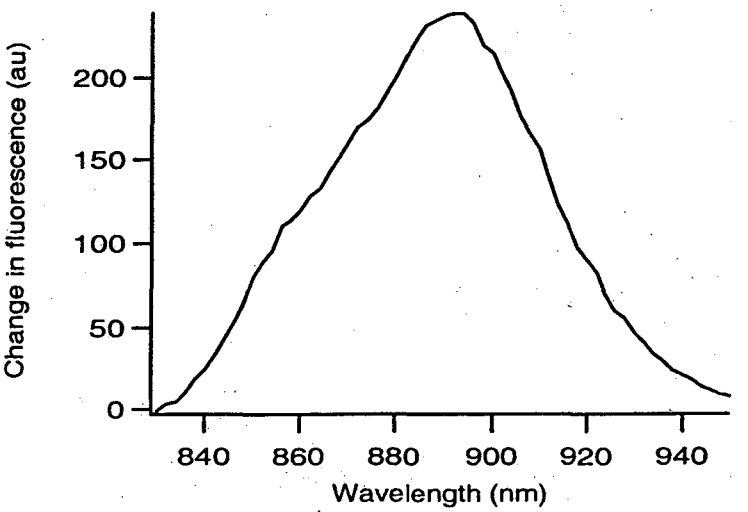

Figure C.1b: Difference in the fluorescence emission spectrum (top spectrum minus bottom spectrum in Figure C.1a) after the addition of potassium ferricyanide (final concentration 3.5 mM).

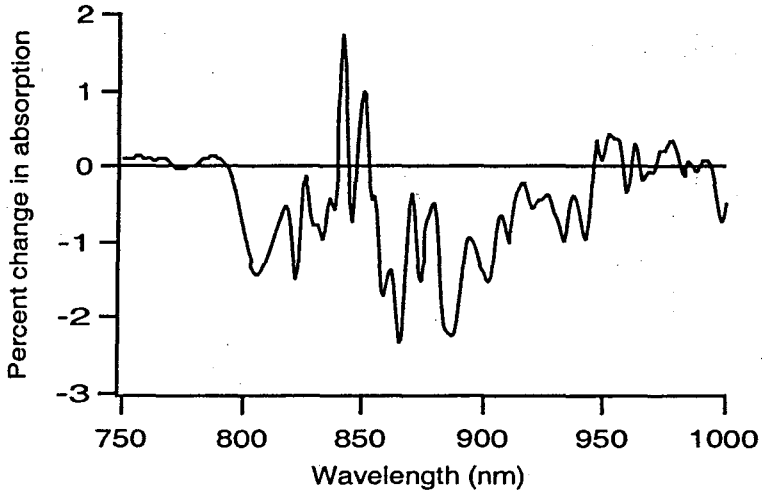

Figure C.2: Change in the near-IR *Rb. sphaeroides* absorption caused by 5 mM ferricyanide.

The fluorescence quenching caused by ferricyanide (which produces oxidizing conditions) is partially reversed by the subsequent addition of ferrocyanide (Figure C.3). Addition of ferrocyanide partially re-reduces the chromatophore solution.

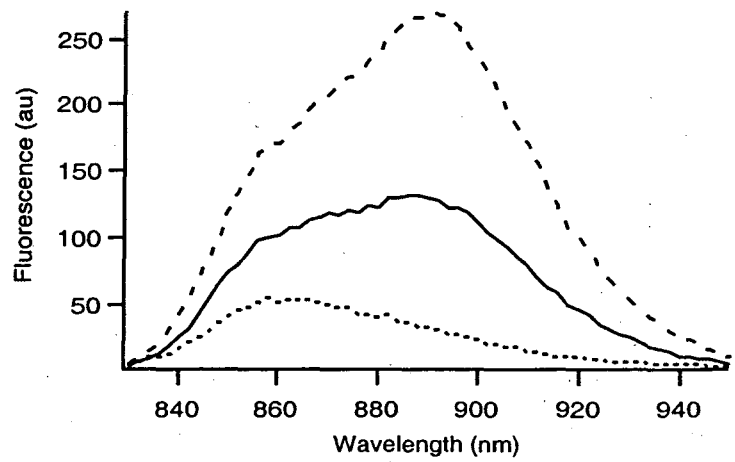

Figure C.3: Untreated *Rb. sphaeroides* chromatophore fluorescence emission (dashed line, top); fluorescence emission after addition of potassium ferricyanide to a final concentration of 3.5 mM (dotted line, bottom); and partial recovery of fluorescence emission after addition of potassium ferrocyanide to a final concentration of 0.1 mM (solid line, middle). Excitation at 800 nm.

However, there is some degree of hysteresis in the ferricyanide-induced oxidation of *Rb. sphaeroides* chromatophores. When ferricyanide (final concentration 5 mM) is added to *Rb. sphaeroides* chromatophores first, followed by addition of ferrocyanide (final concentration 2 mM), the extent of fluorescence quenching is greater than if the same solutions of ferricyanide and ferrocyanide are added simultaneously (Figure C.4).

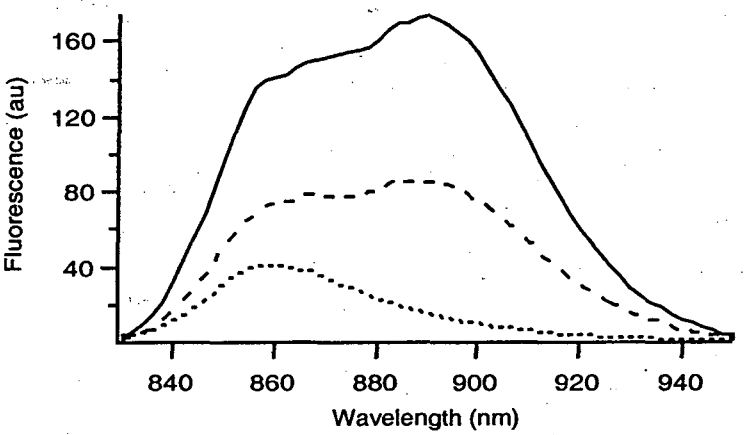

Figure C.4: Fluorescence emission of *Rb. sphaeroides* with 5 mM ferricyanide alone (dotted line, bottom); 5 mM ferricyanide followed by 2 mM ferrocyanide (dashed line, center); and 5 mM ferricyanide with 2 mM ferrocyanide added simultaneously (solid line, top).

The results presented thus far have all been from the Fm state of *Rb. sphaeroides*, which is obtained when the chromatophore solution remains in the excitation beam of the fluorimeter for the duration of the measurement. Ferricyanide also quenches the fluorescence of *Rb. sphaeroides* in the Fo, open trap state, which is obtained when the chromatophores are continuously flowing in the excitation beam of the fluorimeter during the measurement. The fluorescence quenching in the Fo state with 5 mM ferricyanide is shown in Figure C.5.

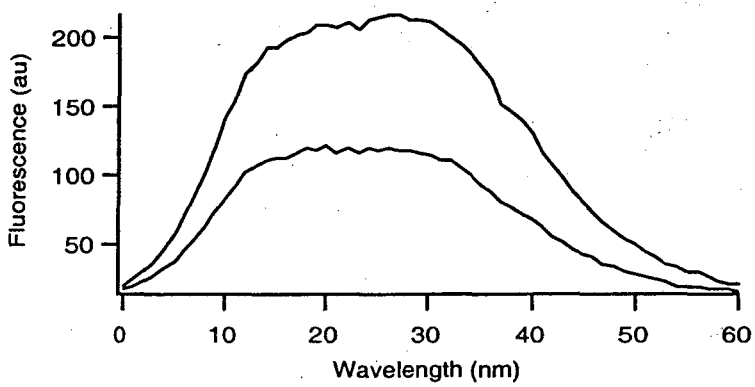

Figure C.5: Fluorescence emission in the Fo state of *Rb. sphaeroides* in the untreated state (top curve) and with 5 mM ferricyanide (bottom curve).

The change in fluorescence can be titrated as a function of the redox potential in solution, which increases with each subsequent addition of ferricyanide. The Fm and Fo state fluorescence of *Rb. sphaeroides* are shown in Figure C.6 as a function of the redox potential. The Fo state fluorescence increases slightly with increasing ferricyanide concentration, until a solution potential of approximately 200 mV is reached, as measured versus an Ag/AgCl electrode. This is the potential at which the special pair becomes oxidized.[4] At redox potentials greater than 200 mV versus Ag/AgCl, the Fo state fluorescence decreases. The Fm state fluorescence also shows two regions of change. At redox potentials less than 200 mV versus Ag/AgCl there is a gradual decrease in the fluorescence emission, and at redox potentials greater than 200 mV versus Ag/AgCl there is a sharp decrease in fluorescence emission (Figure C.6).

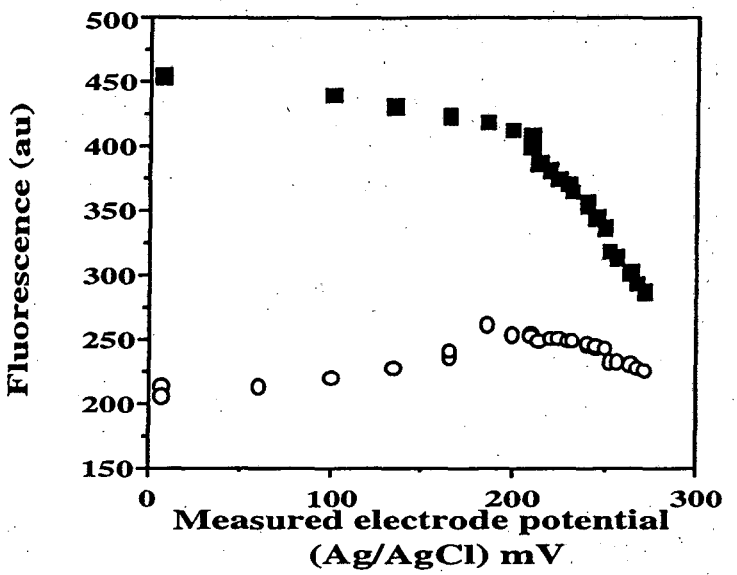

Figure C.6: The Fm (solid squares) and Fo (open circles) state fluorescence emission at 890 nm as a function of solution potential. The solution potential is increased by addition of ferricyanide. Excitation at 800 nm.

Ferricyanide-induced fluorescence quenching is also seen in mutant strains of *Rb. sphaeroides* which lack a reaction center. LM1.1, a strain which has both LH1 and LH2, shows a strong fluorescence quenching in the presence of 4.76 mM ferricyanide (Figure C.7). The extent of quenching is maximum at 890 nm, identical to the wild type fluorescence quenching. At 890 nm, the LM1.1 ferricyanide-treated fluorescence is approximately 11% of the untreated fluorescence. The fluorescence can be partially recovered by subsequent addition of ferrocyanide, final concentration 5 mM, to approximately 65% of the original intensity.

The extent of fluorescence quenching is not as strong in *Rb. sphaeroides* mutant BALM/LH2, which lacks both reaction centers and LH1, but expresses LH2 (Figure C.8). The fluorescence emission at 860 nm (the maximum emission of LH2) in the presence of 4.76 mM ferricyanide is approximately 77% of the untreated

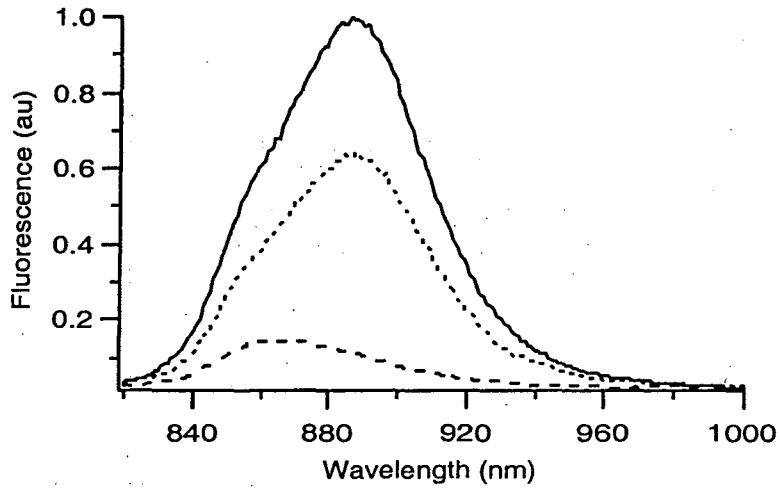

Figure C.7: Fluorescence emission of the *Rb. sphaeroides* mutant LM1.1 (which lacks reaction centers) in the untreated state (solid line, top); after addition of 4.76 mM ferricyanide (dashed line, bottom); and partial recovery of fluorescence after subsequent addition of 5 mM ferrocyanide (dotted line, middle). Excitation at 800 nm.

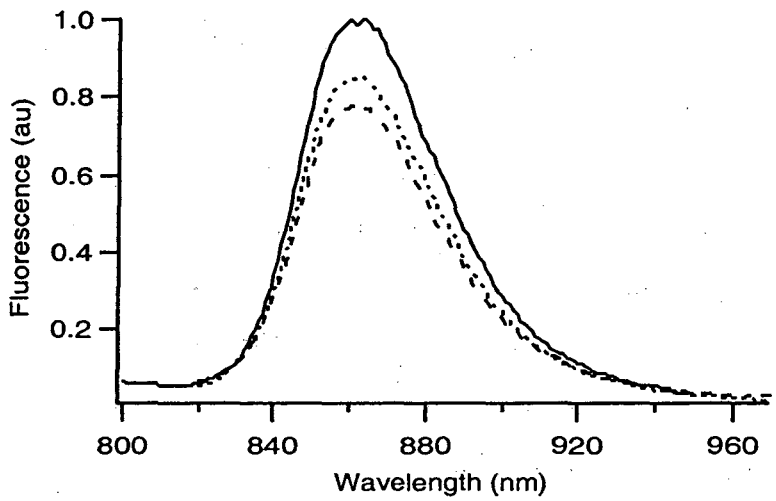

Figure C.8: Fluorescence emission of the *Rb. sphaeroides* mutant BALM/LH2 (which lacks reaction centers and LH1, and expresses LH2) in the untreated state (solid line, top); after addition of 4.76 mM ferricyanide (dashed line, bottom); and partial recovery of fluorescence after subsequent addition of 5 mM ferrocyanide (dotted line, middle). Excitation at 800 nm.

fluorescence, and after subsequent addition of 5 mM ferrocyanide, the fluorescence is restored to approximately 85% of the untreated fluorescence intensity.

A third mutant, RC-1A, expresses LH1 but does not express LH2 or reaction centers. This mutant shows strong quenching in the presence of 4.76 mM ferricyanide. The fluorescence is approximately 18% of its initial intensity at 890 nm (Figure C.9). Fluorescence emission can be recovered by the subsequent addition of 5 mM ferrocyanide, to a level approximately 75% of the initial fluorescence at 890 nm. These results are similar to those seen for LM1.1 and wild-type *Rb. sphaeroides* membranes.

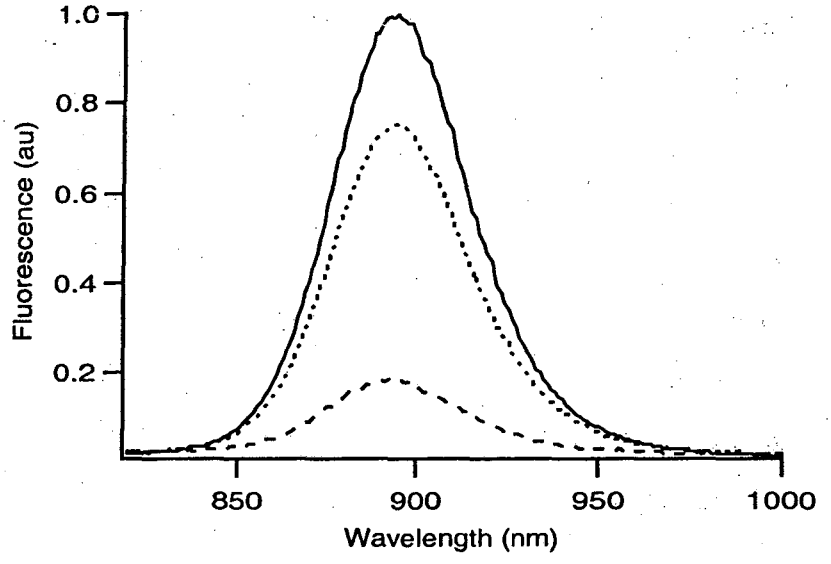

Figure C.8: Fluorescence emission of the *Rb. sphaeroides* mutant RC-1A (which lacks reaction centers and LH2, and expresses LH1) in the untreated state (solid line, top); after addition of 4.76 mM ferricyanide (dashed line, bottom); and partial recovery of fluorescence after subsequent addition of 5 mM ferrocyanide (dotted line, middle). Excitation at 375 nm.

The results from the mutant *Rb. sphaeroides* strains are consistent with a ferricyanide-induced oxidation of pigments in the membrane-bound antenna complexes

of *Rb. sphaeroides* chromatophores, particularly pigments in the LH1 complex. This hypothesis is consistent with previously published results. In the literature, ferricyanide has been shown to oxidize bacteriochlorophyll in light-harvesting complexes which have been isolated with detergents from purple photosynthetic bacteria.[5,6,7] For example, in one of these experiments, 10 mM potassium ferricyanide causes a very mild bleaching of the *Rhodobium marinum* LH1 complex absorption (2-3%), but a large quenching of the fluorescence emission (50%).[5] While these experiments are performed on isolated antenna complexes, the results on the isolated LH1 complex are very similar to what we observe for the membrane-bound *Rb. sphaeroides* LH1 complex in both wild-type and mutant strains.

Regardless of the origin of the fluorescence quenching caused by ferricyanide, the electric-field effect on the fluorescence emission (see Chapter Four) persists under ferricyanide-quenched conditions. Figure C.9 shows the electric-field induced change in fluorescence for wild-type *Rb. sphaeroides* chromatophores in the presence of 10 mM ferricyanide. See Chapters Two and Four for experimental details. Under these oxidizing conditions, the special pair may be at least partially oxidized (the P^+ state), and the fluorescence emission from LH1 is greatly attenuated. Under these circumstances, the electric-field effect is still evident, with a maximum at 890 nm of approximately 5 % per 100 mV (Figure C.10).

The electric field persists in both the Fo and Fm state. Figure C.11 compares the electric-field induced change in fluorescence emission in the Fo and Fm states for untreated chromatophores with the electric-field induced change in the Fo and Fm states in the presence of 10 mM ferricyanide, for an electric field intensity of 100 mV. The electric-field induced fluorescence change, $\Delta F/Fmax$, is reduced but present under ferricyanide-treated conditions.

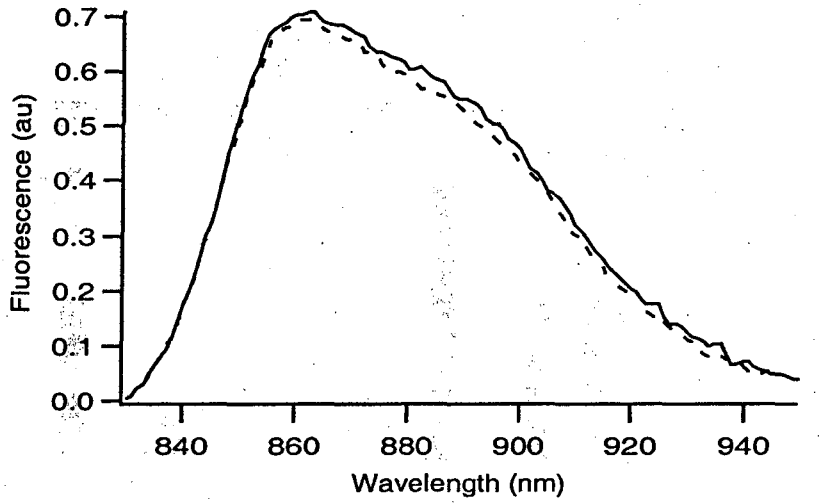

Figure C.9: Electric-field induced change in the wild-type *Rb. sphaeroides* fluorescence under oxidizing conditions of 10 mM ferricyanide. Positive applied field (top line, solid) and negative applied field (bottom line, dashed). Applied field strength 100 mV. Excitation at 800 nm. See Chapters Two and Four for experimental details.

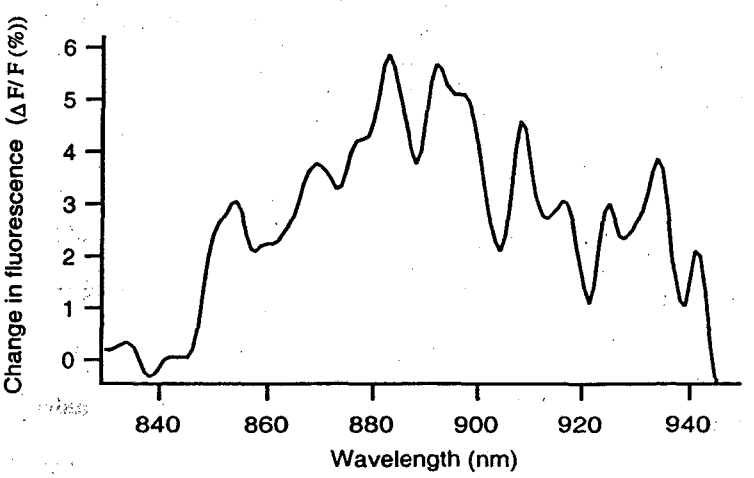

Figure C.10: The difference spectrum of the electric-field induced change in the Fo-state fluorescence spectrum of wild-type *Rb. sphaeroides* chromatophores in the presence of 10 mM potassium ferricyanide.

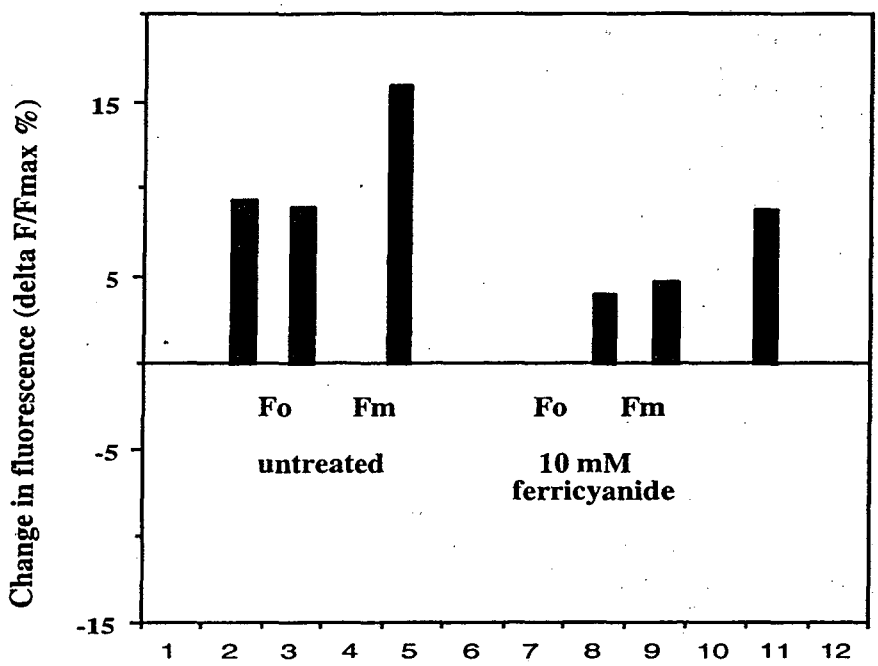

Figure C.11: Comparison of the electric-field induced change (ΔF/Fmax) in fluorescence for untreated *Rb. sphaeroides* chromatophores (left side, Fo and Fm) and chromatophores with 10 mM ferricyanide (right side, Fo and Fm), all cases for 100 mV electric-field potential, excitation at 800 nm.

Summary of experimental findings:

Potassium ferricyanide leads to strong fluorescence quenching in chromatophores of wild-type *Rb. sphaeroides*. Ferricyanide does not cause large changes in the near-IR absorption spectrum of *Rb. sphaeroides* chromatophores. The fluorescence quenching is maximum at 890 nm and fluorescence emission can be partially recovered by re-reduction of the solution through addition of potassium ferrocyanide.

Ferricyanide-induced fluorescence quenching is also observed in membrane preparations of mutant strains of *Rb. sphaeroides* which lack reaction centers. The fluorescence quenching is strongest in those strains which express LH1, and the quenching is maximum at 890 nm which is the emission maximum of LH1. These results are consistent with ferricyanide-induced quenching of fluorescence from the membrane-bound LH1 complex of *Rb. sphaeroides*.

Under these conditions, an electric-field effect still persists. The extent of the electric-field induced fluorescence change in the Fo state is approximately 5% per 100 mV, and in the Fm state approximately 10% per 100 mV. The maximum of the electric-field induced change is at 890 nm, despite the quenching of fluorescence at that wavelength.

References for Appendix C

[1]Goedheer, J.C. (1960) *Biochim. Biophys. Acta* 38: 389-399.

[2]Clayton, R.K. (1966) *Photochem. Photobio.* 5: 679-688.

[3]Vermeglio, A. & Clayton, R.K. (1976) *Biochim. Biophys. Acta* 449: 500-15.

[4]Clayton, R.K. (1962) *Photochem. Photobiol.* 1: 201-208.

[5]Picorel, R., Lefebvre, S. & Gingras, G. (1984) *Eur. J. Biochem.* 142: 304-311.

[6]Bopp, M.A., Jia, Y., Li, L., Cogdell R.J. & Hochstrasser R.M. (1997) *Proc. Natl. Acad. Sci.* 94: 10630-10635.

[7]Law, C.J. & Cogdell, R.J. (1998) *FEBS Letters* 432: 27-30.

Ernest Orlando Lawrence Berkeley National Laboratory
One Cyclotron Road | Berkeley, California 94720

Prepared for the U.S. Department of Energy under Contract No. DE-AC03-76SF00098